Formulation and Evaluation of 5-Fluorouracil and Methotrexate Gold Nanoparticles

A THESIS
SUBMITTED IN PARTIAL FULFILLMENT
OF THE REQUIREMENTS FOR THE DEGREE OF
MASTER OF PHARMACY

in

Pharmaceutics

By

Paras Famta

(Reg.No.11512561)

Under the guidance of

Supervisor

Dr. Vijay Mishra
Associate Professor

Co-Supervisor

Dr. Gopal L. Khatik
Associate Professor

School of Pharmaceutical Sciences
Lovely Professional University, Phagwara
Punjab 144411

(2017)

Dedicated to my guides, Dr. Vijay Mishra and Dr. Gopal Lal Khatik.

Statement by the candidate

This is to submit that this written submission in my thesis entitled **"Formulation and Evaluation of 5-Fluorouracil and Methotrexate Gold Nanoparticles"** represents original ideas in my own words and where other ideas and words have been included; I have adequately cited and referenced the original sources. I also declare that i have struck to all the principles of academic honesty and integrity and have not misrepresented or fabricated or falsified any idea/data/fact/source in my submission. I understand that any violation of the above will be cause for disciplinary action by the school and can also evoke penal action from the sources which thus have not been properly cited or from whom proper permission have not been taken when required.

Patents related to API, process, product, method and equipments, if any, have been examined to ensure non infringing approach to the existing patents.

This thesis encompasses the information generated by me based on experimental work carried out in the institute. I assure and hold full responsibility for its genuineness.

(**Paras Famta)**

Forwarded Through

(Co-Supervisor)

Dr. Gopal Lal Khatik
Associate professor
Department of Pharmaceutical Chemistry
Lovely Institute of Technology (Pharmacy)
Lovely Professional University, Phagwara

(Supervisor)

Dr. Vijay Mishra
Associate Professor
Department of Pharmaceutics
Lovely Institute of Technology (Pharmacy)
Lovely Professional University, Phagwara

Certificate by Supervisor

The work described in this thesis entitled **"Formulation and Evaluation of 5-Fluorouracil and Methotrexate Gold Nanoparticles"** has been carried out by **Mr. Paras Famta** under my supervision. we certify that this is his bonafide work. The work described is original and has not been submitted before for purpose of getting degree in any university. The candidate has performed the work with his dedication to the best of my satisfaction.

(Co-Supervisor)

Dr. Gopal Lal Khatik
Associate professor
Department of Pharmaceutical Chemistry
Lovely Institute of Technology (Pharmacy)
Lovely Professional University, Phagwara

(Supervisor)

Dr. Vijay Mishra
Associate Professor
Department of Pharmaceutics
Lovely Institute of Technology (Pharmacy)
Lovely Professional University, Phagwara

Date:
Place: LPU, Phagwara

Certificate by School

This is to certify that the project dissertation entitled, **"Formulation and Evaluation of 5-Fluorouracil and Methotrexate Gold Nanoparticles"** submitted by **Mr. Paras Famta** under the guidance of **Dr. Vijay Mishra** being duly certified and approved by the guide, and accepted for submission to Lovely Professional University in partial fulfilment of the requirements for the award of the degree of Masters in Pharmacy.

Dr. S. Tamilvanan
Professor
Head of domain
School of Pharmaceutical Sciences
Lovely Professional University, Punjab

Dr. Monica Gulati
(Senior Dean)
Head of School
School of Pharmaceutical Sciences
Lovely Professional University, Punjab

ACKNOWLEDGEMENT

Towards the completion of my thesis it is a pleasurable aspect that I communicate my thankfulness to all those who have been influential in the completion of this task.

I am thankful to my supervisor ***Dr. Vijay Mishra****, Associate Professor, Lovely School of Pharmaceutical Sciences, Lovely Professional University who has helped me complete my project with his excellent ideas, guidance, motivation, attention. I appreciate his never ending support and always having my back me in every situation due to which I was able to cope with every challenge in my project. I thank him for creating an environment where I can express my ideas and clear my doubts. I thank him for teaching me new things every day and always having faith in me.*

I would also like to thank my co-supervisor ***Dr. Gopal Lal Khatik****, Associate professor, Domain of pharmaceutical chemistry, Lovely Professional university, Punjab. I am extremely thankful to him for his constant encouragement, guidance, attention and motivation for completing my project work. I thank him for always being so kind to me and for helping me troubleshoot every challenge with his excellent ideas. I can never thank him enough for providing me the working area and resources to complete my project.*

I am very obliged to ***Dr. Monica Gulati****, Sr. Dean, School of Pharmaceutical Sciences and* ***Dr. S. Tamilvanan,*** *Head of department of pharmaceutics, Lovely School of Pharmaceutical Sciences , Lovely Professional University for giving his support to proceed my project work*

I also acknowledge with a deep sense of reverence, my gratitude towards ***Mr. Gopal Krishan*** *and* ***Mr. Satish Tiwari*** *who timely provided me all the materials and*

*resources required. **Mr. Hansraj, Mr. Manawar, Mr. Vijay Kumar, Mr. Anil Kumar** and **Mr. Prithavi** were very helpful during my project work.*

*I would like to express my heartiest gratitude to my friends **Jaskiran Kaur**, **Nuni Sagar**, **Deepak Ghai**, **Harish Rathee, Yusuf Nawaz Khan, Pushpak Mehriwala and Swati Patial** as without their love and support it would not have been possible to complete the task.*

*I owe my loving thanks to my brother **Mani Famta** who is always there to help me with his excellent ideas and support.*

*I would like to thank my parents **Mr. Anil Famta** and **Mrs Jyoti Famta** who have always been with me. It was due to my parent's dream, ambition, and sacrifice that I get so much ability to face all challenges during my research work today.*

*Acknowledgment can't be completed without expressing gratitude to our Chancellor **Mr. Ashok Mittal** who provided the facilities, equipment, and faculty for the research work.*

At last but not least gratitude goes to all my friends who directly or indirectly helped me to complete this project report, as well as expressing my apology that I could not mention personally one by one.

Date: 23-05-2017 *Paras Famta*

Place: Jalandhar

List of contents

List of Figures

List of Tables

List of symbols and Abbreviations

Symbol/Abbreviations	Full Form
%	Percentage
AFM	Atomic force microscopy
Au	Element gold
Au^{+}	Aurous ion
Au^{3+}	Auric ion
AUC	Area under curve
AuNR	Gold nanorods
BSA	Bovine serum albumin
BP	British pharmacopoeia
C_{max}	Maximum drug concentration in blood
Cl	Total plasma clearance
c(RGD)	cyclo-[L-arginyl-glycyl-L-alpha-aspartyl-D-phenyl alanyl-L-lysyl]
Co	Cobalt
CT Scan	Computerized tomography scan
CTAB	Cetyl trimethyl ammonium bromide
CNS	Central nervous system
DCC	N,N'-Dicyclohexylcarbodiimide
DNA	Deoxyribonucleic acid
DLS	Dynamic light scattering
DSC	Differential scanning calorimetry
DCM	Dichloromethane
DMF	Dimethylformamide
et al.	And co-workers
etc.	Et cetera
EDX	Energy dispersive X-ray spectroscopy
EAAS	Enzyme amplified array sensing
5-FU	5-Fluorouracil
5-FA	5-Fluorouracil-1-Acetic Acid
FTIR	Fourier transform infrared spectroscopy

5-FdMP	Fuorodeoxyuridine monophosphate
5_FUMP	Floxuridine monophosphate
5-FUDP	Floxuridine diphosphate
5-FUTP	Floxuridine triphosphate
GNP	Gold nanoparticles
GFP	Green fluorescent light
Gd	Gadolinium
GSH	Glutathione
GIT	Gastrointestinal tract
$HAuCl_4$	Chloro auric acid
HRTEM	High resolution transmission electron microscopy
^1H	Proton
i.v.	Intravenous
IR	Infrared radiations
JP	Japanese pharmacopoeia
KrF	Krypton fluoride laser
KBr	Potassium bromide
Ltd.	Limited
Λ max	Lambda max
MTX	Methotrexate
MRT	Mean residence time
MRI	Magnetic resonance imaging
mPeg	Modified polyethylene glycol
MTAB	16- Mercaptohexadecyltrimethyl ammonium bromide
MCF- 7	Michigan cancer foundation 7 cell lines
NIR	Near infrared radiation
Nd:YAG	Neodymium-doped Yttrium Aluminium garnet
NaOH	Sodium hydroxide
NMR	Nuclear magnetic resonance

PEG	Polyethylene glycol
PEG-5-FUA	5-Fluorouracil conjugate polyethylene glycol
PEG-MTX	Methotrexate conjugated polyethylene glycol
PTT	Photothermal therapy
PVP	Polyvinyl pyrrolidone
PPE	Poly paraphenylene ether
PLGA	Poly lactic co-glycolic acid
PAI	Photoacoustic imaging
pH	Power of hydrogen
PBS	Phosphate buffered saline solution
pKa	Negative base-10 logarithm of the acid dissociation constant
Pvt.	Private
RES	Reticuloendothelial system
RME	Receptor mediated endocytosis
RNA	Ribonucleic acid
Rpm	Revolutions per minute
SPR	Surface plasmon resonance
SAED	Selected electron diffraction
siRNA	Small interfering RNA
TOAB	Tetraoctylammonium bromide
TEM	Transmission electron microscopy
TA	Thermal analysis
TGA	Thermogravimetric analysis
THP	Tumor homing peptides
UV	Ultraviolet
Vis	Visible
Vd	Volume of distribution
XRD	X-ray diffraction
XPS	X-ray photoelectron microscopy

X-ray	X-radiations
mm	millimetre
µm	Micrometre
nm	nanometre
mg	milligram
Kg	kilogram
h	hour
m^2	Metre square

List of Terminology

Antibody: An antibody (Ab), also known as an immunoglobulin, is a large, Y-shaped protein produced mainly by plasma cells that is used by the immune system to neutralize pathogens such as bacteria and viruses.

Anisotropic property: A physical property which has a different value when measured in different directions.

Antimetabolite: A substance that interferes with the normal metabolic processes within cells, typically by combining with enzymes.

Biocompatible: A substance is called biocompatible, if it is not harmful or has any toxic effect on the body tissues.

Biosensor: A device which uses a living organism or biological molecules, especially enzymes or antibodies, to detect the presence of chemicals.

Biodistribution: The distribution of a compound within a biological system or within an organism.

Buffer: A solution which resists changes in pH when acid or alkali is added to it.

Chemotherapy: The treatment of disease by the use of chemical substances, especially the treatment of cancer by cytotoxic and other drugs.

Cytokinesis: The cytoplasmic division of a cell at the end of mitosis or meiosis, bringing about the separation into two daughter cells.

Corona: Crown like structure, covering the particles in all directions.

Capping agent: Agent used for the coating of nanoparticles. They prevent the agglomeration of the nanoparticles.

Cytotoxic: Any agent or process that kills cells.

Carcinomatosis: A pathological condition characterized by the presence of carcinomas that have metastasized to many parts of the body.

Characterization: A description of the distinctive nature or features of an object.

Diagnosis: The identification of the nature of an illness or other problem by examination of the symptoms.

Esterification: A chemical reaction in which two reactants form an ester as the reaction product.

Fluorescence: The visible or invisible radiation produced from certain substances as a result of incident radiation of a shorter wavelength such as X-rays or ultraviolet light.

Fibroblast: A cell in connective tissue which produces collagen and other fibres.

Grafting: It is a technique of attaching one living tissue with another living tissue.

Hydrophobic: Physical property of a material due to which it repels water.

Hydrophilic: Physical property of a material due to which it mixes with water.

Immunology: The branch of medicine and biology related to immune system.

Ischemia: An inadequate blood supply to an organ or part of the body.

Ligand: A molecule that binds to another (usually larger) molecule.

Laser ablation: Laser ablation is the process of removing material from a solid (or occasionally liquid) surface by irradiating it with a laser beam.

Monodisperse: It is a property of a colloid in which it possesses particles of uniform size.

Multidentate: Ability to form bonds at more than one point.

Macrophage: A large phagocytic cell found in stationary form in the tissues or as a mobile white blood cell, especially at sites of infection.

Myelosuppression: It is the decrease in production of cells responsible for providing immunity (leukocytes), carrying oxygen (erythrocytes), and/or those responsible for normal blood clotting (thrombocytes).

Nanotechnology: The branch of technology that deals with dimensions and tolerances of less than 100 nanometres.

Nanoparticles: A particle with the dimensions in the range of nanometres.

Oscillation: Regular variation in magnitude or position about a central point.

Osponization: Antibody opsonization is the process by which a pathogen is marked for ingestion and eliminated by a phagocyte. Osponin protein binds to the membrane, due to which phagocytes are attracted towards the pathogen.

Photothermal therapy: Photothermal therapy refers to efforts to use electromagnetic radiation (most often in infrared wavelengths) for the treatment of various medical conditions, including cancer. This approach is an extension of photodynamic therapy, in which a photosensitizer is excited with specific band light.

PEGylation: PEGylation is the process of both covalent and non-covalent attachment of polyethylene glycol polymer chains to molecules and structures of different size range, such as a drug, therapeutic protein or vesicle.

Pharmacokinetics: The branch of pharmacology concerned with the movement of drugs within the body.

Phase transfer catalyst: A phase-transfer catalyst or PTC is a catalyst that facilitates the migration of a reactant from one phase into another phase where reaction occurs.

Physiosorption: It is a process in which the electronic structure of the atom or molecule is barely perturbed upon adsorption.

Preformulation studies: It can be defined as an investigation of physical and chemical properties of a drug substance - alone and or when combined with excipients.

Resonance: Resonance or mesomerism is a way of describing delocalized electrons within certain molecules or polyatomic ions where the bonding cannot be expressed by one single Lewis structure.

Surface plasmon resonance: It is the resonant oscillation of conduction electrons at the interface between negative and positive permittivity material stimulated by incident light.

Simulation: It is the imitation of a situation or a process.

Spectrum: It used to classify something in terms of its position on a scale between two extreme points.

Tumor: A swelling of a part of the body, generally without inflammation, caused by an abnormal growth of tissue, whether benign or malignant.

Thrombocytopenia: Deficiency of platelets in the blood.

Xenograph: A tissue graft or organ transplant from a donor of a different species from the recipient.

Abstract

Nowadays, cancer is one of the leading life taker worldwide. We are still to find an efficient treatment without toxic side effects. Nanotechnology has shown enormous potential as a drug delivery system in the cancer treatment. In recent works, gold nanoparticles (GNP) have shown good potential as an anticancer agent because of its unique physico-chemical properties and Photo Thermal Ablation property. In this study, we report the formulation of 5-Fluorouracil (5-FU) and Methotrexate (MTX) functionalized GNPs for the treatment of breast cancer. The GNPs were prepared by the reduction of chloroauric acid with trisodium citrate. 5-FU was converted into its derivative 5- Fluorouracil-1 Acetic Acid (5-FUA) with the help of chloroacetic acid. The FTIR results confirmed the synthesis of 5-FUA. The anticancer agents 5-FUA and MTX were conjugated to Polyethylene glycol 6000 (Peg 6000) with the help of N,N'-Dicyclohexylcarbodiimide (DCC). The UV-Visible Spectroscopy, FTIR and proton NMR results confirmed the conjugation on Peg 6000. The gold nanoparticles were capped with drug conjugated Peg 6000 using PEG linker technique. The formulation was characterized by UV-Visible spectroscopy, ^{1}H NMR and Atomic Force Microscopy (AFM). The qualitative in-vitro studies using MDA-MB-231 breast cancer cell lines showed uptake of the formulation by the cancer cells. This, illustrates GNP formulation as a promising Drug Delivery System to breast cancer.

Keywords: Gold nanoparticles, Methotrexate, 5-Fluorouracil, Breast cancer, Cell line study.

1. INTRODUCTION

Nanoparticles (NPs) are the materials having particle size in the range of 1 to 100 nm. The NPs offer various properties, which can be utilized to formulate new formulations and to get more stable products (Dreaden et al., 2012). The NPs are 100 to 1000 times smaller when compared with human cells; consequently, they can enter inside cells and organelles. The NPs are utilized to focus on the DNA, proteins, enzymes and cell receptors intracellular and extracellular. Contingent on their size, NPs can go through various biological barriers like blood brain barrier (BBB) and skin. Biological processes and events leading to cancer occur at nanoscale and inside the cells, NPs offer alluring plan to target such cases (Patra et al., 2009).

1.1 Gold nanoparticles

The gold nanoparticles (GNPs) show various physicochemical, optical and electronic properties, which make it a superb contender for anticancer chemotherapy and imaging agents. These arrangements of properties make them flexible, biocompatible and practically more precise, consequently they can focus on the targeting the drug more proficiently prompting low toxicity. The GNPs are a brilliant possibility to convey drugs and imaging agents with high susceptibility of degradation and poor pharmacokinetics (Dreaden et al., 2012). The GNPs can convey hydrophobic dyes and drugs by ensnaring them in hydrophobic alkanethiol pockets (Kim et al., 2009). Because of their small particle size and biocompatible behavior, GNPs can concede long circulating lifetimes to agents susceptible to enzymatic and environmental degradation. GNPs have the property to be surface functionalized with high densities ($1x10^6$ μm^{-2}) of ligands, which is higher when compared with other NPs. Thus, the binding affinity of the formulation can be optimized according to a disease type or patient. Attributable to the properties, for example, capacity to frame NPs of various sizes and high loading density of ligands, multivalent GNPs with high avidity can be shaped. High avidity results in elevated specific take-up at the target site (Tassa et al., 2010; Dreaden et al., 2012). Plasmonic NPs, for example, GNPs have a special property of surface plasmon resonance (SPR) due to which the radiative and non-radiative properties of the GNPs are expanded.

The GNPs as alluring contender for the conveyance of drug payloads specifically into cancer cells because of its physicochemical properties including moderately high biocompatibility and simplicity in conjugation to biomolecules, fit

for enhancing drug delivery and expanded targeting efficacy (Cabral et al., 2014, Bao et al., 2014, Perez-Herero et al., 2015).

AuNPs have been effectively used to deliver i) drugs and contrast agents that otherwise exhibit low solubility and poor pharmacokinetics and ii) compounds that are naturally susceptible to enzymatic degradation, as well as those that display low intracellular penetration (e.g. siRNA) (Conde et al., 2012).

The GNPs based frameworks are absolutely critical to beat the limitations of cancer therapy including side effects and multi-drug resistance (Lin et al., 2016). The GNPs can be surface functionalized with active ligands at high densities e.g. 100 times higher than that attainable with conventional liposomes (Torchilin et al., 2001).

Interactions of near IR (700-900 nm) with GNPs brings about surface plasmons resonances (SPR), which is directly related to the photothermal effects (Zhong et al., 2014). Many reports have demonstrated that GNPs have equipped for modifying the cell cycle including cell division, signaling, and proliferation. Tumor cell targeted GNPs can instigate DNA damage, cytokinesis arrest, and apoptosis (programmed cell death) (Giljohann et al., 2010, Boisselier and Astruc 2009; Lim et al., 2011).

The GNPs are versatile platforms for the design of recognition components toward particular biological targets. Additionally, the improved radiative properties responsible for fluorescence quenching, surface enhanced Raman scattering, and in addition their electrochemical action, can be bridled to signal the transduction of binding events. Thus, incorporation of GNPs can improve framework while upgrading the sensitivity of biosensors. The typical size of GNPs, which is ten thousand times smaller than human cells and comparable to large biological molecules such as enzymes and antibodies, leads to interactions with biomolecules, both at the surface and inside cells, which may revolutionize disease diagnosis and treatment. GNPs can act as either photothermal therapeutic (PTT) agents or probes for in vitro or in vivo bioimaging because of their high absorption and scattering cross areas in the visible-NIR range, by virtue of the purported localized SPR (Bodelóna et al., 2017). The electrons of the conduction band of GNPs undergo collective surface oscillations, called surface plasmon resonance (SPR), which originate high absorption and scattering cross sections (Jain et al. 2006).

1.2 Fabrication of GNPs

Techniques for making diverse GNPs can be sorted into two principles such as Bottom up and Top down strategies (Eustis et al., 2006).

The bottom up strategy incorporates nanosphere lithography, chemical, photochemical, electrochemical, templating, sonochemical and thermal reduction strategies (Schaal et al., 2012). This strategy includes assembly of atoms (produce by reduction of ions) into craved nanostructures. Top down strategies such as vapor deposition, pulsed wire discharge, arc discharge method, milling, photolithography and electron beam lithography require the expulsion of matter from the bulk material to get the coveted nanostructure (Sun et al., 2006).

Since both techniques can create GNPs of desired shape and size, each have their own disadvantages e.g., poor monodispersity in case of bottom up method and extensive waste of material in top down method. Commonly utilized bottom up strategies (Shah et al., 2014) for making GNPs are given below:

1.2.1. Turkevich technique

The Turkevich technique was first portrayed in 1951 and is a standout amongst the most regularly utilized strategies for fabrication of spherical GNPs in the size range of 10-20 nm. The principle of this technique includes reduction of gold ions (Au^{3+}) to gold atoms (Au^{0}) in the presence of reducing agents like citrate (Turkevich et al., 1951; Frens et al., 1973), ascorbic acid, amino acids or UV light (Sivaram et al., 2011; Niidome 2003). Size of GNPs is additionally balanced by utilizing different capping/stabilizing agents.

Initially the Turkevich technique was restricted by the narrow range of GNPs that could be generated by this strategy. However, a few advances in the original technique have allowed for researchers to expand the size of GNP that can be produced by means of this strategy. In 1973, Frens found that by changing the proportion of reducing to stabilizing agents, GNPs of particular size, extending from 16-147 nm can be accomplished. Afterward, the roles of pH, temperature and sodium citrate concentration were better comprehended, taking into consideration for the development of a particle growth model (Kumar et al., 2007).

1.2.2. Brust strategy

The Brust strategy was first demonstrated in 1994 (Brust et al., 1994). This technique is a two phase process to produce 1.5-5.2 nm GNPs utilizing organic

solvents and by changing the proportion of thiol to gold. The Brust strategy was motivated from Faraday's two phase system. The technique includes exchange of gold salt from aqueous solution to an organic solvent e.g. toluene utilizing a phase transfer agent e.g. tetraoctylammonium bromide (TOAB). The gold is then reduced utilizing sodium borohydride in presence of alkanethiol, which stabilize the GNPs resulting in a color change of the reaction from orange to brown. Schriffin and co-workers reported the purification of GNPs stabilized with dodecanethiol from TOAB (Waters et al., 2003).

1.2.3. Seeded growth technique

While the Turkevich and Brust techniques can create spherical GNPs, the GNPs can also exist in assortment of nanostructures such as rods (Gole et al., 2004; Sau et al., 2004), cubes (Skrabalak et al., 2008), tubes (Bridges et al., 2013) and so on. The most widely favored procedure to acquire GNPs in different shapes is seed mediated growth. The basic principle of this method is to first produce seed particles by reducing gold salts with a strong reducing agent like sodium borohydride. The seed particles are then added to a solution of metal salt in presence of a weak reducing agent like ascorbic acid and structure guiding agent to counteract further nucleation and accelerate the anisotropic growth of GNPs. Geometry of gold nanostructures can be changed by differing the concentration of seeds, reducing agents and structure directing agents (Chuan et al., 2007).

1.2.4. Laser ablation strategy

Laser ablation strategy has got much consideration because of its adaptability, simplicity, control on fabrication parameters and chemical contaminants free products (El-Sayed et al., 2013). In this strategy, the size distribution of NPs is influenced by the parameters of laser and the nature of the encompassing fluid. The nanosecond lasers like Nd:YAG laser and KrF Excimer laser have been widely utilized for the fabrication of GNPs in liquid media (Imam et al., 2012; Scaramuzza et al., 2016).

1.2.5. Xia method

Xia et al modified the Turkevich strategy by quickly adding a blend solution of $HAuCl_4$ and sodium citrate into boiling water. This method allowed reproducible preparation of GNPs in water with a fairly narrow size distribution. The uniform quasi-spherical shape gave a trace amount of silver nitrate ($AgNO_3$) in the $HAuCl_4$/citrate blend (Xia et al., 2009).

As compared with the commonly used Turkevich method, two distinct characters of this approach are (1) aqueous solutions of citrate and $HAuCl_4$ are well mixed at room temperature and then rapidly added to boiling water and (2) the citrate/$HAuCl_4$ mixture contains a trace amount of Ag^+ ions. Because of these two modifications, this methodology can (1) efficiently minimize the effect of citrate to buffer the pH of the reaction media and thus change the type and reactive activity of auric ions to guarantee a dominant presence of highly active $AuCl_3(OH)$- ions, (2) significantly speed up the nucleation and growth rate of GNPs due to Ag^+ ion catalyzed oxidation of citrate to SADC to largely narrow the NP size distribution, and (3) reshape the polycrystalline GNPs into a quasi-spherical shape with the aid of Ag^+ ions due to their Au facet selective deposition. In the case of synthesis of Au NPs of sizes ranging from 10 to 40 nm, our approach efficiently makes up the shortages of the classical Turkevich method with respect to the reproducibility and uniformity of the NP size and shape (Xia et al., 2010).

1.3. Characterization techniques for GNPs

1.3.1. Morphology characterization

Electron microscopy including transmission electron microscopy (TEM) and scanning electron microscopy (SEM) makes use of the wave character of electrons, but is analogous to optical microscopy in that an image of an object is constructed from the scattering pattern of a focused beam of electrons. The technique of high resolution transmission electron microscopy (HRTEM) together with selected electron diffraction (SAED) and energy dispersive X-ray spectroscopy (EDX) can be utilized to analyze the crystal structure and composition of objects. X-ray diffraction (XRD) is meanwhile one of the most important techniques for the determination of structure and composition.

For SPR, UV-visible spectroscopy provides valuable information regarding shape, size, interparticle distance, and aggregation of nanoparticles. Dynamic light scattering (DLS) analysis determines the average hydrodynamic size and size distribution profiles of the particles in solution.

1.3.2. Surface characterization

X-ray photoelectron spectroscopy (XPS) is an essential tool to analyze surface atomic layers of NPs within several nanometers from the surface. Information of atomic composition and chemical state of the surface atoms can be obtained from

XPS spectra. Fourier transform infrared (FT-IR) spectroscopy is meanwhile a powerful tool to characterize functional groups of the surface protecting organic layers. Thermal analysis (TA) including thermogravimetric analysis (TGA) and differential scanning calorimetry (DSC) can be used to analyze the amount of organic residues and surface melting properties.

1.3.3. Theoretical simulation

The surface plasmon phenomenon is basically a resonance between light and conductive matter, and thus it can be comprehensively analyzed by Maxwell equations.23 The Mie theory provides an exact solution of the equations, but is limited to analysis of the morphology of spheres and spheroids.

Recent advances in electrodynamic theory make it possible to determine numerically converged solutions for nanoparticles of arbitrary shapes with dimensions up to a few hundred nanometers. The discrete dipole approximation (DDA) (Yang et al., 1995) and finite difference time domain (FDTD) (Novotony et al., 1997) methods are generally used for analyzing absorption and scattering and bands of gold nanoparticles.

1.4 Properties of GNPs

Gold nanoparticles (GNPs) have been extensively used for applications both in biomedical (e.g. bio-imaging and Drug delivery) (Ghosh et al., 2008) and technology (e.g. photonics) due their unique optical properties. These optical properties are conferred by the interaction of light with electrons on the GNP surface. At a specific wavelength (frequency) of light, collective oscillation of electrons on the GNP surface cause a phenomenon called SPR (Cai et al., 2008; Sayed et al., 2005), resulting in strong extinction of light (scattering and absorption). The particular wavelength of light where this occurs is strongly dependant on the GNP size, shape, surface and agglomeration state.

Some physicochemical properties of GNPs, including size (surface area), shape, surface charge and coating, agglomeration, and dissolution rate, are particularly important for determining their biological interactions and impacts. Smaller particles have a larger surface area and therefore, have greater toxic potential. It is well known that the shape of gold nanostructures can dramatically affect their physical and chemical properties. Frequently utilized gold nanostructures in the

biomedical field include gold spherical, nanowires, nanorods, nanoplates, and nanocubes (Dreaden et al., 2012; Sharma et al., 2015).

1.4.1. Optical properties of GNPs

The influence of GNP size on the SPR is to affect the absorption maximum (λ_{max}), which increases from 520-570 nm for 20 and 100 nm spherical GNPs, respectively (Huang et al., 2010). Particles with sizes above 100 nm have broader peaks spanning into the 600 nm range due to the presence of both transversal and longitudinal SPRs. In comparison, GNPs with diameters below 2 nm do not exhibit SPR. The difference in extinction between different sized and shapes GNPs can conveniently be utilized for multiplexing. The GNPs have a broad absorption band in the visible region of the electromagnetic spectrum. Mie was the first researcher to formulate the nature of the optical band as a surface plasmon effect, in the so-called "Mie theory". The characteristics of the band arise from the collective oscillation of free-conduction electrons induced by an interacting electromagnetic field, and their resonances are noted as surface plasmon (Figure 1). In fact, the electric field of the incoming radiation causes the formation of a dipole in the nanoparticle. The specific resonance frequency depends on a number of parameters such as nanoparticle composition, morphology, concentration, solvent refractive index, surface charge, and temperature. Meanwhile, such a resonance wavelength for rod-shaped NPs depends on the angle of the electric field. This results in two oscillations, transverse and longitudinal, that lead to two plasmon bands. The transverse SPR band occurs at a wavelength close to that of spherical GNPs, while the longitudinal band is in the region 600-900 nm, depending on their aspect ratio (length/width) (Alekseeva et al., 2006; Tokonami et al., 2012).

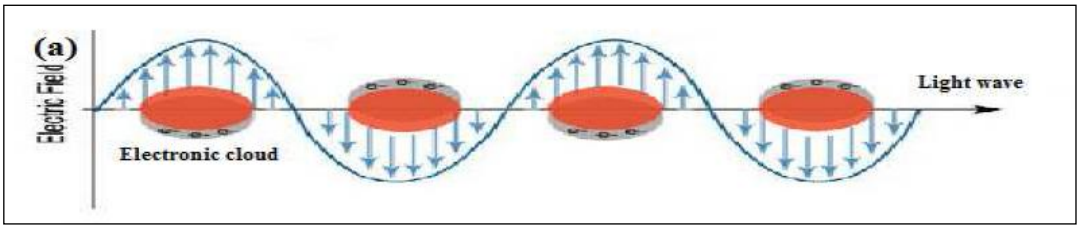

Fig. 1.1: Schematic presentation of localized surface plasmon resonance (SPR)

A major determinant of the optical properties of GNPs is their shape. Therefore synthesizing GNPs of different shapes, SPR can easily be tuned to give absorption maxima from around 500 nm into the near-infrared part of the spectrum. For example, spherical collodial gold have absorbance maxima between 515-570 nm

as described above, while irregular shaped NPs such as gold nanorods, and urchin shaped GNPs (also called gold nanostars) have absorption maximum in the near-infrared region of the spectra. The difference in absorption properties between spherical and irregular-shaped GNPs of the same average size is caused by an anisotropic (uneven) distribution of the surface electron layers (Dreaden et al., 2012; Sharma et al., 2015).

1.5. Pharmacokinetics of GNPs

Among various types of GNPs, one special and most widely used form is the polyethylene glycol (PEG)-coated GNPs because PEGylation prolongs circulation time. Cho et. al. studied the compartmental pharmacokinetics of 13 nm PEG coated GNPs in mice after intravenous (i.v.) injection of 0.85 or 4.26 mg/kg at various time points up to 7 days. Plasma C_{max} and Area Under Curve (AUC) were dose-dependent; terminal elimination $T_{1/2}$, Mean Residence Time (MRT), total plasma clearance (Cl), and volume of distribution (Vd) were not affected by dosage. The blood $T_{1/2}$ of the 4.26 and 0.85 mg/kg dose groups were 32.65 and 28.50 h, respectively. Cho et. al. then examined the influence of particle size (4, 13, and 100 nm) on the long-term kinetics of PEG-coated GNPs after a single i.v. injection (0.85 mg/kg) in mice. Kinetics of small (4 and 13 nm) GNPs showed similar patterns, i.e., plasma concentrations remained high for 24 h and dramatically dropped 7 days after injection. In contrast, large (100 nm) GNPs had a much lower (~100-fold) plasma concentration and were completely cleared at 24 h after injection (Cho et al., 2007; Cho et al., 2010).

Biodistribution of GNPs depends on multiple factors, including the size, surface modification, surface charge, opsonization including protein corona formation, and administration route (Cho et al., 2007; Cho et al., 2010). To increase biocompatibility, metallic NPs are generally coated with natural or synthesized polymers (e.g., PEG) or peptides, which are normally distinct from the core. These surface-coating materials can be cleaved off and then degraded. This is a general metabolic pathway for bioconjugated GNPs designed as drug carriers (Lin et al., 2015). The GNPs can be excreted from the body via renal and hepato-biliary clearance. Many factors can affect elimination of GNPs, including size and surface chemistry. Excretion of GNPs is generally low due to opsonization with persistent and primary accumulation in the liver, spleen, and mesenteric lymph node, even for small-

size particles. For example, nearly ~50% of 1.4 nm GNPs was found in the liver and only ~9% was excreted into urine 24 h after i.v. injection in rats (Semmler-Behnke et al., 2008).

1.5.1. Aggregation of GNPs

Aggregation state of GNPs has an effect on their optical properties. This fact can be used to monitor GNP stability, both over time, and upon addition of salt-containing buffers, which at high enough concentrations leads to particle aggregation, The red-shift or Bathochromic shift in absorption maximum caused by aggregation of nanoparticle, or particles in close proximity, which have successfully been utilized in many assays as a detection mechanism. Chegel et al studied on the interactions between citrate-stabilized GNPs and organic compounds bearing various functional groups in an aqueous medium. As a result, authors had found that organic compounds containing both thiol and amine groups strongly promote the aggregation of GNPs due to their cooperative functionalities (Chegel et al., 2012) for cell uptake and toxicity of GNP. Albanese et al had developed a simple technique to produce transferrin-coated GNP aggregates of different sizes and characterized their uptake and toxicity in three different cell lines (Albanese et al., 2011).

1.6. Surface chemistry and functionalization

The GNPs are capped with citrate, tannic acid, or polyvinyl pyrrolidone (PVP) capping agents. Citrate as capping agent weakly associates with the nanoparticle surface and is often used because the weakly bound capping agent provides long term stability and is readily displaced by a range of other molecules including amines, thiols polymers, proteins and antibodies (Gangwar et al., 2012; Mirza et al., 2011; Senoudi et al., 2014). Tannic acid is a multidentate capping ligand that can be displaced with many thiol containing molecules. Tannic acid is generally used as a capping agent in applications where high particle concentrations are required. PVP is a polymer that binds strongly to the GNP surface. It provides greater stability than citrate or tannic acid capping agents, but is more difficult to displace. It is important to remember the surface of most NPs is dynamic and is strongly influenced by the local environment. Different conditions also affect the particle in different ways. GNPs used in biological applications are commonly coated with polyethylene glycol (PEG) (Marcelo et al., 2015), bovine serum albumin (BSA) (Khullar et al., 2012) proteins, peptides, oligonucleotides or numerous other polymer. Binding molecules to

a gold surface can be accomplished by physisorption or by taking advantage of extremely stable thiol-gold bonds. The GNPs can be functionalized with molecules that 'flip' the surface charge of the negatively charged GNPs to a positively charged surface. Particles can also be functionalized to provide reactive groups (for example, amine- or carboxy-terminated surfaces) for subsequent conjugation by the customer. Dielectric shells (for example, silica, aluminium oxide, and TiO2) with a precisely controlled thickness can be used for encapsulating the particles (Bahadur et al., 2011).

1.7. Biomedical applications

The GNPs show a variety of promising applications. These are presented in Fig 1.2.

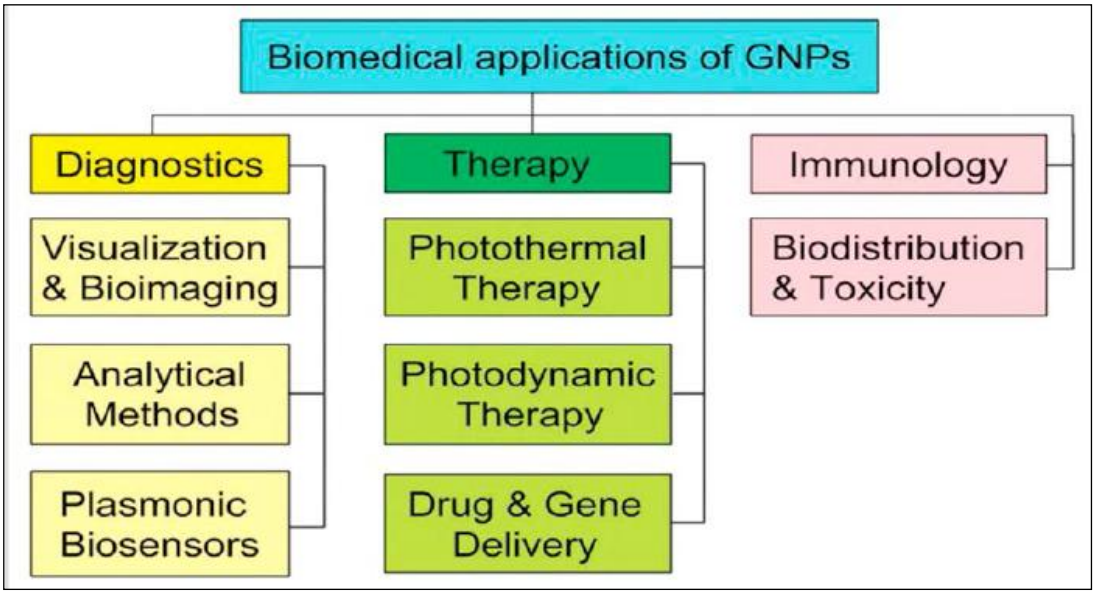

Fig 1.2: Biomedical applications of GNPs

1.7.1 Sensing

The GNPs are easily conjugated with oligonucleotides or antibodies for the detection of target biomolecules, permitting in vitro revealing and diagnostics applications for diseases such as cancer (Huo et al., 2011). For example, in the “bio-barcode assay”, which is a very sensitive method for sensing target proteins and nucleic acids, GNPs play an important role (Hill et al., 2007). Developing GNPs conjugated with both barcode oligonucleotides and target-specific antibodies, and magnetic micro-particles (MMPs) functionalized with monoclonal antibodies for the target cells is the main principle of the “bio-barcode assay”. These complexes cause a large quantity of barcode oligonucleotides, create both identification and quantification possibility of the target (Thaxton et al., 2009). Aptamer-conjugated GNPs were applied to sense small molecule and cancer cells by merging the

selectivity and affinity of aptamers with the spectroscopic properties of GNPs (Medley et al., 2008; Zhang et al., 2010). Under optimal conditions, an aptamer-nanoparticle strip biosensor (ANSB) exhibited a detection limit of 4000 lymphoma (Ramos) cells utilizing visual detection and 750 Ramos cells with a strip reader (Liu et al., 2009).

"Chemical nose" is a new method employing non-covalent conjugates of fluorophore and GNP, which is developed to create high sensitivity sensors for sensing of bio-molecular targets (Miranda et al., 2010). This complex create a proper bio-detection technique to "lock and key" specific recognition based methods, applying an array of selective receptors to produce a pattern, which is able to recognize analytes. The first sensor system was based on quaternary ammonium-functionalized GNPs with poly para-phenyleneethynylene (PPE) as a fluorescence transduction element that can be quenched by cationic GNPs (Bajaj et al., 2009). The PPE can be dislocated from the complex because of Competitive binding of analyte, cause the recovered fluorescence from PPE and also creating a clear signal. By this technique it was possible to distinguish 12 different species of bacteria with 95% accuracy. Furthermore, this method was applied to distinguish normal, malignant and metastatic cells in a quick and accurate assay. To provide higher sensitivity (5000 cells comparative to the previous 20000) in sensing of mammalian cancer cells, green fluorescent protein (GFP) replaced the polymer transducer (Bajaj et al., 2010). Lately, the array-based sensing technique was modified to an enzyme-amplified array sensing (EAAS) method, where the sensitivity is amplified via enzymatic catalysis (Miranda et al., 2010). This system is based on competitive binding of analyte protein with the GNP, freeing the β-galactosidase (β-Gal) and re-establishing its activity. Enzyme-amplified fluorescent information of the binding event can be created through cleavage of substrate, letting the identification of proteins.

1.7.2 Imaging

1.7.2.1 Fluorescence based imaging

In 1969, for the first time the fluorescence of bulk gold, which is very weak with a quantum yield in the order of 10^{-10}, observed by Mooradian et al. Amazingly, in Nano-scale, GNPs such as rods or shells show strong fluorescence with a quantum yield of up to 10^{-3} (Zheng et al., 2003; Zheng et al., 2012). This fluorescence property can be adjusted to the near IR window (600-800 nm), a region where light infiltrates

tissues comparatively well (Durr et al., 2007; Zhang et al., 2010). Gold nanorods (AuNRs) as result of the intermittent oscillation of the surface electrons along the x and y axis show transversal and longitudinal Plasmon resonance bands. When the aspect ratio of the rod, for a given diameter, increases the longitudinal band shifts to the red while transversal band remains unaffected. For instance, AuNRs with an aspect ratio of 2 exhibited a maximum emission at 540 nm, while enhancement the aspect ratio to 5.4 results in a maximum emission at 740 nm. These properties could be useful in biosensing of DNA, where with functionalized AuNRs with sequences, when complementary sequences were added, the AuNRs cumulative and the fluorescence signal reduced (John, 2005).

1.7.2.2 X-ray based imaging

Due to electron density and high atomic number of Au, they provide efficient absorption of X-ray radiation which is larger than iodine-based contrast agents that currently applied in the hospital, especially in 120 and 140 Kv X-ray tubes (Galper et al., 2012). Moreover, longer circulation times of GNPs toward current agents result in prolonged imaging, targeting to specific cell types and cell tracking (Arifin et al., 2011; Cormode et al., 2008). Such properties, as well as their biocompatibility toward other elements has caused to the examination of GNPs as contrast agents for X-ray based imaging methods such as CT scan (Aydogan et al., 2010; Hainfeld et al., 2011; Davaran et al., 2014). An in vivo CT contrast performance study, of 38 nm GNP coated with PEG as a blood-pool contrast agent for X-ray in mice has already done by Cai et al. (Cai et al., 2007). Injected GNPs dose was about 493 µg Au/kg. Prolonged improvements in contrast were observed in the blood vessels at 24 h post-injection. Comparatively, the contrast created from same doses of current X-ray contrast agents decreases within short time (2 or 3 min). By addition of other contrast creating materials to Au nanostructures, it is possible to create multi-functional systems that offer contrast for CT along with other imaging methods such as fluorescence or magnetic resonance imaging (MRI) (van Schooneveld et al., 2010). For example, Gd chelate-coated GNPs, provided for both MRI and CT (Figure 3) (Alric et al., 2008).

Spectral CT is a new method, which allows multicolor imaging via splitting of the X-ray beam into 6 components based on the energy, which was used to image and individualize GNPs gathered in macrophages in iodine in vasculature, atherosclerotic plaques, besides calcified material, concurrently (Cormode et al., 2010). Furthermore

these NPs localization in macrophages was spotted by immunofluorescence due to their incorporation with fluorophore Rhodamine. This technique also has been applied with gold nanoclusters targeted with antibodies through an avidin-biotin graft to fibrin for specific detection of clots formed in vitro.

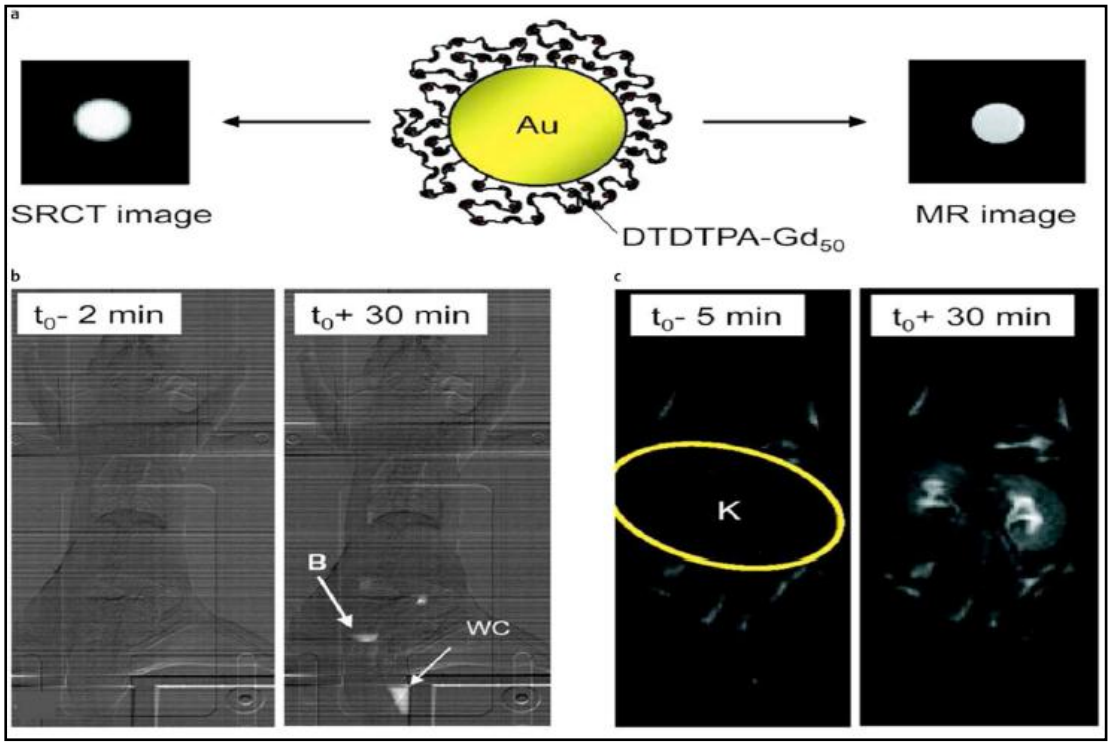

Fig 1.3: GNPs functionalized with Gd for dual (SRCT and MRI) imaging

1.7.2.3 Optical imaging via GNPs

Supernatural light scattering is one of the GNPs properties, which is not detected in non-plasmonic NPs. The GNPs scattering influenced by changing in size and shape, create an ability to adjust the agent to have optimal light scattering performance. For instance, the optical cross section and the reflection constant increase with size, cause more efficient light scattering by larger rather than smaller NPs (Jain et al., 2006). Furthermore, GNPs do not have photobleaching problem, compared with fluorescent probes applied in optical imaging (He et al., 2008). Such properties encourage researches of GNPs as contrast agents for light scattering imaging (Craig et al., 2010; JunáZhen et al., 2010).

Qian et al. monitored resonant light scattering from GNPs, by employing dark field microscopy to image cancer cells for 2 cell cycles. Visualization of GNPs entry to the cell nucleus or the cytoplasm and their localization was observable after cell division due to their strong scattering signals. The light scattering of GNPs was

applied to distinguish tumorous cells from healthy cells, where 35 nm GNPs were improved with an anti-EGFR antibody and incubated with a non-malignant epithelial cell line and 2 malignant oral epithelial cell lines (Asadi et al., 2016). About 600 % higher signal could easily be detected and found in malignant compared with non-malignant cells when incubated with antibody modified GNPs. There is no significant difference in uptake between the cell lines with non-targeted GNPs and seemed to aggregate within the cells, as showed by a red-shift of their absorption maximum from 545 to 552 nm.

1.7.3. GNPs mediated drug delivery

Non-spherical NPs may have some benefits comparatively with the spherical-nanoparticle as a useful delivery system, and Au nanorods (AuNRs) are a promising choice. The AuNRs was first synthesized by Dr. Martin in 1992 (Badrzadeh et al., 2014). In terms of delivery mechanisms the size and shape act a major role (Champion et al., 2007; Daraee et al., 2014). Though, colloidal dispersion more than size and shape, is highly dependent on stability. In this case cetyl trimethyl ammonium bromide (CTAB) helps to stabilize the AuNRs, despite free CTAB is usually known as toxic, but there are also reports that nanoparticle limited-CTAB did not show acute cytotoxicity (Alimohammadi et al., 2014). Therefore, surface coating with thiol modified polyethylene glycol (mPEG-SH) (Liao et al., 2005) or with poly(N-isopropylacrylamide (PNIPAAm) polymer (Alimohammadi et al., 2014), which can decrease the toxicity and keep stability is one common approach.

Recently, 16-mercaptohexadecyl trimethylammonium bromide (MTAB), which is a CTAB analogue has been replaced with CTAB, which not only kept the stability but was also reasonable for biological applications (Vigderman et al., 2012). There are many number of in-vitro experiments, that proved surface coating is an important factor in a delivery system which is developed based on AuNRs. Bypassing the biological barriers and attainment to the targeting site would be the following consideration for nanomaterial-based targeted drug delivery after ensuring the colloidal stability. Biological liquids and the plasma proteins cause the first challenge, due to their abundantly distribution. These would unavoidably attach onto the AuNRs and cause reticuloendothelial system (RES) clearance (Yoo et al., 2011). It has been found that in most cases the plasma protein would attach onto the surface of AuNRs irrespective of the ligands and surface charge (Alkilany et al., 2009). Akiyama et al.

assessed the biodistribution of AuNRs in rats with different level of PEG-grafting and noticed that higher PEG grafting result in more RES clearance avoidance and lengthier circulation (Akiyama et al., 2009).

Many covalent and non-covalent strategies have been used for loading drugs onto GNPs. Covalent binding creates stable delivery vehicles, but usually needs intracellular processing of the prodrug (Morgan et al., 2006). In non-covalent loading of drugs, direct release of active drugs could be possible but early release can be a matter. Zubarev and co-workers covalently attached Paclitaxel (PTX), a chemotherapeutic drug to GNPs with 2 nm core (Gibson et al., 2007). This synthetic technique involves the attachment of ethylene glycol as linker with PTX followed by coupling of the subsequent linear equivalent to phenol-terminated GNP and resulting in a well-defined amount of PTX molecules with rather uniform composition.

By several approaches, such as hydrolysis by phosphodiesterase in vitro, efficient release of drugs from covalently attached prodrugs has also been accomplished (Hwu et al., 2009). By Intracellular activation/ release of the loaded drug, reducing the side effects of drug could be possible because of delivery of inert forms of the drug. Glutathione creates a non-enzymatic alternative for intracellular drug releasing (Anderson et al., 1998; Jones et al., 2000). This method based on variance in the intracellular GSH concentration (about 2-9 mM) compared with the extracellular thiol levels (about 9 μM cysteine). An external stimulus for releasing of payload offers a complementary approach to endogenous agents for time and site specific delivery of drugs (Giri et al., 2005). The light-controlled release of caged drugs has been expanded where the activity of the drug was repressed by binding it to GNPs via a photocleavable covering group (Agasti et al., 2009). In this method, anticancer drug 5-fluorouracil (5-FU) was attached to GNPs via an o-nitrobenzyl group that could be excellently detached by applying near-UV (360 nm) irradiation. Likewise, GNPs could be coated with monolayer of zwitterionic ligands due to providing solubility and prevent cellular uptake (Agasti et al., 2009).

In another study, another kind of drug, histamine which is a cell-signaling agent conjugated on GNPs via carbamate connection that could be detached through the photocleavage reaction of the o-nitrobenzyl group upon near-UV radiation (Nakanishi et al., 2009). Efficient custody of histamine supported its biological activity deterrence while linked to GNPs and result in comprehensive recovery after

photo-release from the particle surface. Non-covalent method of encapsulation of drugs into GNP monolayers creates direct release of unchanged drugs. This approach based on the employ of ligands to produce hydrophobic pockets into the monolayer, where these hydrophobic properties come from the radial nature of the ligands. Furthermore, the charge on surface can be applied to control the interactions of the NPs with cell membranes. The hydrophobic drugs encapsulated into the hydrophobic pockets of zwitterionic ligand-functionalized GNPs (Kim et al., 2009). Non-specific interactions with bio-macromolecules and low cell uptake can be possible with these zwitterionic head-groups. The encapsulated drugs were released into MCF-7 cells by membrane- interceded diffusion, as confirmed by fluorescence microscopy.

Remarkably, the NPs presented no toxicity even at a concentration of 28 μM, thus the biocompatibility of these particles attached to proper sizes (diameter 10-150 nm) make these systems capable choice for passive targeting employing the enhanced permeability and retention (EPR) effect (Torchilin et al., 2011). Many other methods have been progressed to rectify the monolayer of the GNPs with small molecule drugs. For example, at acidic pH there was achievement in efficient release of nitric oxide (NO) from GNPs, where NO was proficiently loaded on GNPs by covalent binding with polyamine ligands through formation of an acid labile N-diazeniumdiolate. In acidic media (about pH 4), these water-soluble NPs showed improved release profile. The range of NO release properties can be manipulated by controlling over the type and amount of amine in the monolayer (Panahi et al., 2016).

2. LITERATURE REVIEW

- Chauhan et al., (2017) formulated nano-graphene oxide gold nanometal composite loaded with doxorubicin and using folic acid as targeting moiety for active tumor targeting. This nano-formulation presented a chemotherapy and photo-thermal ablation strategy for the treatment of cancer. Authors reported that the irradiation with near infrared radiations enhanced the drug release and gold nanoparticles (GNPs) release in the cellular vicinity (Chauhan et al., 2017).
- Fernandes et al., (2017) formulated GNP formulation (TargetNanoTS265) conjugated with monoclonal antibody against epidermal growth factor receptor (anti-EFGR D-11) as a targeting moiety and a Co(II) coordination compound $[CoCl(H_2O)(phendione)_2][BF_4]$ (phendione = 1,10-phenanthroline-5,6-dione) (TS265) as a cancer cells anti-proliferative agent. The efficacy of this nanoformulation, were evaluated in vitro using cancer cell models and in vivo using mice xenografts. Treatment of HCT116-derived xenographs tumors with TargetNanoTS265 led to 93% tumor reduction (Fernandes et al., 2017).
- Kumawat et al., (2017) reported a method to increase the particle size of the thiol capped GNPs using high energy electron beam of Field emission gun transmission electron microscope. Authors reported that the electron beam causes coalescence of finer gold nanoclusters to form bigger nanoparticles (Kumawat et al., 2017).
- Nirmala et al., (2017) used grape polyphenols as the reducing and stabilizing agents for the synthesis of GNPs having 20-40 nm in size. The synthesized GNPs showed apoptosis in the cancer cells owing to increase in the reactive oxidative species production, apoptotic morphological change and membrane potential loss (Nirmala et al., 2017).
- Rafique et al., (2017) studied the nature, size and dispersity of GNPs synthesized by different lasers used in laser ablation method. They found that both low power continuous wave diode laser and nanosecond pulsed neodymium-doped yttrium aluminium garnet (Nd:YAG) laser yielded crystalline GNPs. The Nd:YAG yielded GNPs in the size range of 12-49 nm whereas, low power laser yielded 5-20 nm sized GNPs (Rafique et al., 2017).
- Saber et al., (2017) formulated cyclo-[L-arginyl-glycyl-L-alpha-aspartyl-D-phenylalanyl-L-lysyl [C(RGD)] labelled chitosan capped GNPs for the delivery of

sunitinib malate to the tumor vasculature for the treatment of angiogenesis. Confocal microscopy showed enhanced absorption of targeted formulation (Saber et al., 2017).

- Dhamecha et al., (2016) formulated doxorubicin loaded gold nanoparticles. Authors formulated GNPs via green synthesis and loaded doxorubicin by incubation method. Doxorubicin loaded GNPs showed better activity (81% tumor suppression) as compared to free doxorubicin (48% tumor suppression) (Dhamecha et al., 2016).
- Galbiati et al., (2016) evaluated Tumor Homing Peptides (THP) on the basis of their selectivity towards MCF-7 cell lines in comparison to noncancerous 3T3-L1 fibroblast cells. These THP-gold nanoconjugates exhibited good selectivity and binding affinity by flow cytometry, and low cytotoxicity as assayed by cell death experiments (Galbiati et al., 2016).
- Guo et al., (2016) investigated the effect of active targeting by transferrin and folic acid on the delivery of non-viral gene delivery to the prostate cancer. Transferrin conjugated GNP formulation showed increase cellular uptake by PC-3 cells and Folic acid conjugated GNP formulation delivered siRNA in LNCaP cells (Guo et al., 2016).
- Harrison et al., (2016) compared two methodologies of PEGylation i.e. Mixed monolayer method and PEG liker method. Authors found that GNPs formulated with both the methods were stable in ionic solutions but GNPs conjugated with mixed monolayer method showed some changes in gel electrophoresis migration profile. Authors reported that receptor mediated endocytosis (RME) peptide greatly enhanced the cell internalization of GNP (Harrison et al., 2016).
- Iodice et al., (2016) formulated formulation consisting of ulta-small gold nanoclusters (6 nm) entrapped inside the larger polymer nannoconstruct made of Poly Lactic Co-glycolic acid which is stabilized superficially by lipid-PEG layer. These formulations increased gold thermal production by 2 folds. The superior photothermal performance of these formulation was assessed in vitro on monolayers of breast cancer cells (SUM-159) and tumor spheroids of glioblastoma multiforme cells (U87-MG) (Iodice et al., 2016).
- Jazayeri et al., (2016) reviewed various physical and chemical methods to conjugate antibodies to the GNPs surface (Jazayeri et al., 2016).
- Kim et al., (2016) formulated Doxorubicin/ gold loaded nanoformulation for combination therapy i.e. radiotherapy owing to gold shells and chemotherapy owing to doxorubicin. The nanoformulation was capped with Pluronic F-68 which increased the

stability in systemic circulation. They observed highest anti-tumor activity when both chemotherapy and radiotherapy was used (Kim et al., 2016).

- Manivasagan et al., (2016) synthesized and stabilized GNPs using chitosan oligonucleotide and loaded the formed GNPs with Paclitaxel to investigate chemotherapeutic and photoacoustic imaging (PAI). The formed nano-formulation showed sustained and pH related drug release from the formulation. The formulation showed strong cytotoxic effect in MDA-MB-231 cells. Authors also evaluated it as optical contrast agents for photoacoustic imaging (PAI) (Manivasagan et al., 2016).
- Nag et al., (2016) used transferrin as a targeting agent for the active delivery of paclitaxel loaded GNPs to the cancer cells. Targeted formulation showed higher cytotoxity to the Non-small cell Lung cancer cell lines (HOP-62), higher intracellular uptake andlow haemolytic toxicity (Nag et al., 2016).
- Porcaro et al., (2016) formulated biocompatible and stable GNPs capped with 3-mercapto-1-propansulfonate and 1-thioglucose mixed thiols. The formulation showed increased uptake by the cells as compared with its non-functionalised counter-parts (Porcaro et al., 2016).
- Safwat et al., (2016) formulated 5-Fluorouracil loaded GNPs using two thiol ligands Thioglycolic acid and glutathione. Nanoparticles were further covered with Pluronics to increase their stability. The release was found to be slow and pH dependent. The nanoformulation showed better activity as compared to only 5-fluorouracil against colo-rectal cancer (Safwat et al., 2016).
- Shaat et al., (2016) developed GNPs modified by branched polyethyleneimine for the delivery of siRNA against an oncogene c-Myc. HuH7 cells were transfected with naked siRNA and siRNA GNP formulation. The formulation showed better gene silencing as compared to naked siRNA (Shaat et al., 2016).
- Shi et al., (2016) studied the effect of citrate to gold molar ratio on the size of GNPs synthesized keeping all the other variables constant (Shi et al., 2016).
- Suganya et al., (2016) developed GNPs via green synthesis from the leaf extract of *Mimosa pudica.* The synthesized GNPs were tested for cancer cytotoxicity on MDA-MB-231 and MCF-7 cancer cell lines. Study showed apoptosis in G_0/G_1 to S phase (Suganya et al., 2016).
- Suganya et al., (2016) used pectin an anionic polysaccharide for the synthesis of GNPs. Cytotoxicity of Pectin-GNP was tested on MCF-7 and MDA-MB-231 cell lines.

The treated cell lines showed decrease in viability inferred from the decrease in viability of treated cells. p-GNPs mediated apoptosis induction is evident from increase in sub-G1 population, DNA damage in comet assay and retention of Annexin V FITC/ PI double stain by the cells (Suganya et al., 2016).

- Taghdisi et al., (2016) formulated polyvalent aptamers-Daunorubicin-GNPs and it's efficacy was tested on its efficacy was assessed in Molt-4 cells (human acute lymphoblastic leukemia T-cell, target). Flow cytometry showed that the formulation was internalized by the cancerous cells and not the normal cells. The formulation had more cytotoxicity in Molt-4 cells as compared to Daunorubicin alone (Taghdisi et al., 2016).
- Tang et al., (2016) reported one step method for synthesis of GNPs and stabilization with PEG using flash nanoprecipitation technique. By this technique 13 to 62 nm PEG stabilized GNPs can be synthesized (Tang et al., 2016).
- Ashwanikumar et al., (2014) reported synthesis of random copolymer poly-lactic-co-glycolic acid (PLGA) grafted on branched polyethyleneinmine. 5-Fluorouracil and methotrexate were loaded on this copolymer. Methotrexate was used as the targeting moiety. 5-Fluorouracil and Methotrexate together form synergistic anticancer agents. The cellular uptake studies showed higher uptake of the drugs into cancer cells (Ashwanikumar et al., 2014).
- Li et al., (2014) formulated a prodrug of 5-fluorouracil by developing an acetic acid group on the uracil ring for the attachment of drug to the PEG. Authors also synthesized multi-hydroxyl PEG derivative for increased loading of drug on the PEG. The 5-Fluorouracil-Acetic acid was conjugated on the modified PEG by ester bond with 10.58% increase in the loading efficiency (Li et al., 2014).
- Chen et al., (2013) reported a new technique for PEGylation i.e. Living PEGylation. Authors develop GNPs conjugated with different density of PEG and studied the effect targeting ligands for effective targeting to the cancer cells (Chen et al., 2013).
- Ding et al., (2013) formulated PEG-Paclitaxel derivative and conjugated it on the GNPs. The water solubility of paclitaxel in GNP conjugate increased by 4.6×10^5 times as compared to paclitaxel alone. The formulation showed prolonged circulation, targeted release of paclitaxel inside the tumor cells and an increase in tumor cytotoxicity (Ding et al., 2013).
- Wang et al., (2013) reported the concept of critical stabilizing concentration (CSC). They reported that PEGylation stabilized GNPs only if the PEG conjugation

concentration reached higher than CSC. They also reported that high molecular weight PEG stabilized GNPs better than low molecular weight GNPs but low molecular weight PEG yielded high conjugation density (Wang et al., 2013).

- Dasog et al., (2011) worked on brust schriffin method to synthesize bigger sized stabilized GNPs by using hydroborates as the reducing agents (Dasog et al., 2011).
- Manson et al., (2011) reported the stability study of GNPs functionalized with different PEG densities in water, phosphate-buffered saline solution (PBS), phosphate-buffered saline solution containing bovine serum albumin (PBS/BSA), and dichloromethane (DCM). Study showed with an increase in PEG density the stability increased (Manson et al., 2011).
- Qian et al., (2011) reported a method to develop GNPs conjugated with PEG molecules. Firstly they prepared bare surfaced negatively charged GNPs by laser ablation method and then conjugating with PEG. They reported that PEG conjugation to gold surface is very efficient and can be controlled (Qian et al., 2011).
- Kah et al., (2009) studied the effect of PEG chain length, size of gold nanoshells and PEG density on Gold nanoshell surface on uptake of nanoformulation by macrophages. Authors found that nanoshells having saturated PEG density minimise the macrophage uptake (Kah et al., 2009).
- Perrault et al., (2009) found a method of producing spherical GNPs with better dispersity as compared to traditional citrate method with the help of hydroquinone. This method involved of generation of gold seeds which are grown with the help of hydroquinone to form spherical bigger GNPs (Perrault and Chan, 2010).
- Ji et al., (2007) reported the effect of pH on the size and shape of the GNPs and observed that citrate also acted as a buffer which regulated the change in pH (Ji et al., 2007).
- Liu et al., (2007) studied the stability of mixed monolayer PEGylated GNPs in high ionic strength solutions. Authors reported that stability increased with increasing PEG length, decreasing nanoparticle size and increasing PEG density. Authors also reported that long chain PEG, such as PEG 5000 does not affect activity of targeting moiety in mixed monolayer PEGylated GNPs (Liu et al., 2007).
- Kimling et al., (2006) studied the reduction process of gold chloride by citrate and ascorbic acid. They initiated the reaction either by heat or ultraviolet radiation and studied the effect of gold to citrate concentration on the size of the GNPs. The size

dispersion of 13 to 16% was obtained below the size range of 40 nm. The bigger particles tend to develop elongated shape and poor size dispersion. Authors suggested that GNPs formation process is a multiple step process involving of particles appearance, collapse of particles to form bigger particles and growth of particles to form spherical GNPs (Kimling et al., 2006).

- Brust et al., (1994) developed a two-phase method for synthesizing GNPs ranging from 1.5 to 5 nm using sodium borohydride as the reducing agent. They synthesized alkane-thiol layer stabilized GNPs (Brust et al., 1994).
- Frens, (1973) further worked on Turkevich's work and studied the effect of different amount of trisodium citrate solution on the size of the GNPs created. They got nanoparticles in the range of 12 to 150 nm by changing the amount of trisodium citrate. Bigger nanoparticles were created by reducing the concentration of trisodium citrate. At low concentration the results were less reproducible (Frens, 1973).
- Turkevich et al., (1951) created GNPs using trisodium citrate as the reducing agent. Using this method, nanoparticles in the range of 12 to 150 nm can be created reproducibly with less root-mean-square deviation. They also studied the effects of temperature, citrate concentration and citrate dilution on the GNPs size and % deviation (Turkevich, John; Cooper, 1951).

3.1. RESEARCH ENVISAGED

The object of the present study was to develop and characterize 5-Fluorouracil and Methotrexate loaded gold nanoparticles.

3.1.1. Rationale for selecting gold nanoparticles

The gold nanoparticles (GNPs) possess a number of distinct physical, chemical, electronic and optical properties, which make them as promising nanocarrier for the treatment, diagnosis and imaging of diseases. The GNPs can be synthesized monodispersely over the range of 1.5 to 150 nm with the ability to load high density of ligands and drugs. Small sized GNPs can be employed to circumvent the reticuloendothelial system (RES) and for the passive targeting of the drug to the tumors owing to the leaky vasculature of the tumors. The electronic and optical properties of the GNPs arise from the collective oscillation of the conducting electrons (known as surface plasmons) present on the surface of these particles. Surface plasmons, results in the dipolar charge density distribution across the surface of the GNP and can absorb the photons of the same frequency resulting increment in the energy of the electrons. This property is used for the photothermal therapy (PTT) where the local temperature of the tumor is increased by irradiating with the laser of near infrared (NIR) window (650-900 nm). Hyperthermia can cause cell death in tumor by generation of heat shock proteins, DNA damage, denaturation of proteins, metabolic signaling inhibition etc. Hyperthermia can also lead to fast unloading of the drug in the tumor interstitium. As gold nanoparticle is a heavy metal, it can also be used for the radiotherapy by release of the Auger electron in the tumor area, which can lead to DNA damage. Hence, GNPs can act as nanocarriers for combination therapy including chemotherapy, photothermal therapy and radio therapy (Dreaden et al., 2012).

3.1.2. Rationale for PEGylation of GNPs

It was reported that increasing both the GNP size and the polyethylene glycol (PEG) density over the surface of GNP, increase the blood half-life of the GNP formulation (Perrault et al., 2009). PEGylation reduces the chances of GNPs identification by the RES, which leads to more biocompatibility and less immunogenicity. In PEG linker technique, PEG serves as a linker to conjugate the drug or ligands on the surface of the GNPs. Further PEG can be easily functionalized

with different functional groups on the both ends for conjugation with GNPs as well as the drug (Dreaden et al., 2012; Perrault et al., 2009).

3.1.3. Rationale for selection of 5-Fluorouracil and Methotrexate drug combination

In current scenario multi-drug formulations have attracted the researchers due to their better therapeutic activities and less chances of forming a multi-drug resistant cancer. 5-Fluorouracil (5-FU) is one of the first line drugs for many cancers but it has various short comings i.e. very short plasma half-life. Hence, to avoid this side-effects Methotrexate (MTX) is used in combination with the 5-FU. The MTX has structural similarity with the folic acid and actively internalized in the cancerous cells by over expressed folate receptors on the cancer cell membrane. The synergistic effect of 5-FU and MTX advocated that the combination has better therapeutic activity as compared to that of single drug (Ashwanikumar et al., 2014).

3.2 PLAN OF WORK

3.2.1. Literature survey

3.2.2. Procurement of chemicals/ drug sample

3.2.3. Preformulation study

A. Identification of drug

- Melting point determination
- UV spectroscopy
- FT-IR spectroscopy

B. Partition coefficient determination

C. Solubility profile of drug

D. Determination of λ_{max} (asorption maxima) of drug in

- PBS pH 7.2
- Distilled water

3.2.4. Synthesis of GNP and PEG conjugation

3.2.5. Development and characterization of drug loaded PEGylated GNP

- UV spectroscopy
- FT-IR spectroscopy
- ^{1}H-NMR spectroscopy
- Atomic force microscopy

- Drug content in GNP formulations
- Drug entrapment efficiency

3.2.6. In vitro study

- Determination of *in-vitro* drug release
- Determination of hemolytic toxicity
- Cell internalization study (Confocal microscopy)

3.2.7. Compilation of data, statistical treatment and submission of thesis

3.3. DRUG PROFILE

3.3.1. 5-Fluorouracil

5-Fluorouracil (5-FU) belongs to the antimetabolite category of the anti-cancer drugs. It inhibits the formation of thymidine, important in DNA biosynthesis (Goodman and Gillman's, 2006; Tripathi, 2003).

3.3.1.1 Chemical profile

- **Chemical structure**

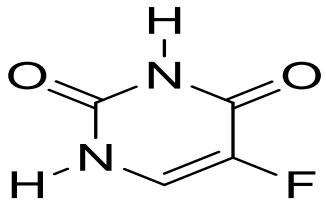

5-fluoro-1H-pyrimidine-2,4-dione

- **Molecular formula:** $C_4H_3FN_2O_2$
- **Molecular weight:** 130.078 g/mole
- **Description:** White, crystalline powder; odorless; pKa is 8.02.
- **Solubility:** 5-FU is sparingly soluble in water; slightly soluble in alcohol practically insoluble in chloroform, benzene and ether; soluble in water methanol mixtures.
- **Storage:** It should be stored in well closed containers.

3.3.1.2 Pharmacokinetic and Pharmacodynamic profile

- **Absorption:** Absorption from GIT is unpredictable and incomplete.
- **Half-life:** Plasma half-life of 5-FU is 10 to 20 minutes.
- **Elimination:** Metabolic degradation of 5-Fu occurs various sites such as intestinal mucosa, tumor cells and mainly in liver. 5-10% of dose is excreted through renal excretion in 24 hours.

- **Mechanism of action:** 5-FU is phosphorylated to form active agent floxuridine monophosphate [5-FUMP] and fluorodeoxyuridine monophosphate [5-FdMP]. 5-FUMP is further phosphorylated to form floxuridine triphosphate [5-FUTP] which incorporates in RNA to inhibit RNA functioning. Floxuridine diphosphate [5-FUDP] is reduced by ribonucleotide reductase to form 5-FdMP. The 5-FdMP binds to thymidilate synthetase and inhibits the DNA synthesis.
- **Adverse effects:** Most common side effects include-
  - **CNS:** Acute cerebellar syndrome, myelopathy
  - **Dermatologic:** Dermatitis, pigmentation, skin atrophy, alopecia, nail changes
  - **Gastrointestinal:** Diarrhea, nausea, vomiting, anorexia, mucosal ulceration, stomatitis
  - **Bone Marrow:** Myelosuppression, thrombocytopenia, anemia
  - **Cardiac:** Acute chest pain with evidence of ischemia
  - Hand foot syndrome
- **Route of administration:** 5-FU is administered through I.V. route.
- **Dose:** 500 to 600 mg/m^2 once a week with leucovorin for 6 to 8 weeks.
- **Therapeutic uses:**
  - Treatment of metastatic colon carcinomas, upper gastrointestinal tract carcinomas, breast carcinomas.
  - 5-FU is used with leucovorin as an adjuvant therapy of colorectal cancers and gastric cancers.

Table 3.1 Available marketed preparation of 5-Fluorouracil:

Product	Strength	Manufacturer
Kucil 50 (injection)	500 mg	Khandelwal Laboratories Pvt Ltd.
Fluracil (injection)	500 mg	Biochem Pharmaceutical Industrial Ltd
Fluracil (injection)	250 mg	Biochem Pharmaceutical Industrial Ltd
Flutas (injection)	500 mg	Intas Laboratories Pvt Ltd

3.3.1.3 Analytical profile

IP (1996) incorporates spectrophotometric method for determination of 5-FU. The acidic solution was extracted with chloroform filtered, diluted and absorbance was measured at maximum of 266 nm (IP, 1996).

3.3.2 Methotrexate

Methotrexate (MTX) is an example antimetabolites class of antineoplastic drugs. It acts as an antifolate and binds to the enzyme dihydrofolate reductase and prevents the formation of tetrahydrofolic acid coenzyme **[**Goodman and Gillman's, 2006; Tripathi, 2003; BP, 2009**]**.

3.3.2.1 Chemical profile

- **Chemical Structure**

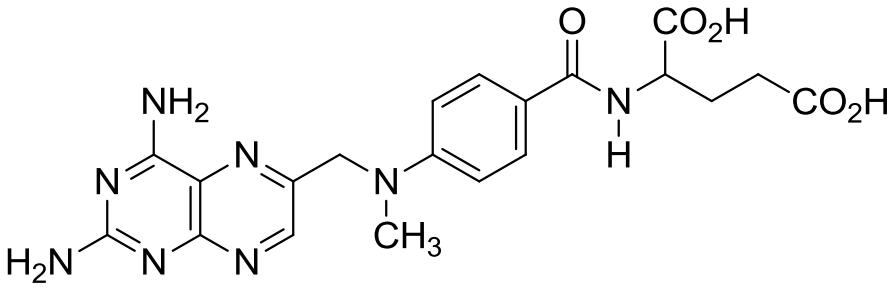

Methotrexate

- **Molecular Formula:** $C_{20}H_{22}N_8O_5$
- **Molecular Weight:** 454.447 g/mole
- **Description:** yellow, crystalline powder; odourless; pKa is 4.7.
- **Solubility:** Insoluble in water, alcohol, chloroform, ether; slightly soluble in 0.1N Hydrochloric acid, 0.1 N NaOH, methanol and water solutions, dimethylformamide.
- **Storage:** It should be stored in cool place. Keep container tightly closed in a dry and well-ventilated place. Storage temperature is 2-8°C.

3.3.2.2 Pharmacokinetic and Pharmacodynamic profile

- **Absorption:** MTX is well absorbed orally.
- **Protein binding:** Plasma protein binding is about 50%.
- **Peak plasma concentration:** Peak plasma concentration attained by the drug is 1 to 10 µM after I.V. administration of 25 to 100 mg/m^2 doses.
- **Half-life:** After I.V. administration drug disappears in triphasic manner. The rapid distribution phase is followed by second renal clearance phase (Half-life 2 to 3 hours). The third phase has a half-life of 8 to 10 hours.
- **Elimination:** MTX follows the renal excretion and 90% of a dose is eliminated unchanged from the body through urine.

- **Mechanism of action:** MTX is an antifolate drug belonging to the category of antimetabolites. It binds almost irreversibly to the enzyme dihydrofolate reductase preventing the formation of tetrahydrofolic acid from dihydrofolic acid. Tetrahydrofolic acid is important in DNA synthesis and cell replication. The toxic effects of MTX can be reduced by leucovorin, which is a fully reduced folic acid.
- **Adverse effects:**
  - Bone marrow depression and intestinal epithelium degradation are the primary toxicities.
  - Myelosuppression may occur in patients with compromised renal function.
- **Route of administration:** Mainly administered orally, intramuscularly and intravenously.
- **Dose:** The usual dose of MTX for treatment of psoriasis is 2.5 mg orally daily for 5 days followed by at least two days rest or 10 to 25 mg i.v. weekly. The usual dose of MTX for treatment of acute lymphoblastic lymphoma is 30 mg/m^2 intramuscularly weekly divided in two doses (in children).
- **Therapeutic uses:**
  - Acute lymphoblastic leukemia
  - Psoriasis
  - Rheumatoid arthritis.
  - Meningeal carcinomatosis

Table 3.2 Available marketed preparation:

Product	Strength	Manufacturer
Neotrexate (Tab)	2.5 mg	IPCA Laboratories Ltd.
Neotrexate (injection)	50 mg/ 2 ml	IPCA Laboratories Ltd.
Biotrexate (Cap)	250 mg	Khandelwal Laboratories Pvt Ltd.

3.3.2.3 ANALYTICAL PROFILE

Agrawal et al reported simple, sensitive and selective RP-HPLC method with UV detection for the estimation of MTX in pharmaceutical formulation and in spiked plasma developed and validate in his work. Chromatographic separation of drug is performed with a 250 x 4.6 mm, 5 μm diameter particles RP C-18 column and the mobile phase consisted of a mixture of methanol and water (80:20, v/v), containing 0.1%

HPLC grade glacial acetic acid for the adjustment of pH to 4.5. Isocratic elution at a flow rate of 1 ml/min with UV detection at 256 nm at ambient temperature is used in this method. The proposed RP-HPLC method is successfully applied for the determination of MTX in pharmaceutical preparation and spiked plasma samples (Agrawal et al., 2010).

Patel et al reported two simple, precise and economical UV methods have been developed for estimation of Methotrexate in bulk formulation. Method A involves measurement of UV absorbance in zero order derivativeat 303 nm. Method B deals with area under curve measurement (AUC method), which involves the calculation of integrated value of absorbance with respect to wavelength between 294-308 nm. The drug follows Beer-Lambert's law in the concentration range of 3-10 μg/mL in both the methods (Patel et al., 2015).

4.1 Experimental Requirements

4.1.1 Chemicals

Table 4.1 The chemicals used in the study are listed below.

Chemicals	Manufacturers
5-Fluorouracil	HiMedia Laboratories, Mumbai, India
Methotrexate	Sigma Aldrich Pvt. Ltd. Bangalore, India
Chloroauric Acid	Lobachemie Pvt. Ltd., Mumbai, India
Tri sodium Citrate	Lobachemie Pvt. Ltd., Mumbai, India
Hydrochloric acid	Lobachemie Pvt. Ltd., Mumbai, India
Millipore water	Bio-Age Equipment Ltd., Mohali, Punjab, India
Sodium hydroxide pellets	Lobachemie Pvt. Ltd., Mumbai, India
Chloro Acetic Acid	Burgoyne Burbidges & Co., Mumbai, India
Ethyl Acetate	LobaChemie Pvt. Ltd., Mumbai, India
N, N-Dicyclohexyl Carbodiimide	LobaChemie Pvt. Ltd., Mumbai, India
Polyethylene Glycol 6000	Central Drug House Pvt. Ltd., New Delhi, India
Triethylamine	Molychem, Mumbai, India
Dimethylformamide	LobaChemie Pvt. Ltd., Mumbai, India
Silver nitrate	Thomas baker (chemicals) Pvt. Ltd.

4.1.2 Equipment

Table 4.2 List of equipment along with their manufacturers.

Equipment	Manufacturers
Electronic weighing balance	CY360, Shimadzu Co. Ltd., Japan
Magnetic Stirrer	Remi 5MLH, Vasai, Mumbai, India
UV Spectrophotometer	UV-1800, Shimadzu Co. Ltd., Japan
Infrared Spectrophotometer	FTIR 8400 S
Thin Layer Chromatography Plates	Merck, India
Hot air oven	Cadmach Drying Oven, Cadmach Machinary Ltd., Ahmadabad, India
Cooling Centrifuge	REMI C 12, Vasai, Mumbai, India
Melting Point apparatus	Popular India, (Ambala cant., India)
Particle size analyzer	Beckmann coulter delta nano

4.2 PREFORMULATION STUDIES

Preformulation studies are crucial to characterize drugs for proper designing of drug delivery system. The preformulation studies, performed in this project include-

identification of drugs (physical appearance, melting point, IR spectra and UV λ_{max}), quantitative solubility studies, and estimation of drug. The drug 5-Fluorouracil was purchased from HiMedia Laboratories (India) and Methotrexate was purchased from Sigma-Aldrich Chemicals Pvt. Ltd., Bangalore (India).

4.2.1 5-FLUOROURACIL (5-FU)

4.2.1.1 Physical appearance and melting point

- **Physical appearance:** The drug 5-FU was found as white, odorless crystalline powder.
- **Melting point:** The melting point was determined in a melting point apparatus (Popular, India) and was found to be 280-282°C (Table 4.1).

4.2.1.2 Solubility studies

Solubility of 5-FU was determined in different solvents. The 5-FU (10 mg) was added in 10 mL of different solvents in tightly closed test tubes. These test tubes were shaken for about 30 min using vortex shaker (REMI) and solubility was determined (Table 4.2).

4.2.1.3 Drug identification

- **Determination of absorption maxima (λ_{max}):** The ultraviolet spectrophotometry was used to identity validation of the supplied drug. The drug (5 mg) was dissolved in 200 mL of methanol and distilled water (1:1) solution and the resulting solution was scanned in the range 200-400 nm using Shimadzu 1800 (Japan) UV-Visible spectrophotometer. UV/Visible spectrum of 5-FU is presented in Figure 4.1.
- **Infrared spectral assessment:** Infrared (IR) spectrum of any compound gives information about the groups present in the particular compound. IR spectrum of 5-FU was taken out using KBr pellets (Figure 4.2). Various peaks in IR spectrum were interpreted for presence of different groups (Table 4.3). Infrared spectroscopy of 5-FU was carried out by Shimadzu FTIR 8400 S (Japan) Spectrophotometer at Lovely Professional University, Phagwara. The IR spectrum was matched with reference spectra (Figure 4.3) (BP 2009).

4.2.1.4 Estimation of drug

In the present study a spectrophotometric method based on ultraviolet absorption at λ_{max} 266 nm was selected for quantitative estimation of drug **(IP 2007)**.

- **Preparation of standard curve of 5-FU in distilled water:** Accurately weighed 5 mg of 5-FU was transferred into a clean and dry 50 mL stoppered volumetric flask and was dissolved in minimum quantity of water. The volume was made up to 50 mL with distilled water. From the above solution 0.2, 0.4, 0.6, 0.8, 1.0, 1.2 and1.4, 1.6 mL was withdrawn separately in different 10 mL volumetric flasks and volume was made up to 10 mL with distilled water in each case. This produced the concentrations of 2, 4, 6, 8, 10, 12, 14 and 16 µg/mL, respectively. Absorbance of these solutions was recorded at λ_{max} 266 nm against distilled water as blank using Shimadzu 1800 (Japan) UV/Visible spectrophotometer. Observations are recorded (Table 4.4) and standard curve is presented in Fig. 4.4.

Table 4.1 Physical characterization of 5-Fluorouracil

Parameters	**Observation**	**Reported**	**References**
Physical appearance	White crystalline powder	White crystalline powder	**IP 2007**
Melting point	280-282ºC	282-283ºC	**Drug Bank**
UV-Visible scan	λ_{max}	λ_{max}	**IP 2007**
Distilled water	266 nm	266 nm	

Table 4.2 Solubility of 5-Fluorouracil different solvent systems

Solvents	**Solubility**	**Reported**	**References**
Chloroform	- - - -	- - - -	
Ether	- - - -	- - - -	**IP 2007**
Ethanol	+ +	+ +	
Distilled water	+ + +	+ + +	

Practically insoluble - - - -; Slightly soluble + +; Sparingly Soluble + + +

Table 4.3 IR Spectral analysis of 5-Fluorouracil sample

Wave No. (cm^{-1})	Interpretation
1649	C=C stretching
1732	C=O stretching
2829	C-H stretching

Table 4.4 Standard curve of 5-Fluorouracil in distilled water at λ_{max} 266 nm

Concentration (µg/mL)	Absorbance	Statistical parameters
2	0.048	
4	0.093	**Correlation coefficient**
6	0.134	r^2 =0.9996
8	0.168	
10	0.213	**Equation of Line**
12	0.255	y = 0.0206x +0.0076
14	0.294	
16	0.335	
18	0.381	
20	0.421	

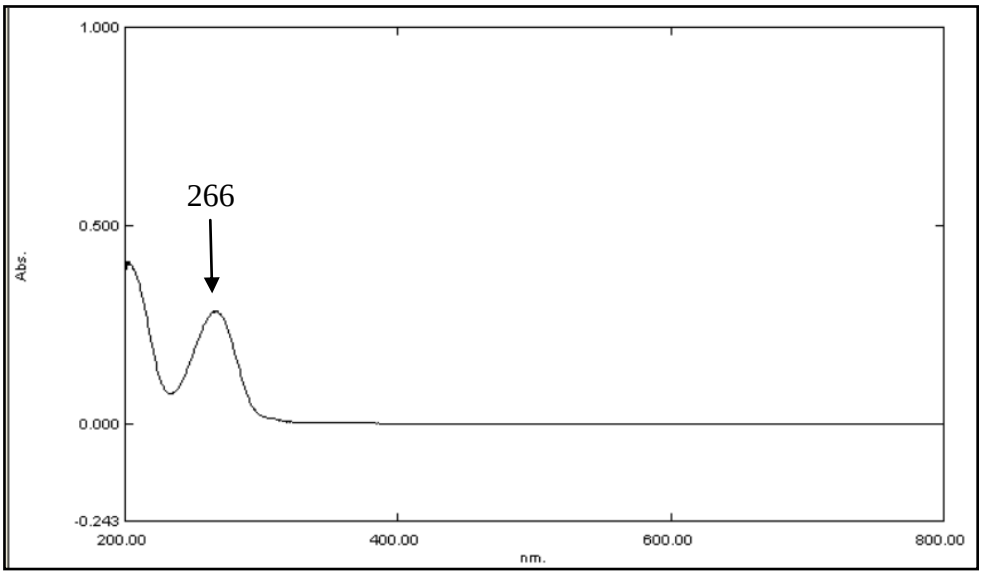

Fig. 4.1 UV/Vis spectrum of 5-Fluorouracil

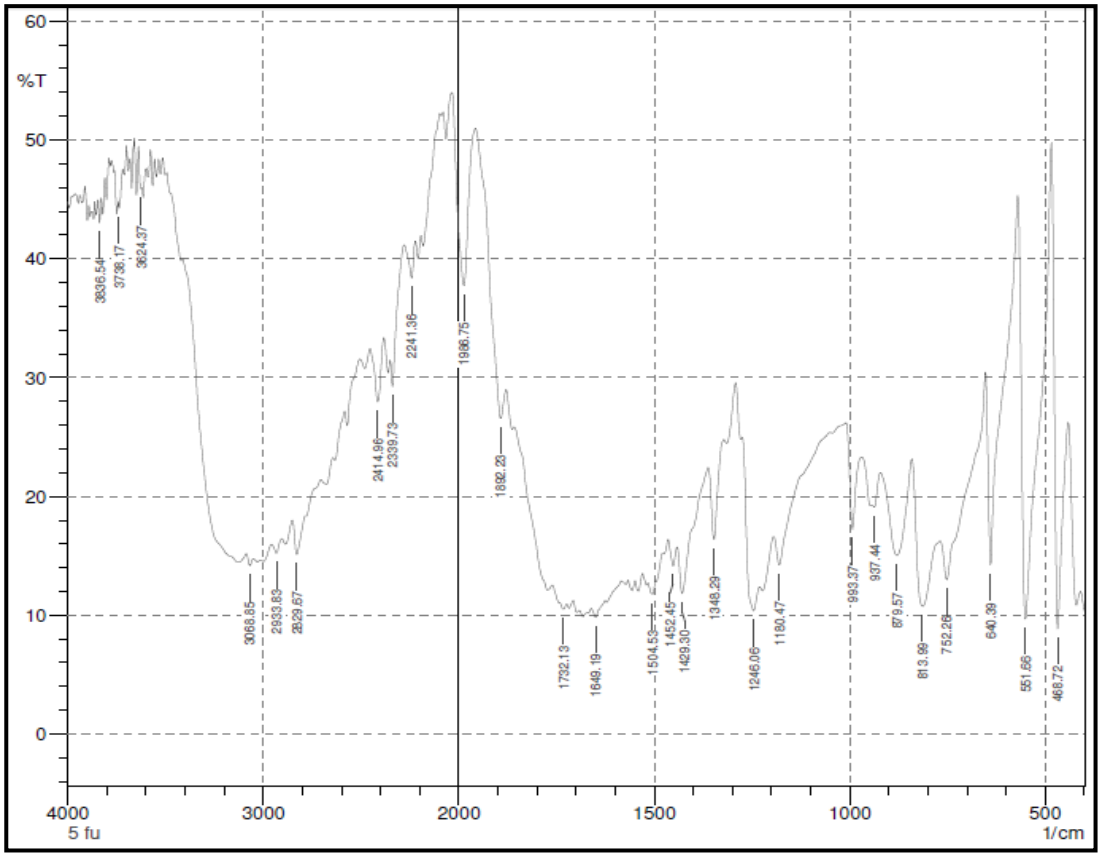

Fig. 4.2 IR spectrum of 5-Fluorouracil

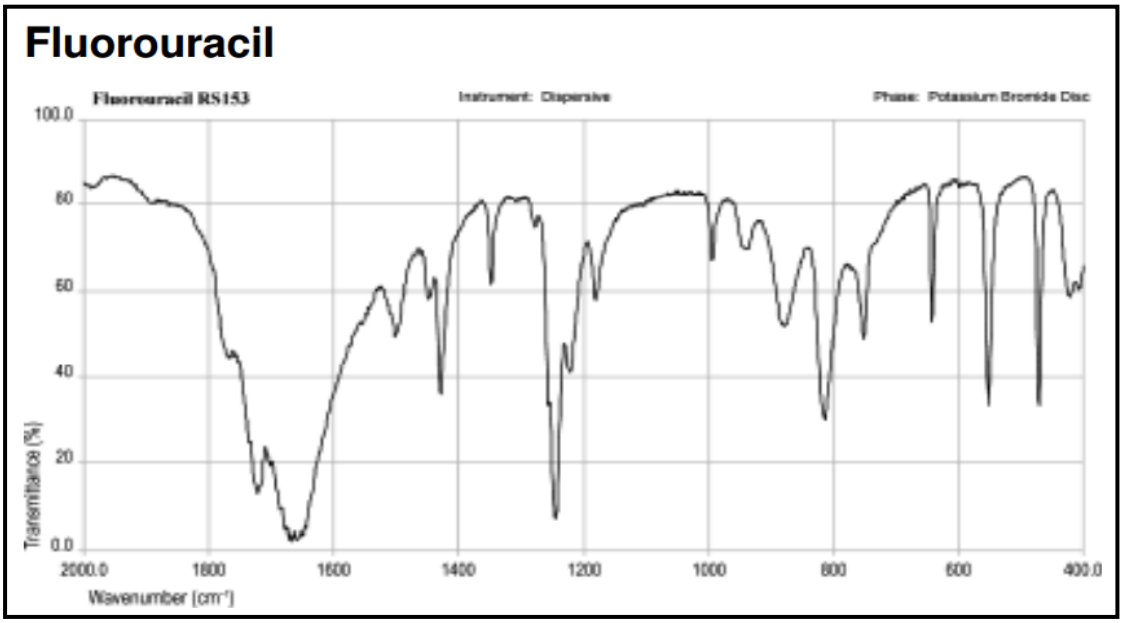

Fig. 4.3 Reference IR spectrum of 5-Fluorouracil (BP 2009)

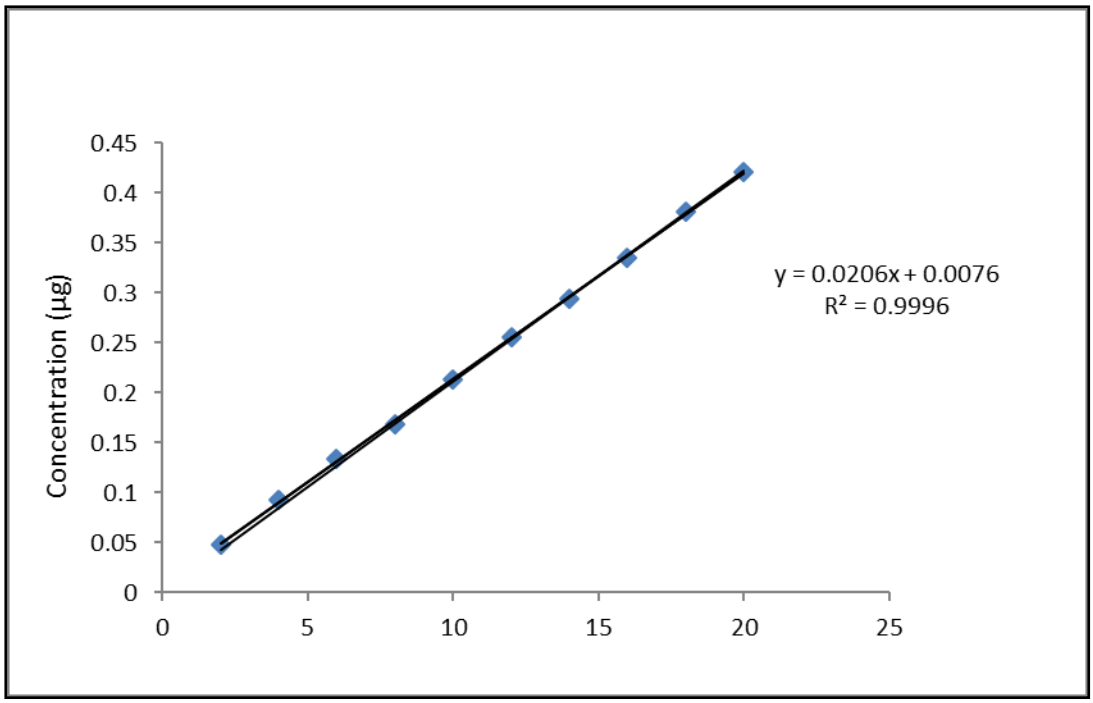

Fig 4.4 UV Standard curve of 5-Fluorouracil

4.2.2 METHOTREXATE (MTX)

4.2.2.1 Physical appearance and melting point

- **Physical appearance:** The drug MTX was found as yellow colored odorless crystalline powder.
- **Melting Point:** The melting point was determined in a melting point apparatus (Popular, India) and was found to be 194-197°C (Table 4.5).

4.2.2.2 Solubility studies

Solubility of MTX was determined in different solvents. MTX (10 mg) was suspended in 10 mL of different solvents in tightly closed test tubes. These test tubes were shaken using vortex Shaker (REMI) and solubility was determined (Table 4.6).

4.2.2.3 Drug identification

- **Determination of absorption maxima (λ_{max}):** The drug (5 mg) was dissolved in 100 mL of 0.1 N Hydrochloric acid buffer pH 2.0 solution. From the above solution 1 ml solution was diluted to 10 ml with 0.1 N Hydrochloric acid solution pH 2.0. The resulting solution was scanned in the range 200-400 nm using Shimadzu 1800 UV-Visible spectrophotometer. UV/Visible spectrum of MTX is presented in Fig.4.5.

- **Infrared spectral assessment:** Infrared (IR) spectrum of MTX was taken out using KBr pellets (Fig. 4.6). Various peaks in IR spectrum were interpreted for presence of different groups (Table 5.7). Infrared spectroscopy of MTX was carried out by Shimadzu 8400 S (Japan) FT-IR Spectrophotometer. The obtained IR spectrum was compared with reference IR spectrum given in Japanese Pharmacopoeia (JP 2014) (Fig 4.7).

4.2.2.4 Estimation of drug

In the present study a spectrophotometric method based on ultraviolet absorption

at λ_{max} 258.50 nm was selected for quantitative estimation of drug **(IP 2007)**.

Standard curve of Methotrexate in Hydrochloric Acid Buffer pH 2.0

- **Preparation of hydrochloric acid buffer (pH 2.0):** Phosphate buffer saline was prepared following the official method (IP 2007). 50.0 ml of the 0.2 M potassium chloride was taken in a 200-ml volumetric flask; 13.0 ml 0.2 M hydrochloric acid was added to the volumetric flask. Volume was made up to 200 ml using distilled water.
- **Preparation of standard curve:** The standard curve of MTX in HCl buffer (pH 2.0) was prepared. 10 mg of MTX was dissolved in 50 ml of HCl buffer pH 2.0 to form bulk solution of 200 µg/ml. 0.1, 0.2, 0.3, 0.4, 0.5, 0.6 ml of bulk solution was taken in five 10 ml volumetric flask and volume was made up using HCl buffer 2.0. Absorbance were recorded at λ_{max} 258.50 nm against HCl buffer pH 2.0 as blank using Shimadzu 1800 (Japan) UV/Visible spectrophotometer. Observations are recorded (Table 4.8) and standard curve is presented in Fig. 4.8.

Table 4.5 Physical characterization of MTX

Parameters	Observation	Reported	References
Physical Appearance	Yellow crystalline powder	Yellow crystalline powder	**IP 2007**
Melting Point	194-197ºC	195ºC	**Drug Bank**
λ_{max} in HCl buffer pH 2.0	258.50, 302, 372 nm	258, 303, 371 nm	**IP 2007**

Table 4.6 Solubility of Methotrexate in different solvent systems

Solvents	Solubility	Reported	References
Chloroform	- - - -	- - - -	
Ether	- - - -	- - - -	**IP 2007**
Ethanol	- - - -	- - - -	
Distilled water	- - - -	- - - -	
0.1 N HCl	+ +	+ +	
0.1 N NaOH	+ +	+ +	

Insoluble - - - - ; Slightly soluble + +

Table 4.7 IR Spectral analysis of Methotrexate sample

Wave No. (cm^{-1})	Interpretation
1602	C=C stretching
1645	C=O stretching
2953	C-H stretching
3358	N-H stretching
3742	O-H stretching

Table 4.8 Standard curve of MTX in HCl buffer (pH 2.0) at λ_{max} 258.50 nm

Concentration (µg/mL)	Absorbance	Statistical Parameters
2	0.093	
4	0.171	**Correlation coefficient**
6	0.244	$R^2 = 0.9985$
8	0.339	
10	0.429	**Equation of Line**
12	0.487	$y = 0.0401x + 0.0123$
14	0.573	
16	0.652	

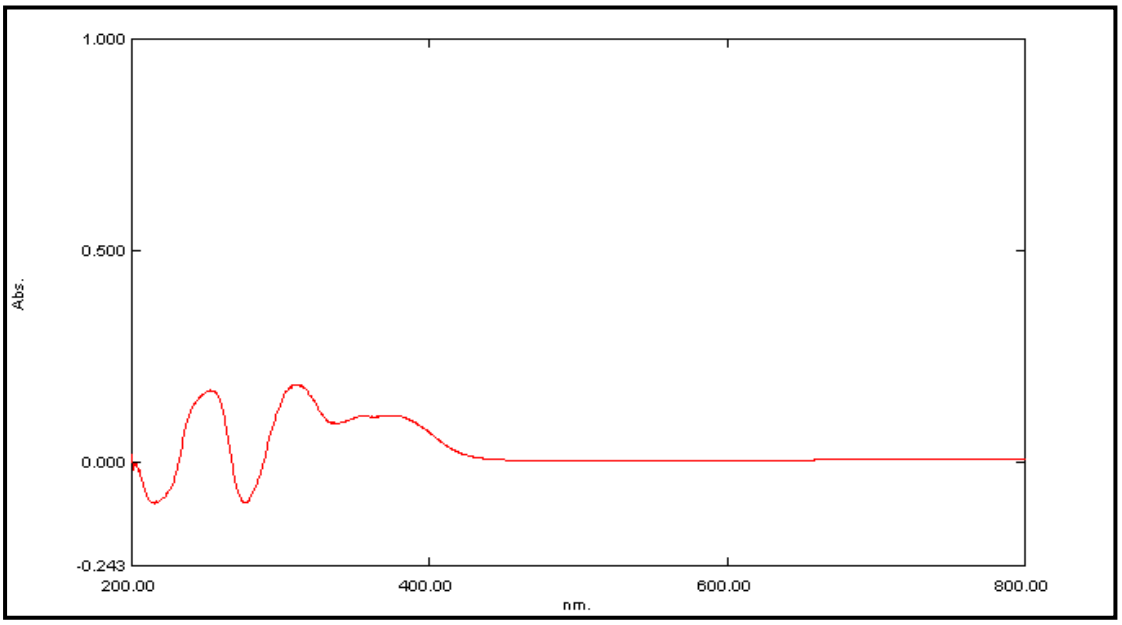

Fig 4.5 UV-Vis Spectrum of MTX

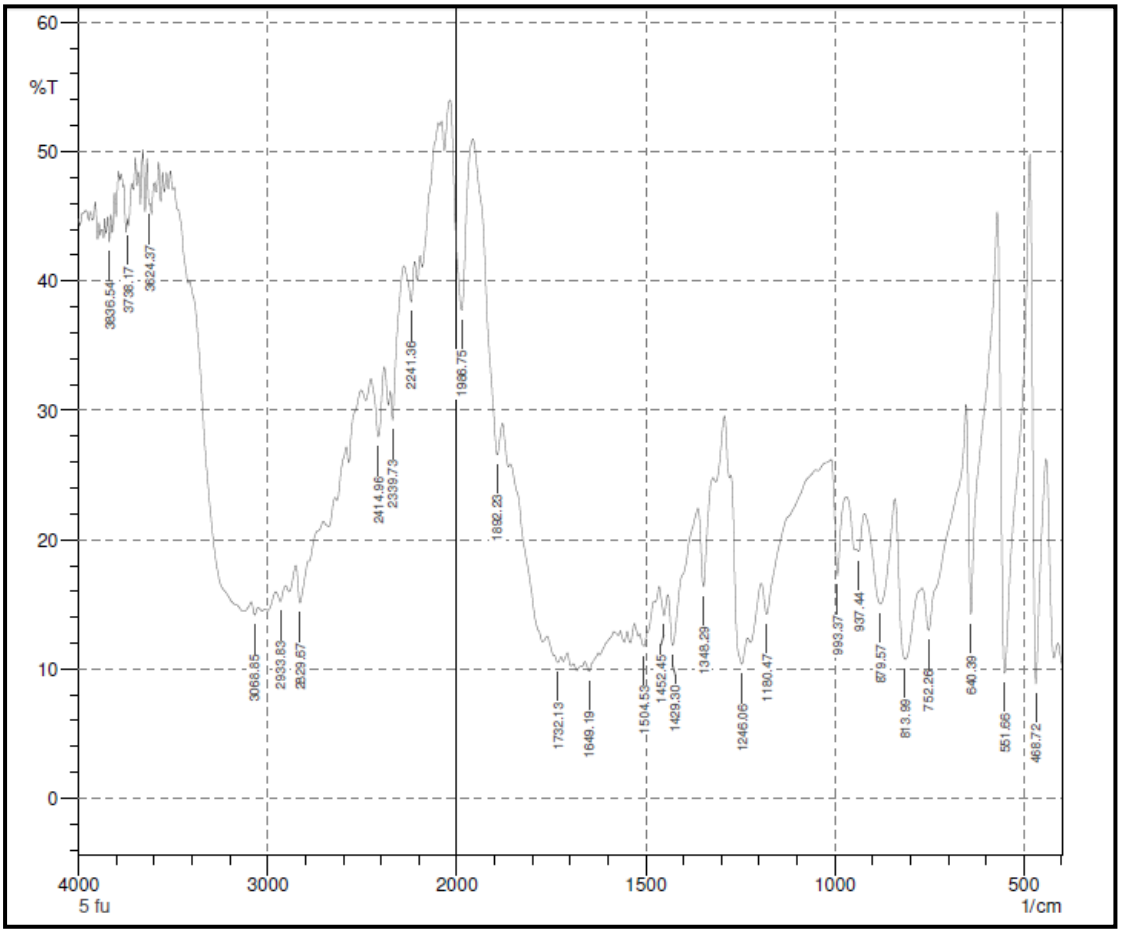

Fig 4.6 IR spectrum of MTX

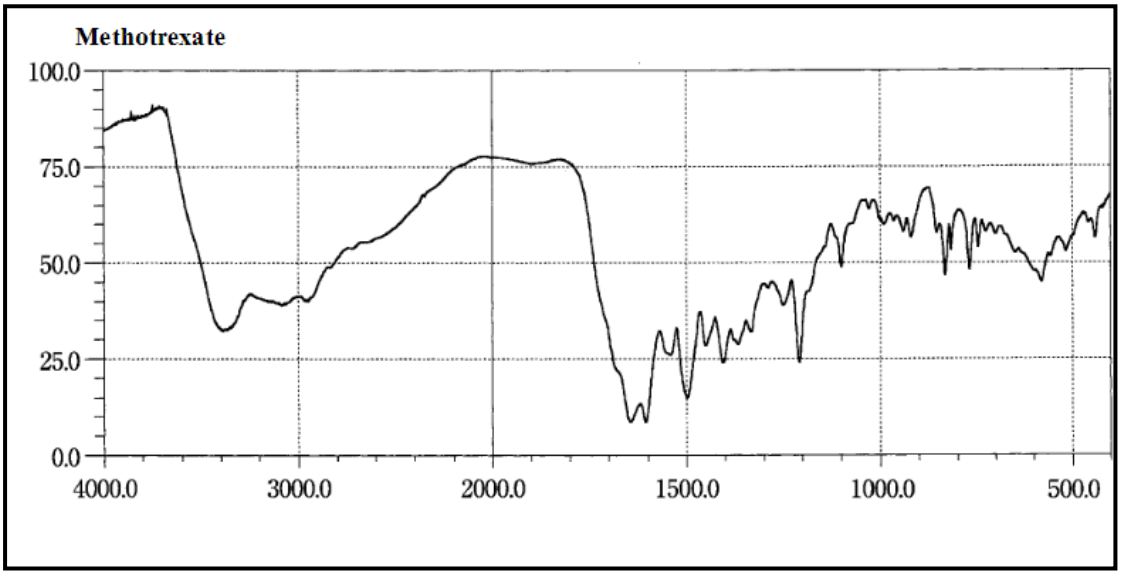

Fig. 4.7 Reference IR spectra of MTX (JP 2014)

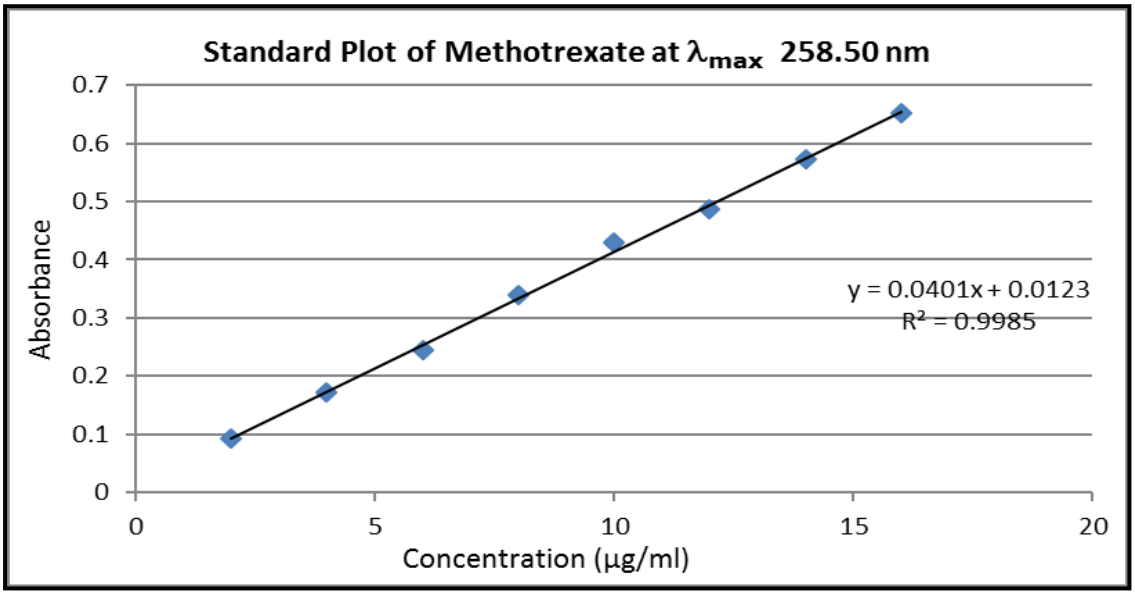

Fig 4.8 Standard curve of MTX

4.3 FORMULATION DEVELOPMENT AND CHARACTERIZATION

4.3.1 Formulation Development

4.3.1.1 Preparation of GNPs

Gold nanoparticles were prepared using Turkevich's trisodium citrate method. In this method 100 ml solution of chloroauric acid 0.01% by weight (Sol A) was heated to 100°C. To this preheated solution 1.5 ml of 1% trisodium citrate solution was added with continuous stirring on magnetic stirrer at 1200 rpm. The solution turned transparent,

from transparent to purplish black ultimately leading to wine red solution. The reaction was continued for 25 minutes (Frens 1973; Turkevich et al., 1951)

4.3.1.2 Preparation of 5-fluorouracil-1-acetic acid (5-FUA) from 5-fluorouracil (5-FU)

In this process 500 mg of 5-FU was dissolved in 3.846 mL of 4M NaOH aqueous solution at temperature 55°C with continuous stirring on magnetic stirrer. 2.306 ml of 5M chloroacetic acid aqueous solution was added drop wise to the above preheated solution. The reaction was continued for 10 hours. The mixture was acidified by diluted HCl to obtain 5-FUA (Li et al., 2014).

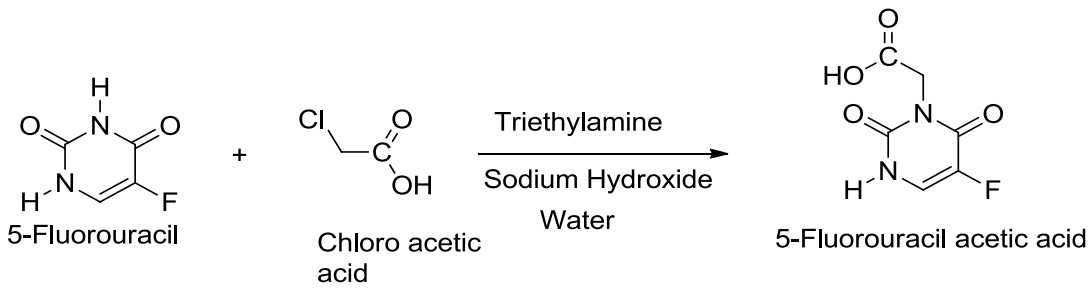

Scheme 1: Synthesis of 5-FUA from 5-FU

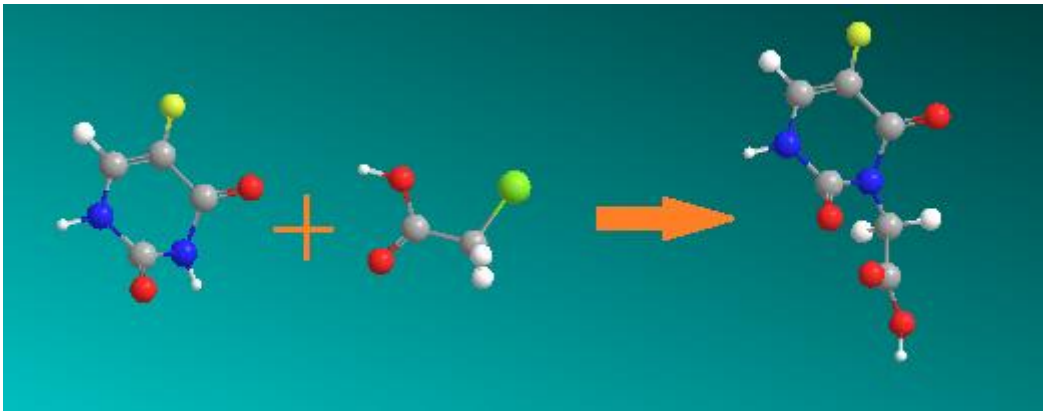

Fig 4.9: Pictorial representation of conjugation of 5-FU with acetic acid to form 5-FUA.

4.3.1.3 Conjugation of 5-FA on PEG6000

In this process 100 mg of 5-FA was dissolved in dimethylformamide (DMF). 3.12 g of PEG6000 was added and stirred for 30 minutes. After 30 min 0.1072g of DCC and 17 µl of triethylamine was added. The reaction was heated to 50° C with continuous stirring for 24 hours. The reaction mixture was concentrated on rotatory evaporator. The concentrated mixture was centrifuged at 12000 rpm. Urea settled

down on the bottom and supernatant was collected. The product was obtained by extracting the supernatant by 20 ml ethyl acetate (Yousefi et al., 2010).

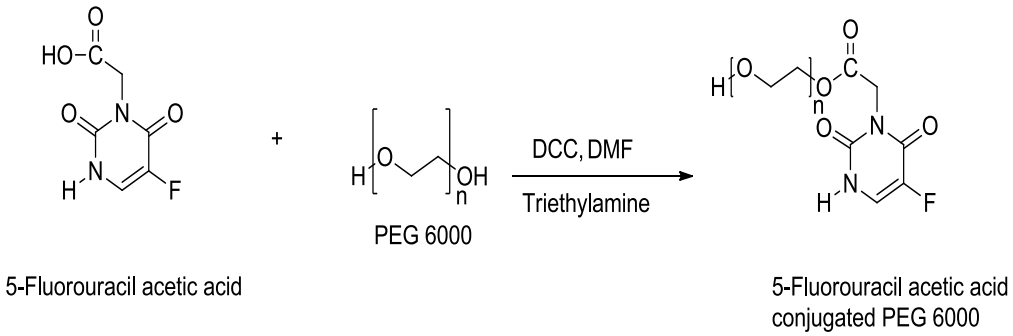

Scheme 2: Synthesis of FUA and PEG conjugate

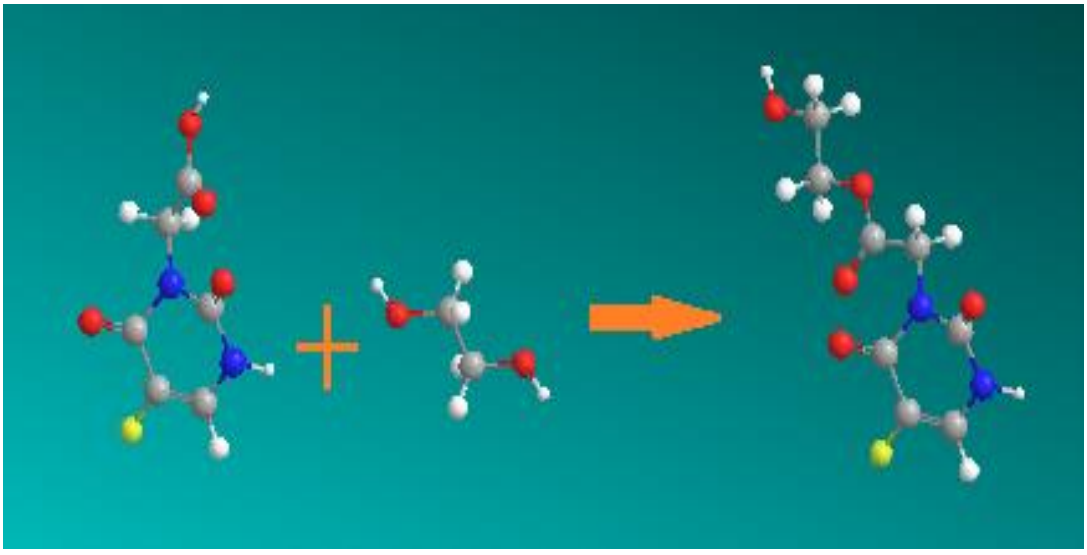

Fig 4.10: Pictorial representation of conjugation of 5-FUA with PEG.

4.3.1.4 Conjugation of methotrexate on PEG6000

100 mg of MTX was dissolved in Dimethylformamide. 1.32 g of PEG6000 was added and stirred for 30 minutes. After 30 min 45.3mg of dicyclohexyl carbodiimide (DCC) and 3.18 µl of triethylamine was added. The reaction was heated to 50° C with continuous stirring for 24 hours. The reaction mixture was concentrated on rotatory evaporator. The concentrated mixture was centrifuged at 12000 rpm. Dicyclohexyl urea (DCU) settled down on the bottom and supernatant was collected. The product was obtained by extracting the supernatant by 20 ml ethyl acetate (Yousefi et al., 2010).

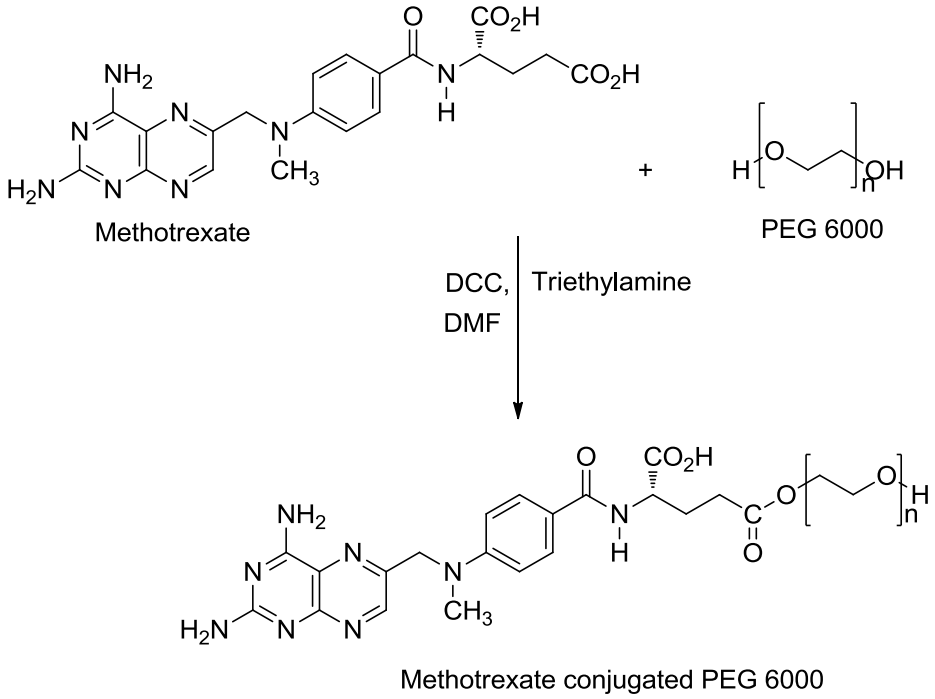

Scheme 3: Synthesis of methotrexate and PEG conjugate.

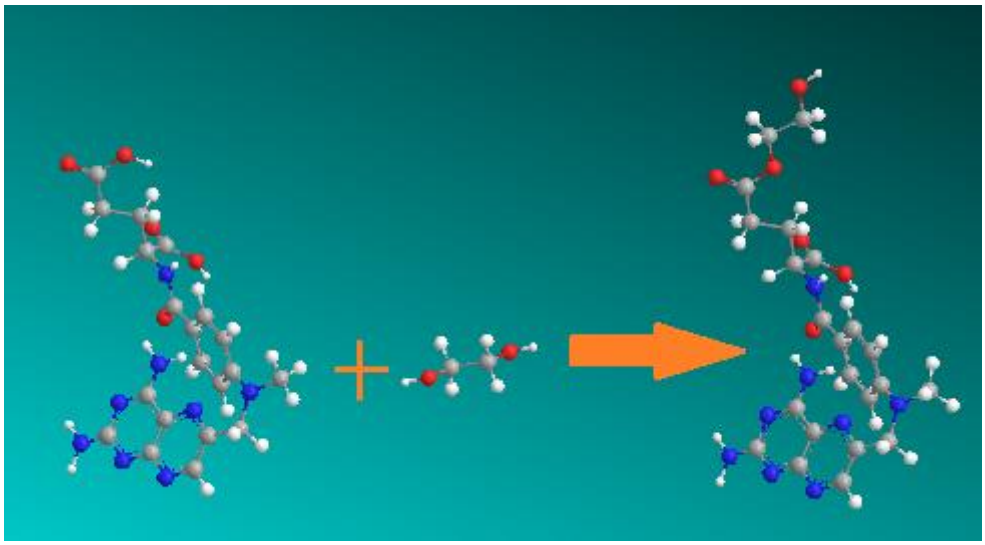

Fig 4.11: Pictorial representation of conjugation of MTX with PEG.

4.3.1.5 Loading of 5-FUA conjugated PEG and MTX conjugated PEG on citrate stabilized GNPs

1.41 g of PEG6000-MTX was dissolved in 10 ml water and 1.368 g of PEG-5-FUA was dissolved in 10 ml. the above solutions were added 50 ml of gold colloid solution [as prepared in process 4.2.1.1. the above solution was stirred continuously for 2 hours. The gold nanoparticles colloid changed color from wine red to pale green (Fig.4.12). After 2 hours, the mixture was centrifuged at 12000 rpm for 90 min. the drug loaded GNP settled down making a pellet. The supernatant was removed.

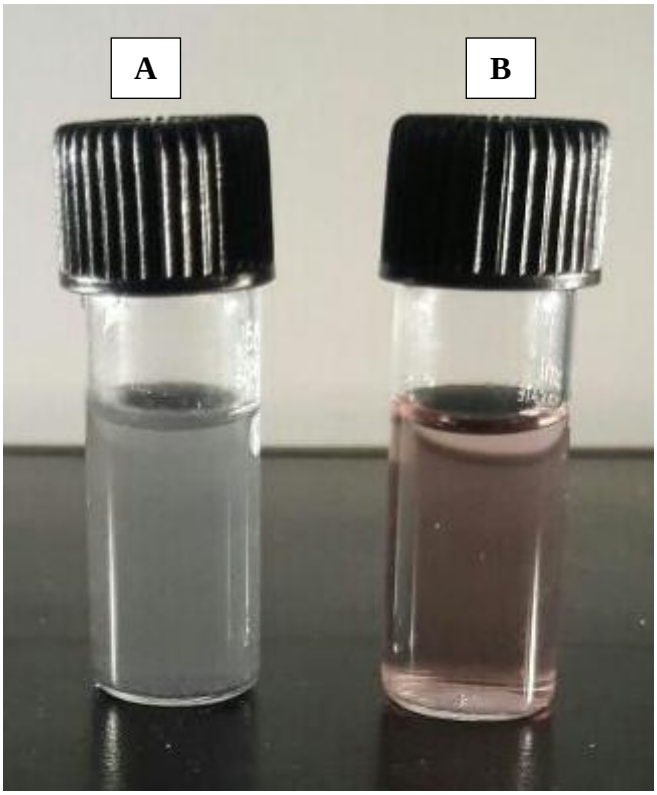

Fig 4.12: Color of GNPs colloid (A) PEG-5-FUA and PEG-MTX loaded GNP, (B) plain GNPs.

4.3.2 Characterization of Gold nanoparticles

- **UV–Visible Spectrum:** The gold nanoparticles prepared in process 4.2.1.1 were taken. The colloid was scanned in the range 200-800 nm using Shimadzu 1800 (Japan) UV-Visible spectrophotometer. 1% by weight trisodium citrate solution was taken as blank. The spectrum showed a peak at 523 nm (Fig.4.13).

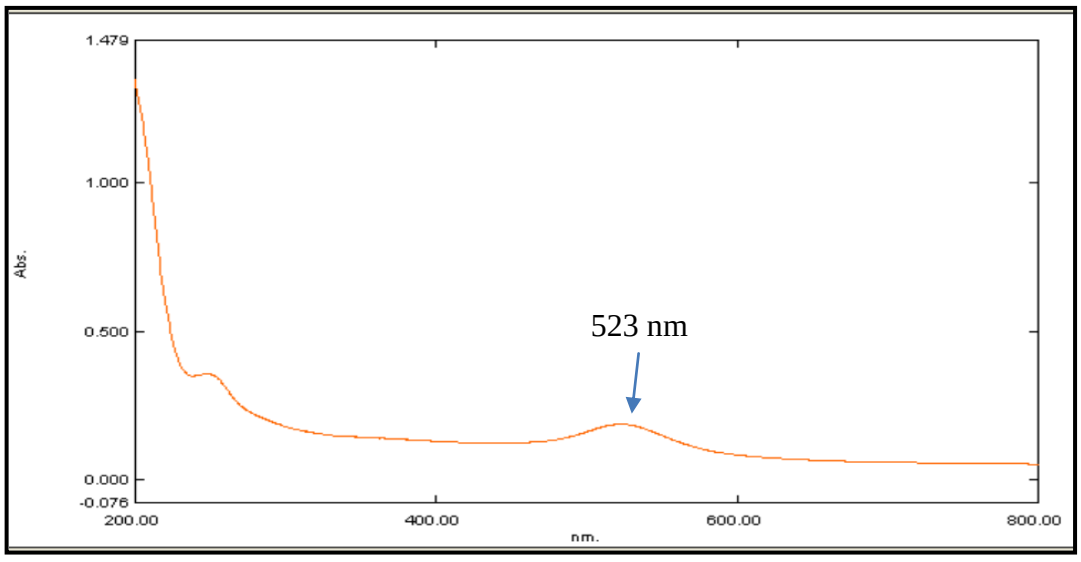

Fig. 4.13: UV-Visible spectrum of gold nanoparticles

Dynamic Light Scattering: It was done at Sophisticated Analytical Instrumentation Facility (SAIF), Panjab University, Chandigarh (Fig.4.14).

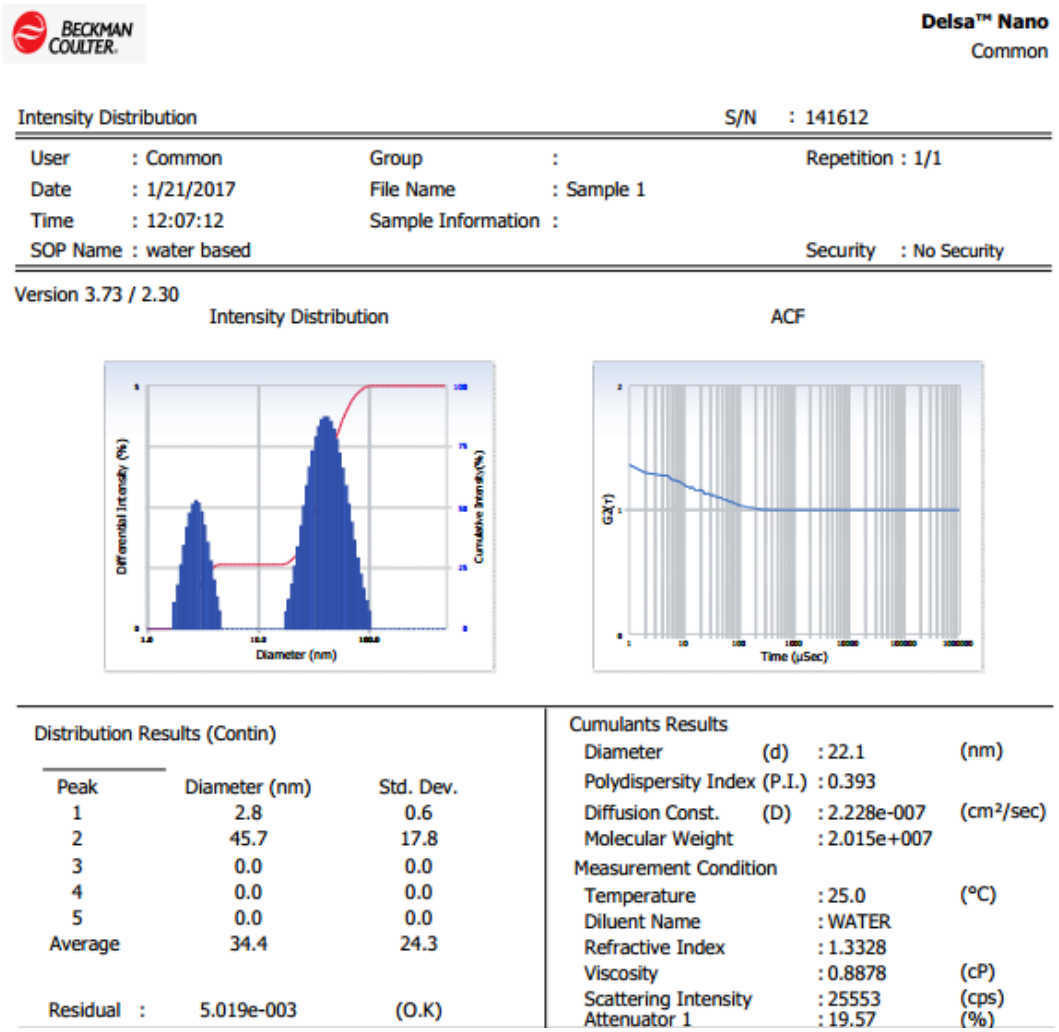

BECKMAN COULTER

Delsa™ Nano
Common

Intensity Distribution S/N : 141612

User	: Common	Group	:	Repetition	: 1/1
Date	: 1/21/2017	File Name	: Sample 1		
Time	: 12:07:12	Sample Information	:		
SOP Name	: water based			Security	: No Security

Version 3.73 / 2.30

Intensity Distribution

ACF

Distribution Results (Contin)

Peak	Diameter (nm)	Std. Dev.
1	2.8	0.6
2	45.7	17.8
3	0.0	0.0
4	0.0	0.0
5	0.0	0.0
Average	34.4	24.3
Residual :	5.019e-003	(O.K)

Cumulants Results

Diameter	(d)	: 22.1	(nm)
Polydispersity Index	(P.I.)	: 0.393	
Diffusion Const.	(D)	: 2.228e-007	(cm^2/sec)
Molecular Weight		: 2.015e+007	
Measurement Condition			
Temperature		: 25.0	(°C)
Diluent Name		: WATER	
Refractive Index		: 1.3328	
Viscosity		: 0.8878	(cP)
Scattering Intensity		: 25553	(cps)
Attenuator 1		: 19.57	(%)

Figure 4.14 Dynamic Light Scattering

4.3.3 Characterization of 5-Fluorouracil acetic acid

- **UV-Visible Spectroscopy:** 5 mg of 5-FUA was taken in 50 ml volumetric flask and dissolved in least amount of distilled water. After dissolution of the drug the volume was made upto 50 ml. 1 ml of the above diluted sample was made up to 10 ml in volumetric flask to form 10 µg/ml solution. UV-visible spectrum was obtained using distilled water as blank. UV-Visible spectrum was obtained using Shimadzu 1800 (Japan) UV-Visible spectrophotometer. A peak was observed at 269.5 nm (Fig. 4.15).

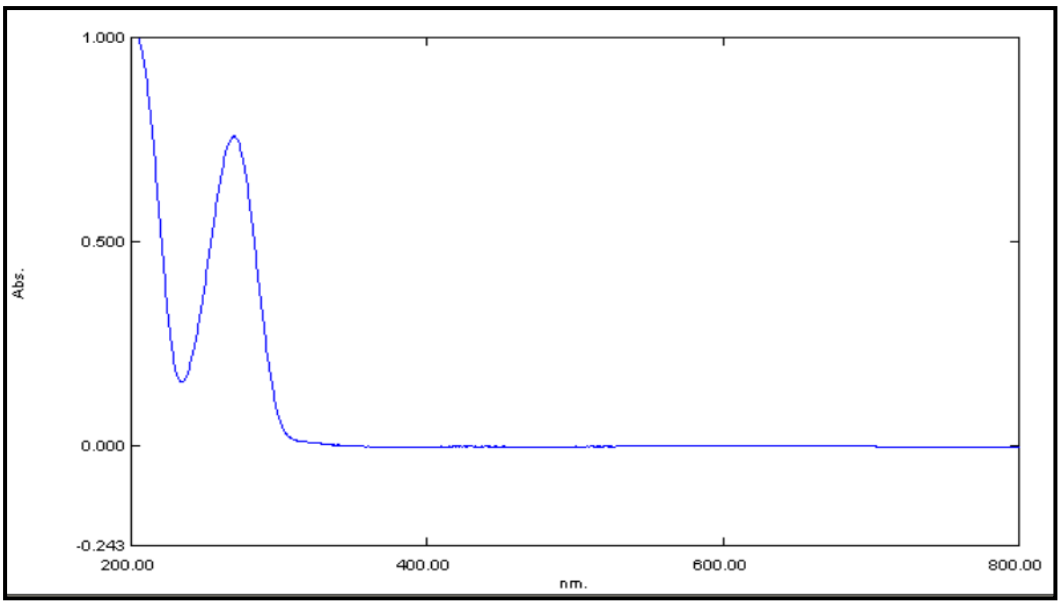

Fig 4.15: UV-Visible spectrum of 5-Fluorouracil acetic acid

❖ **Infrared spectral assessment of 5-FUA:** Infrared (IR) spectrum of any compound gives information about the groups present in the particular compound. IR spectrum of 5-FUA was taken out using KBr pellets (Fig. 4.16). Various peaks in IR spectrum were interpreted for presence of different groups (Table 4.3). Infrared spectroscopy of 5-FUA was carried out by Shimadzu FTIR 8400 S (Japan) Spectrophotometer at Lovely Professional University, Phagwara. The IR spectrum was matched with reference spectra (Fig. 4.3) (BP 2009).

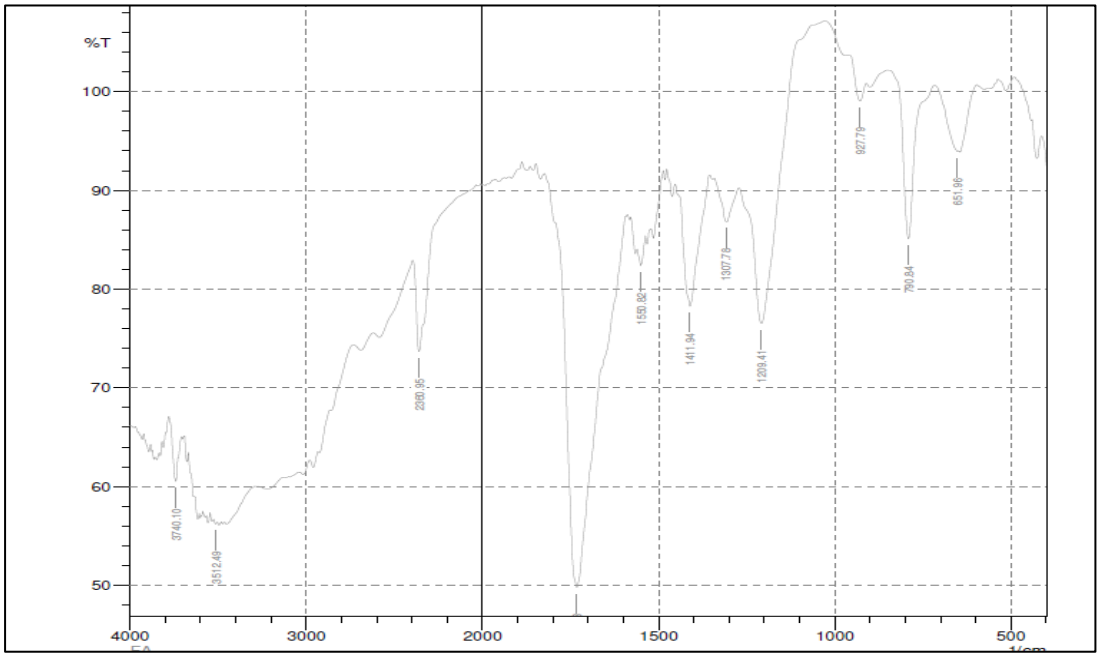

Fig 4.16: Infrared spectroscopy of 5-Fluorouracil acetic acid

4.3.4 Characterization of 5-Fluorouracil acetic acid conjugated PEG6000

- **UV-Visible Spectroscopy:** 10 mg of 5-FA-PEG was taken in 10 ml volumetric flask. It was dissolved in distilled water and volume was made up to 10 ml to prepare 1000 µg/ml solution. 1 ml of above solution was taken in 10 ml volumetric flask and made up to 10 ml using distilled water. UV-Visible spectrum was obtained using Shimadzu 1800 (Japan) UV-Visible spectrophotometer (Fig.4.17).

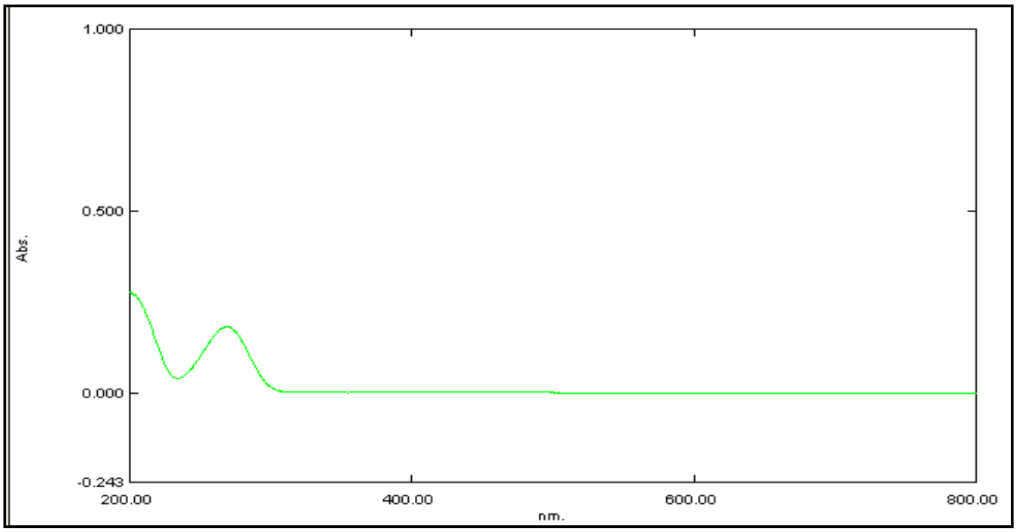

Fig. 4.17: UV-Visible spectrum of 5-Fluorouracil acetic acid conjugated PEG6000

- **Infrared spectroscopy:** IR spectroscopy was performed by making KBr pellets on shimadzu FTIR 8400 S.

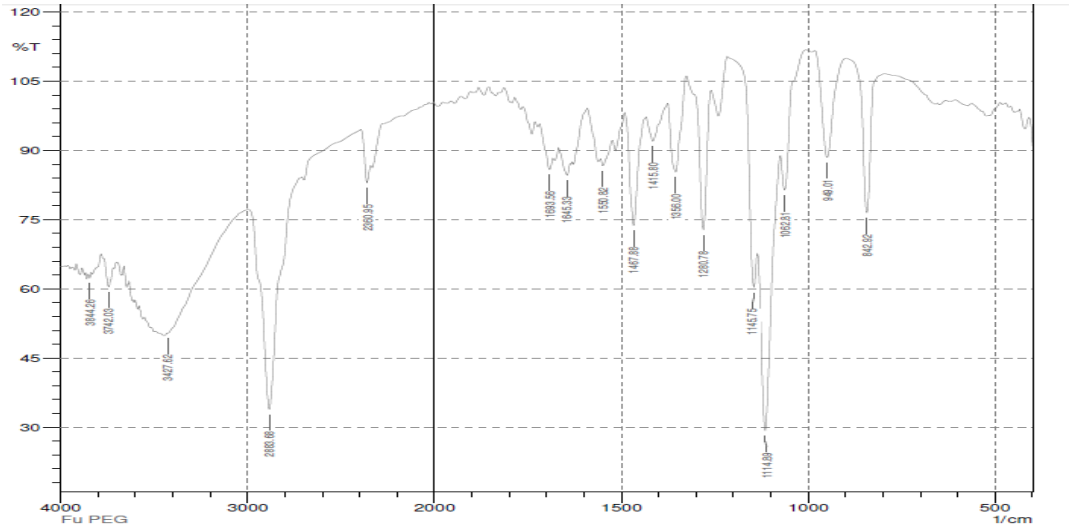

Fig. 4.18: Infrared spectroscopy of 5-Fluorouracil acetic acid conjugated PEG6000

4.3.5 Characterization of Methotrexate conjugated PEG6000

- **UV-Visible Spectroscopy:** 10 mg of MTX-PEG was dissolved in 10 ml of distilled water to prepare 1000 µg/ml solution. 1 ml of above solution was taken in 10 ml volumetric flask and made up to 10 ml using distilled water. UV-Visible spectrum was obtained using Shimadzu 1800 (Japan) UV-Visible spectrophotometer.

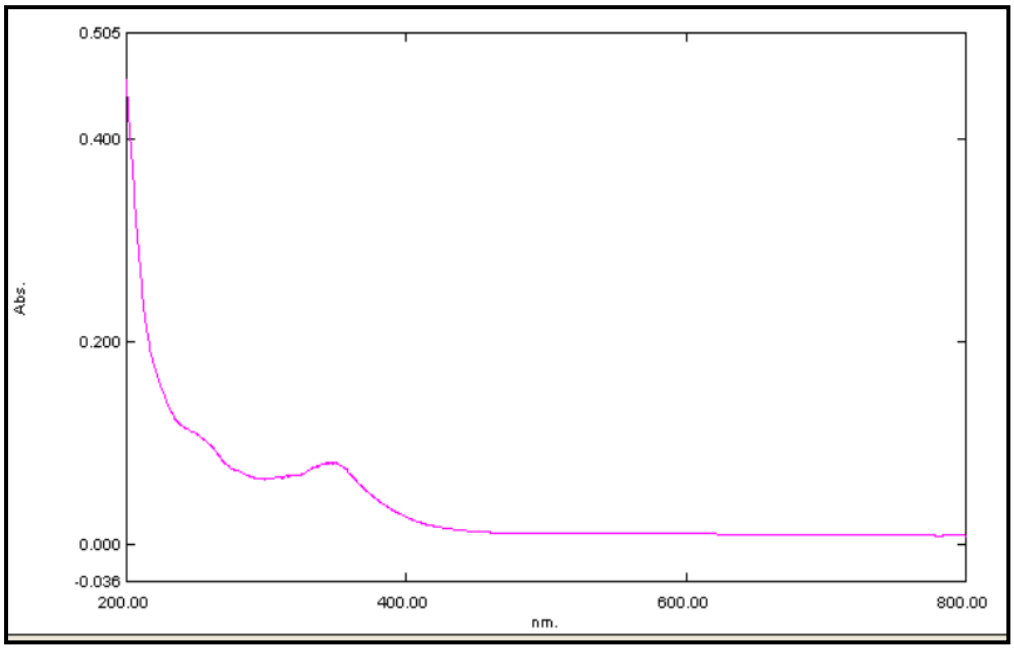

Fig. 4.19. UV-Visible Spectrum of Methotrexate conjugated PEG6000

- **Infrared Spectroscopy:** IR spectroscopy was performed by making KBr pellets on Shimadzu FTIR 8400 S.

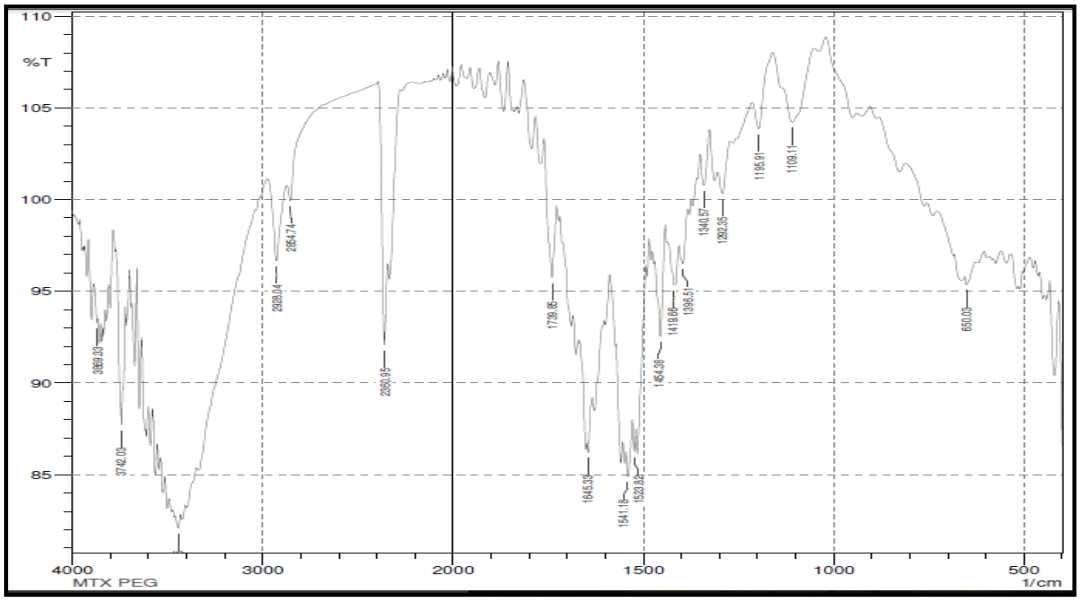

Fig. 4.20. Infrared Spectra of Methotrexate conjugated PEG6000

4.3.6 Characterization of 5-FA conjugated PEG6000 and Methotrexate conjugated PEG6000 loaded gold nanoparticles

- **UV-Visible spectroscopy:** 5 mg of GNP2D was re-suspended in distilled water. UV-Visible spectrum was obtained on Shimadzu 1800 (Japan) UV-Visible Spectrophotometer using distilled water as blank.

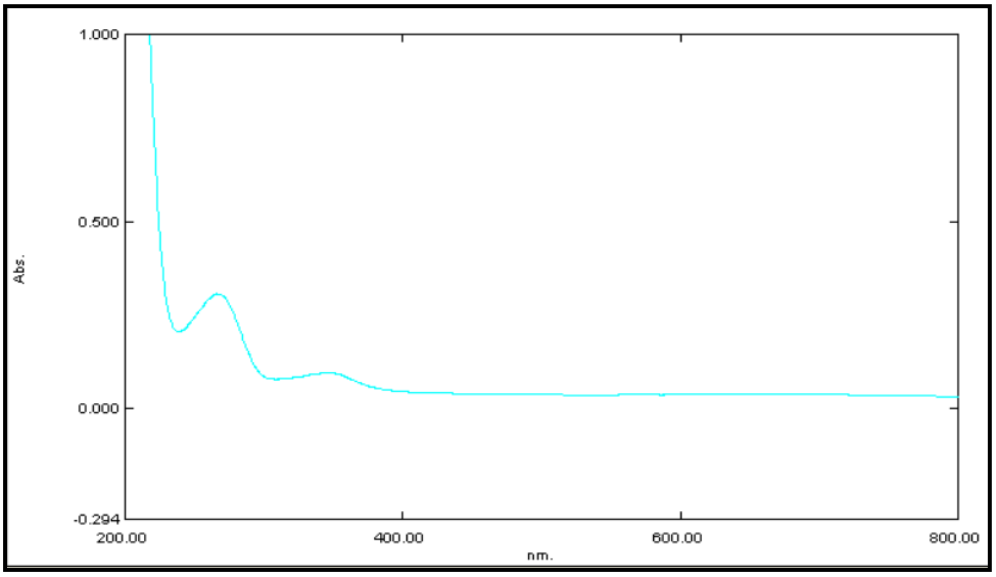

Fig. 4.21. UV-Visible spectrum of Drug loaded Gold Nanoparticles

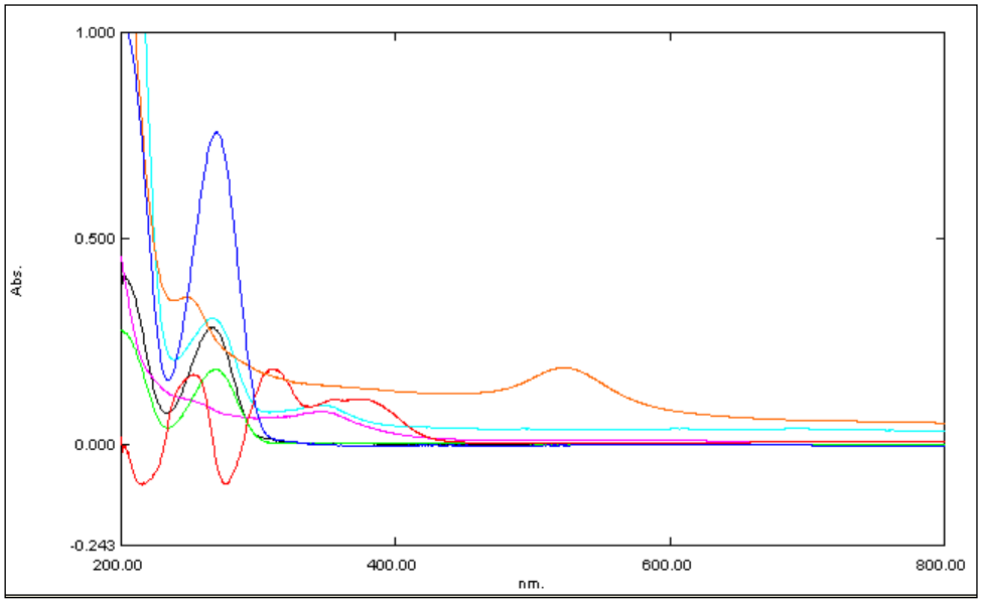

Fig. 4.22: Overlay UV-Visible spectrum of 5-FU (black), 5-FA (blue), 5-FA+PEG6000 (green), MTX (red), MTX+PEG (pink), GNP (saffron), Drug loaded GNP (cyan).

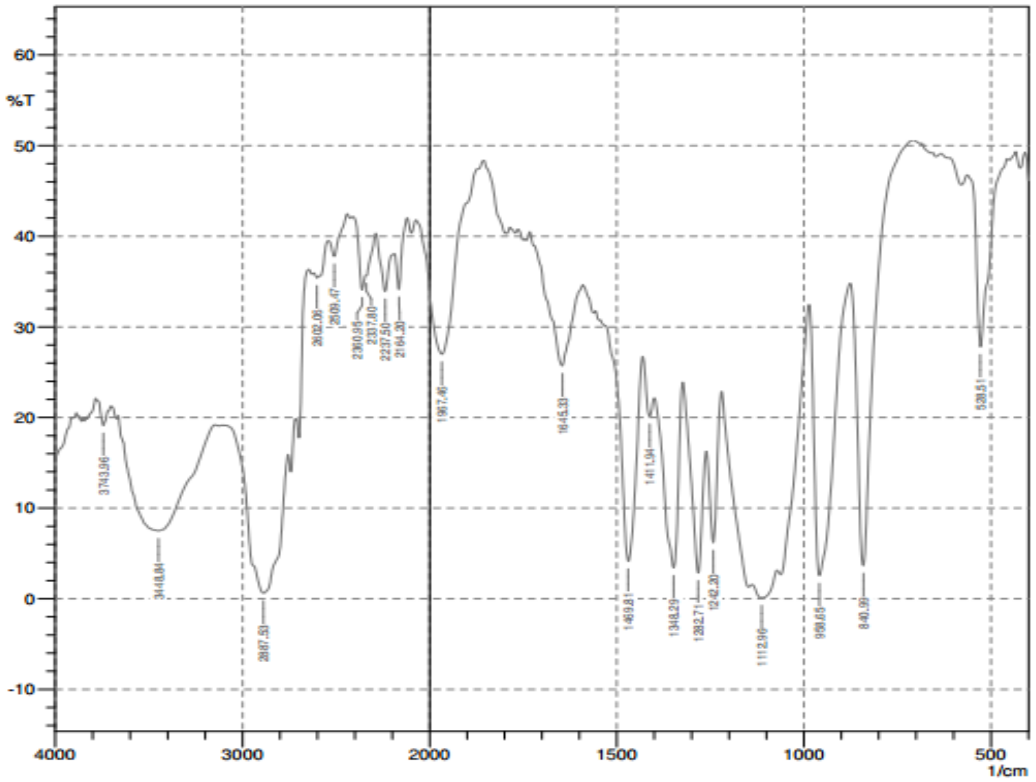

Fig. 4.23. Infrared Spectra of drug loaded GNP.

❖ **Atomic force microscopy:**

The atomic force microscopy **(**AFM) uses an atomically-sharp tip that is brought very close to the sample surface. This technique also predicts the shape and particle size distributions of dendriplexes at various charge ratios, pHs and, salt concentrations. The drug loaded PEGylated GNPs sample was placed on freshly cleaved mica surface and dried in air at room temperature. The samples were examined under atomic force microscope (NT-206; MicroTestMachines Co., Belarus) in tapping mode by using standard AFM cantilevers (MikroMasch, Estonia) in N_2 atmosphere for minimizing the humidity (Pedziwiatr-Werbicka et al., 2013; Perez et al., 2009). AFM studies were performed at SAIF, Punjab University, Chandigarh, India (Fig. 4.24).

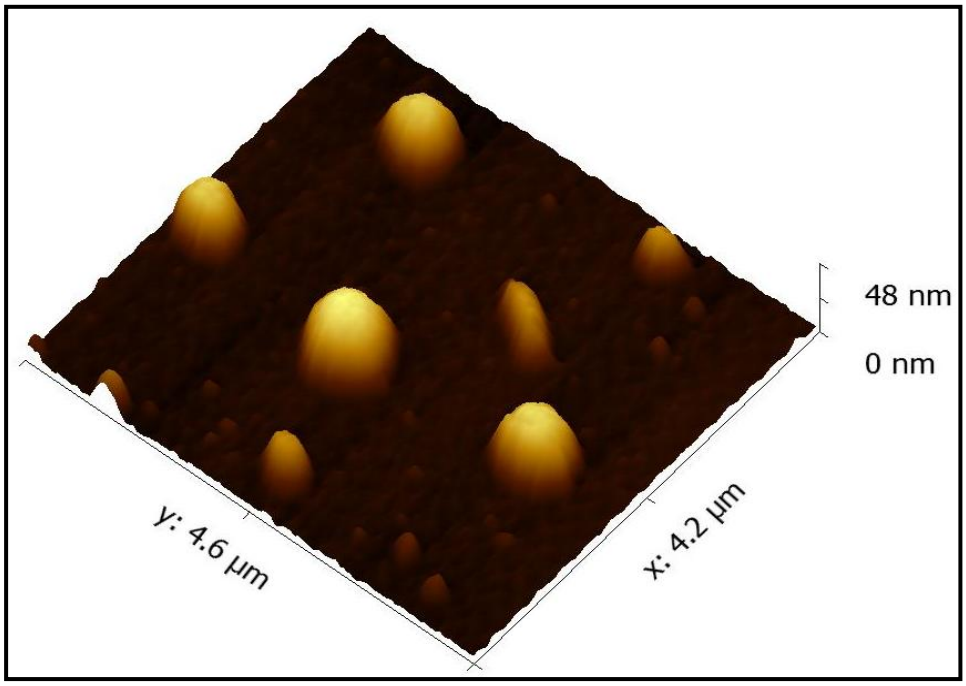

Fig. 4.24: AFM image of drug loaded PEGylated gold nanoparticles

4.4 CELL INTERNALIZATION (CELL UPTAKE) STUDY

Confocal microscopy has been carried out with the help of Carl Zeiss Confocal Micro Scanning Microscope (CLSM510 META, Germany) using plan apochromat objective lens. In brief poly-L-lysine coated slides were prepared and MDA-MB-231 cancer cells were adhered on the slides. Cells seeded at a density of $1x10^6$ cells/well on poly-L-lysine coated glass cover slip in 6 well-plate for 12 h, then cells monolayer's adherent were washed and incubated in fresh medium. Drug loaded PEGylated GNPs were added to triplicate wells and were suspended in Dulbecco Modifed Eagle Medium (DMEM) and added to MDA-MB-231 cancer cells. The system was incubated 4h at room temperature in dark. After incubation, monolayers were washed repeatedly to remove nonadherent GNPs. The cells were fixed in 10% formalin (in Phosphate buffer saline). Nucleus of the MDA-MB-231 cells has been stained using 10 µL of 1 mg/mL DAPI, a nucleus staining dye and mounted with glycerol. The MDA-MB-231 cells internalized GNPs were observed using confocal microscopy of triplicate cover slips for each experimental condition (Fig.4.25). (Garg et al., 2016).

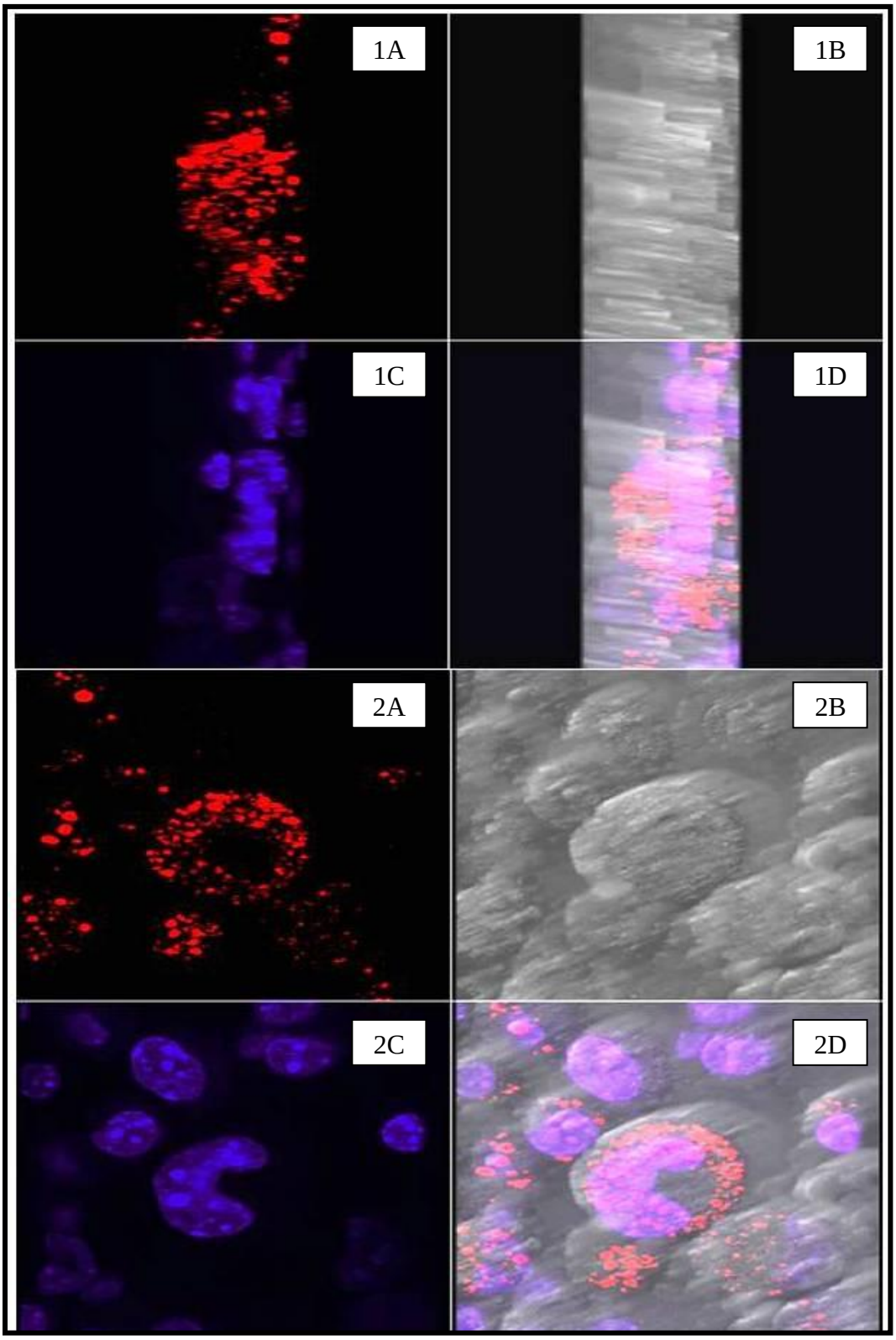

Fig. 4.25: Qualitative cell uptake study of drug loaded PEGylated GNPs. Images 1A-1D and 2A-2D show vertical and horizontal analysis of fluorescence, respectively.

5. RESULTS AND DISCUSSION

5.1 Preformulation

The preformulation studies for both the drugs such physical appearance and melting point which was found coherence with literature. 5-FU was found as white, odorless crystalline powder with a melting point of 280-282°C (Table 4.1). It was soluble in ethanol and distilled water (Table 4.2). 5-FU was identified by ultraviolet spectrophotometry with λ_{max} 266 nm (Fig. 4.1). IR also showed characteristic peaks at 1649 cm^{-1} (C=C stretching), 1732 cm^{-1} (C=O stretching), 2829 cm^{-1} (C-H stretching) (Fig. 4.2). The estimation of FU standard curve was prepared with concentrations of 2, 4, 6, 8, 10, 12, 14 and 16 µg/mL, which showed good linearity with r^2 =0.9996 (Fig. 4.4).

MTX was found as yellow colored odorless crystalline powder with a melting point of 194-197°C (Table 4.5). the solubility study showed that MTX is soluble in 0.1 N HCl and 0.1N NaOH (Table 4.6). MTX was identified by ultraviolet spectrophotometry with λ_{max} 258.50 nm (Fig. 4.5). IR also showed characteristic peaks at 1602 cm^{-1} (C=C stretching), 1645 cm^{-1} (C=O stretching), 2953 cm^{-1} (C-H stretching), 3358 cm^{-1} (N-H stretching), 3742 cm^{-1} (O-H stretching) (Fig. 4.6). The standard curve of MTX in HCl buffer (pH 2.0) was prepared at different concentration and found linear with r^2 = 0.9985 (Fig. 4.8).

5.2 Formulation of GNP loaded with PEG-6000-MTX and PEG-6000-5-FUA

Gold nanoparticles were prepared using Turkevich's trisodium citrate method and characterized by UV spectrophotometry (Frens 1973; Turkevich et al., 1951). The spectrum showed a peak at λmax 523 nm (Fig.4.13) with respect of 20 nm. DLS showed the average diameter of 22 nm.
(http://www.cytodiagnostics.com/store/pc/Introduction-to-Gold-Nanoparticle Characterization-d3.htm , accessed May 15, 2017)

For the conjugation of both the drugs, a PEG-600 conjugates were prepared. To conjugate 5-FU with PEG it was converted to 5-FUA via alkylation reaction with chloroacetic acid as shown in scheme 1 (Li et al., 2014). 5-FUA was characterized by UV which showed λmax 269.5 nm (Fig. 4.14) and IR with characteristic peaks of 1580 cm^{-1} (C=C stretching), 1732 cm^{-1} (C=O stretching), 3512 cm^{-1} (N-H stretching), 3749 cm^{-1} (O-H stretching) (Fig 4.15). Further 5-FUA was conjugated by DCC coupling (Yousefi et al., 2010) and characterized by UV-Visible spectroscopy at λmax 270 nm

(Fig. 4.16), IR with characteristic peaks 1114 cm^{-1} (C-O stretching), 1550 (C=C stretching), 1645 (C=O stretching), 1693 cm^{-1} (C=O stretching), 2883 cm^{-1} (C-H stretching), 3427 cm^{-1} (N-H stretching), 3742 (O-H stretching) (Fig. 4.17).

MTX was directly conjugated with PEG by DCC coupling method (Yousefi et al., 2010). The MTX-PEG conjugate was characterized by UV-Visible Spectroscopy λmax 346 nm (Fig. 4.18) and peak in IR at 1109 cm^{-1} (C-O stretching), 1550 cm^{-1} (C=C stretching), 1645 cm^{-1} (C=O stretching), 1693 cm^{-1} (C=O stretching), 2883 cm^{-1} (C-H stretching), 3427 cm^{-1} (N-H stretching), 3742 cm^{-1} (O-H stretching) showed characteristic peaks (Fig. 4.19)

Thereafter both drugs PEG conjugates were loaded to gold colloid solution [as prepared in process 4.2.1.1), and the competition of reaction monitored by change in color of gold nanoparticles colloid wine red to pale green (Fig.4.12). At the end drug loaded GNP was separated by centrifugation at 3000 rpm.

The drug loaded GNP was showed λmax at 266 and 345 for characteristic peak for 5-FUA and MTX respectively in UV-Visible spectroscopy (Fig. 4.20). The comparison of both free drug, GNP and GNP loaded with drug was done by UV-Visible spectroscopy and overlay drawn which revealed that both the drugs loaed on GNP (Fig. 4.21). The IR spectrum of drug loaded PEG also shoed characteristic peaks at 1112 cm^{-1} (C-O stretching), 1238 (C-O-C stretching), 1645 cm^{-1} (C=O stretching), 2887 cm^{-1} (C-H stretching), 3448 cm^{-1} (N-H stretching), 3743 cm^{-1} (O-H stretching).

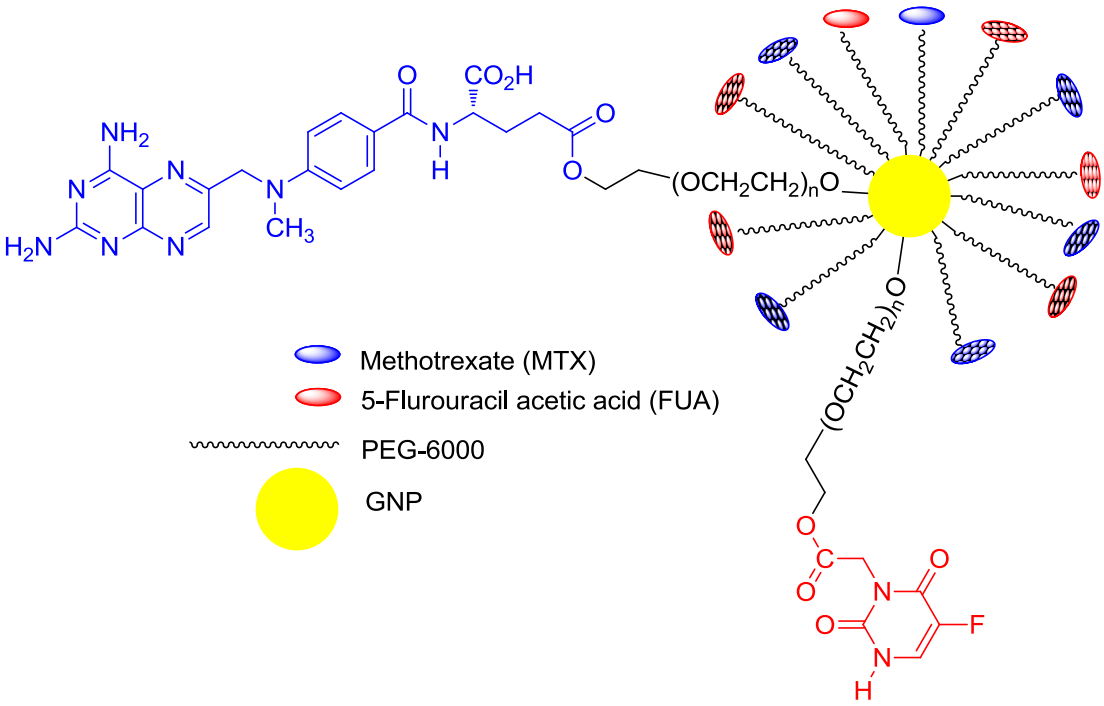

Fig. 5.1: A hypothetical modeled structure of GNP conjugate PEG-MTX and PEG-FUA (Used ChemBioDraw Ultra)

A picture of GNP loaded with PEG-5FUA and PEG-MTX was generated by ChemBio3D Ultra 12.0 (Cambridge Soft) as shown in Fig. 5.1 and Fig. 5.2. Further a hypothetical 3D digram was generated by using n =2 for PEG and 6+6 unit of PEG-5FUA and PEG-MTX (Fig. 5.3).

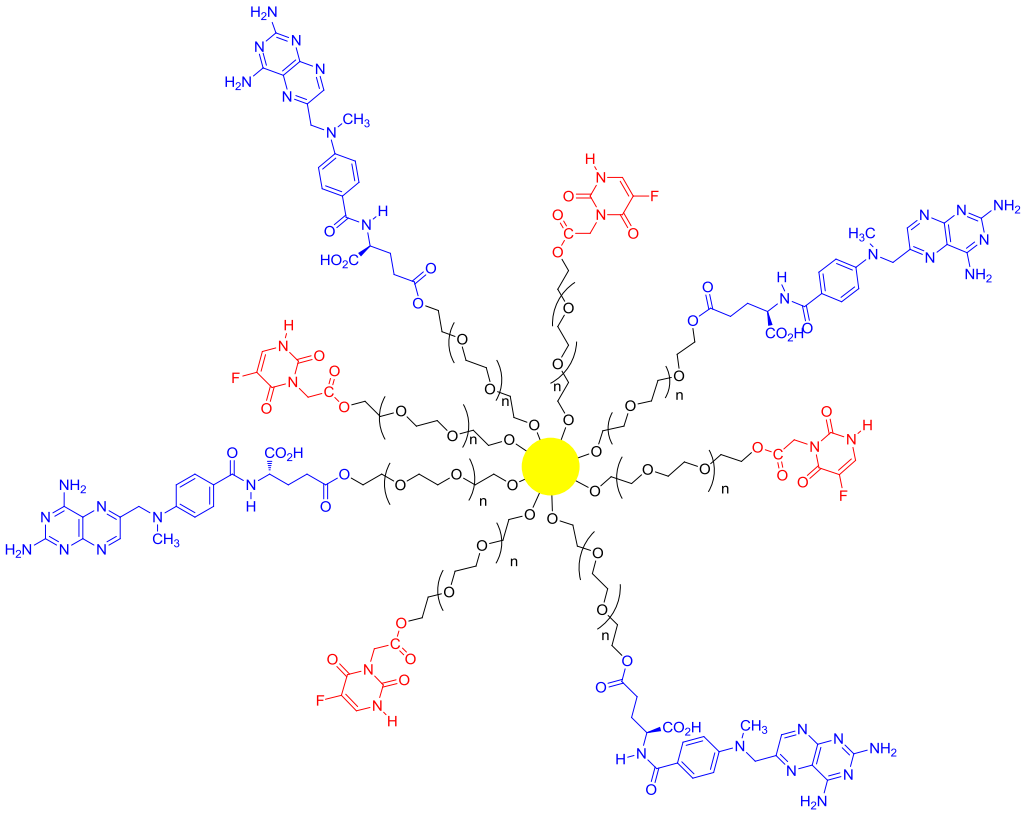

Fig. 5.2: A hypothetical modeled structure of GNP conjugate PEG-MTX and PEG-FUA (Used ChemBioDraw Ultra)

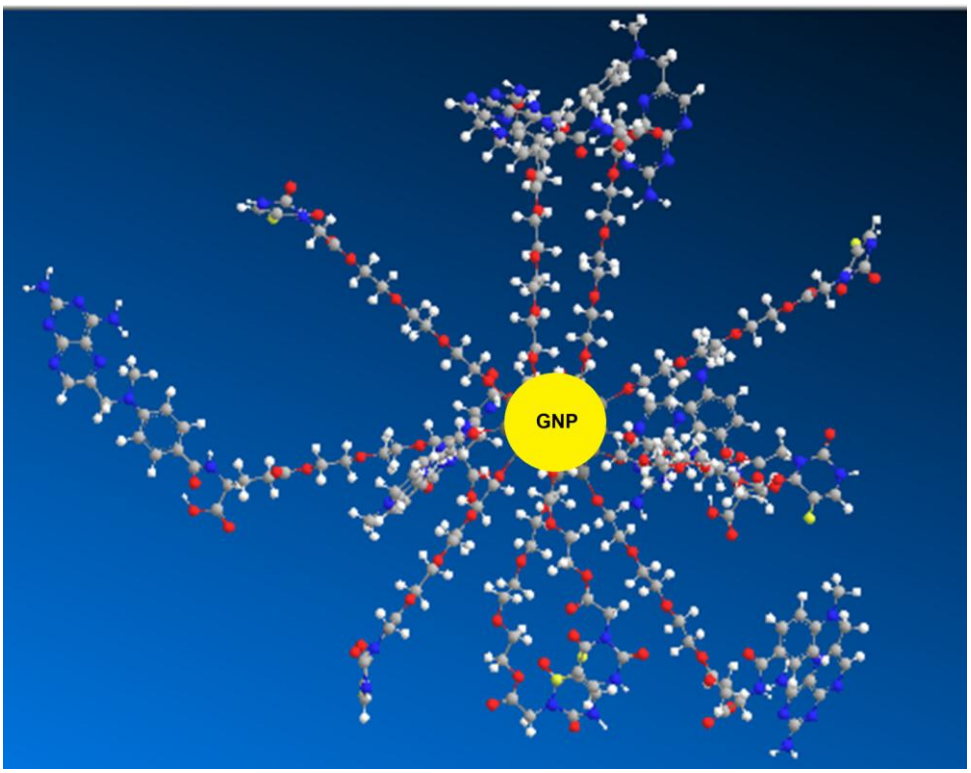

Fig. 5.3. Molecular surface of GNP conjugate with PEG-MTX and PEG-FUA (using n = 2, MTX-PEG =6, FA-PEG =6).

It was expected that GNP is stabilized by PEG conjugate and to understand it we calculated the total energy of GNP and GNP-PEG-drug conjugate with a simpler model as depicted in Fig. 6 using MM2 energy minimization method (ChemBio3D Ultra 12.0; Cambridge Soft). The total energy for GNP was 1748332.4955 kcal/mol whereas GNP-Drug conjugate 532.8317 kcal/mol (used n=2; 6+6 PEG-MTX and PEG-5-FUA conjugates). This shows that the energy of GNP drastically lower down by PEG-drug conjugate and thus lead to increasing the stability.

6. CONCLUSION

Gold nanoparticles (GNPs) were prepared using Turkevich's trisodium citrate method with 20 nm particle size. Conjugation of both the drugs i.e. MTX and 5-FUA with a PEG-600 was done and characterized. Further 5-FUA-PEG and MTX-PEG was directly done with equimolar mixture in GNP solution. A visual monitoring was done with color change of gold nanoparticles colloid wine red to pale green and at the end drug loaded GNP was separated by centrifugation at 12000 rpm upto 90 min.

The drug loaded GNP was showed λ_{max} at 266 and 345 for characteristic peak for 5-FUA and MTX respectively in UV-Visible spectroscopy. The comparison of both free drug, GNP and GNP loaded with drug was done by UV-Visible spectroscopy and overlay drawn which revealed that both the drugs loaed on GNP.

It was expected that GNP is stabilized by PEG conjugate and to understand it we calculated the total energy of GNP and GNP-PEG-drug conjugate with a simpler model using MM2 energy minimization method (ChemBio3D Ultra 12.0; Cambridge Soft). The total energy for GNP was 1748332.4955 kcal/mol whereas GNP-Drug conjugate 532.8317 kcal/mol (used n=2; 6+6 PEG-MTX and PEG-5-FUA conjugates). This shows that the energy of GNP drastically lower down by PEG-drug conjugate and thus lead to increasing the stability. In future the formulation can be studied to evaluate its efficacy in the in-vivo model of breast cancer.

BIBLIOGRAPHY

- Agasti, S. S., Chompoosor, A., You, C. C., et al., Photoregulated release of caged anticancer drugs from gold nanoparticles, J Am Chem Soc, 2009; 131: 5728–5729.Agrawal, A., Rapid RP-HPLC Estimation of Methotrexate in Bulk, Pharmaceutical Preparation and in Spiked Plasma samples, Journal of Pharmacy Research, (2010), 3 (6), 1322.
- Akiyama, Y., Mori, T., Katayama. Y., et al., The effects of PEG grafting level and injection dose on gold nanorod biodistribution in the tumor bearing mice, Journal of Controlled Release, 2009; 139: 81–84.
- Albanese, A., Chan, W. C., Effect of gold nanoparticle aggregation on cell uptake and toxicity, ACS nano, 2011, 5, 5478-5489.
- Alekseeva, A. V., Bogatyrev, V. A., Khlebtsov, B. N., Mel'nikov, A. G., Dykman, L. A., Khlebtsov, N. G., Gold nanorods: Synthesis and optical properties, Colloid J, 2006;68: 661-678.
- Alimohammadi, Y. H., Joo, S. W., PLGA-based nanoparticles as cancer drug delivery systems, Asian Pac J Cancer Prev, 2014; 15: 517–535.
- Alkilany, A. M., Nagaria, P. K., Hexel, C. R., et al., Cellular uptake and cytotoxicity of gold nanorods: molecular origin of cytotoxicity and surface effects, small, 2009; 5: 701–708.
- Alric, C., Taleb, J., Le Duc, G., et al., Gadolinium chelate coated gold nanoparticles as contrast agents for both X-ray computed tomography and magnetic resonance imaging, J Am Chem Soc, 2008; 130: 5908– 5915.
- Anderson, M. E., Glutathione: an overview of biosynthesis and modulation, Chem Biol Interact, 1998; 111-112: 1–14.
- Arifin, D. R., Long, C. M., Gilad, A. A., et al., Trimodal gadolinium-gold microcapsules containing pancreatic islet cells restore normoglycemia in diabetic mice and can be tracked by using US, CT, and positive-contrast MR imaging, Radiology, 2011; 260: 790–798.
- Asadi, N., Davaran, S., Panahi, Y., et al., Application of nanostructured drug delivery systems in immunotherapy of cancer: a review, Artificial cells, nanomedicine, and biotechnology, 2016; 1–6.
- Ashwanikumar, N., Kumar, N. A., Nair, S. A., Kumar, G.S.V., Dual drug delivery of 5-Fluorouracil and Methotrexate through random copolymeric

nanomicelles of PLGA and Polyethylenimine demonstrating enhanced cell uptake and cytotoxicity, Colloids and surfaces B; Biointerfaces, (2014), 122, 520-528.

- Ashwanikumar, N., Kumar, N.A., Nair, S.A., Kumar, G.S.V., 2014. Dual drug delivery of 5-fluorouracil (5-FU) and methotrexate (MTX) through random copolymeric nanomicelles of PLGA and polyethylenimine demonstrating enhanced cell uptake and cytotoxicity. Colloids Surfaces B Biointerfaces 122, 520–528. doi:10.1016/j.colsurfb.2014.07.024
- Aydogan, B., Li, J., Rajh, T., et al., AuNP-DG: deoxyglucose-labeled gold nanoparticles as X-ray computed tomography contrast agents for cancer imaging, Mol Imaging Biol, 2010; 12: 463–467.
- Badrzadeh, F., Rahmati-Yamchi, M., Badrzadeh, K., et al., Drug delivery and nanodetection in lung cancer. Artificial Cells, Nanomedicine, and Biotechnology. Early Online, 2014; 1–17.
- Bahadur, N, M., Watanabe, S., Furusawa, T., Sato, M., Kurayama, F., Siddiquey,I. A., Kobayashi, Y., Suzuki, N., Rapid one-step synthesis, characterization and functionalization of silica coated gold nanoparticles, Colloids and Surfaces A: Physicochemical and Engineering Aspects, 2011;392: 137-144.
- Bajaj, A., Miranda, O.R., Kim, I.B., et al., Detection and differentiation of normal, cancerous, and metastatic cells using nanoparticle-polymer sensor arrays, Proc Natl Acad Sci U S A 2009; 106: 10912–10916.
- Bajaj, A., Rana, S., Miranda, O. R., et al., Cell surface-based differentiation of cell types and cancer states using a gold nanoparticle-GFP based sensing array, Chemical Science 2010; 1: 134–138.
- Bao, C., Conde, J., Polo, E., del Pino, P., Moros, M., Baptista, P. V., Grazu, V., Cui, D., de la Fuente, J. M., A Promising road with challenges: where are gold nanoparticles in translational research? Nanomedicine (Lond). 9 (2014) 2353–2370.
- Bodelóna, G., Costasa, C., Pérez-Justea, J., Pastoriza-Santosa, I., Liz-Marzán., L. M., Gold nanoparticles for regulation of cell function and behaviour, Nanotoday, 2017, 13, 40-60.

- BOISSELIER, E., and ASTRUC, D., Gold nanoparticles in nanomedicine: preparations, imaging, diagnostics, therapies and toxicity. Chemical Society Reviews, 2009, 38, 1759-1782.
- Bridges, C. R., Dicarmine, P. M., Fokina, A., Huesmann, D., Seferos, D. S., Synthesis of gold nanotubes with variable wall thickness. J. Mater. Chem. A, 2013, 1, 1127-1133.
- Brust, M., Walker, M., Bethell, D., Schiffrin, D.J., Whyman, R., 1994. Synthesis of Thiol-derivatised Gold Nanoparticles in. Chem. Commun. 801–802. doi:10.1039/c39940000801
- Brust, M., Walker, M., Bethell, W., Schriffin, D. J., Whyman, R., Synthesis of thiol-derivatised gold nanoparticles in a two phase liquid system. J. Chem. Soc., (1994), 801-802.
- Cabral, R. M., Baptista, P. V., Anti-cancer precision theranostics: a focus on multifunctional gold nanoparticles. Expert Rev. Mol. Diagn., 14 (2014) 1041-1052.
- Cai, Q. Y., Kim, S. H., Choi, K. S., et al., Colloidal gold nanoparticles as a bloodpool contrast agent for X-ray computed tomography in mice, Invest Radiol, 2007; 42: 797–806.
- Cai, W., Gao, T., Hong, H., Sun, J., Applications of gold nanoparticles in cancer nanotechnology, Nanotechnology, science and applications, 2008 10.2147/NSA.S3788.
- Champion, J. A., Katare, Y. K., Mitragotri, S. Particle shape: a new design parameter for micro-and nanoscale drug delivery carriers, Journal of Controlled Release, 2007; 121: 3–9.
- Chauhan, G., Chopra, V., Tyagi, A., Rath, G., Sharma, R.K., Goyal, A.K., 2017. "Gold nanoparticles composite-folic acid conjugated graphene oxide nanohybrids" for targeted chemo-thermal cancer ablation: In vitro screening and in vivo studies. Eur. J. Pharm. Sci. 96, 351–361. doi:10.1016/j.ejps.2016.10.011
- Chegel, V., Rachkov, O., Lopatynskyi, A., Ishihara, S., Yanchuk, I., Nemoto, Y., Hill, J. P., Ariga, K., Gold Nanoparticles Aggregation: Drastic Effect of Cooperative Functionalities in a Single Molecular Conjugate, The Journal of Physical Chemistry C, 2012;116: 2683-2690.

- Chen, H., Paholak, H., Ito, M., Sansanaphongpricha, K., Qian, W., Che, Y., Sun, D., 2013. "Living" PEGylation on gold nanoparticles to optimize cancer cell uptake by controlling targeting ligand and charge densities. Nanotechnology 24, 355101. doi:10.1088/0957-4484/24/35/355101
- Cho, W. S., Cho, M., Jeong, J., Choi, M., Han, B. S., Shin, H. S., Hong, J., Chung, B. H., Jeong, J., Cho, M. H., Size dependent tissue kinetics of PEG-coated gold nanoparticles, Toxicology and applied pharmacology, 2010,245, 116-123.
- Cho, W. S., Cho, M., Jeong, J., Choi, M., Cho, H. Y., Han, B. S., Kim, S. H., Kim, H. O., Lim, Y. T., Chung, B. H., Jeong, J., Acute toxicity and pharmacokinetics of 13 nm- sized PEG-coated gold nanoparticles, Toxicology and applied pharmacology, 2009;239: 16-24.
- Conde, J., Ambrosone, A., Sanz, V., Hernandez, Y., Marchesano, V., Tian, F., Child, H., Berry, C. C., Ibarra, M. R., Baptista, P. V., et al. Design of multifunctional gold nanoparticles for in vitro and in vivo gene silencing. ACS Nano 6 (2012) 8316–8324.
- Cormode, D. P., Roessl, E., Thran, A., et al., Atherosclerotic plaque composition: analysis with multicolor CT and targeted gold nanoparticles, Radiology, 2010; 256: 774–782.
- Cormode, D. P., Skajaa, T., van Schooneveld, M. M., et al., Nanocrystal core high-density lipoproteins: a multimodality contrast agent platform, Nano Lett, 2008; 8: 3715–3723.
- Craig, G. A,, Allen, P. J., Mason, M. D., Synthesis, characterization, and functionalization of gold nanoparticles for cancer imaging, Methods Mol Biol, 2010; 624: 177–193.
- Daraee, H., Etemadi, A., Kouhi, M., et al., Application of liposomes in medicine and drug delivery, Artificial cells, nanomedicine, and biotechnology, 2014; 1–11.
- Dasog, M., Hou, W., Scott, R.W.J., 2011. Controlled growth and catalytic activity of gold monolayer protected clusters in presence of borohydride salts. Chem. Commun. (Camb). 47, 8569–8571. doi:10.1039/c1cc11813g
- Davaran, S., Alimirzalu, S., Nejati-Koshki, K., et al., Physicochemical characteristics of Fe3O4 magnetic nanocomposites based on

poly(Nisopropylacrylamide) for anti-cancer drug delivery, Asian Pac J, Cancer Prev 2014; 15: 49–54.

- Dhamecha, D., Jalalpure, S., Jadhav, K., Jagwani, S., Chavan, R., 2016. Doxorubicin loaded gold nanoparticles: Implication of passive targeting on anticancer efficacy. Pharmacol. Res. 113, 547–556. doi:10.1016/j.phrs.2016.09.037
- Ding, Y., Zhou, Y.-Y., Chen, H., Geng, D.-D., Wu, D.-Y., Hong, J., Shen, W.-B., Hang, T.-J., Zhang, C., 2013. The performance of thiol-terminated PEG-paclitaxel-conjugated gold nanoparticles. Biomaterials 34, 10217–10227. doi:10.1016/j.biomaterials.2013.09.008
- Dreaden, E. C., Austin, L, A., Mackey, M.A., El- Sayed, M. A., Size matters: gold nanoparticles in targeted cancer drug delivery, Therapeutic delivery, 2012;3: 457-478.
- Durr, N. J., Larson, T., Smith, D. K., et al., Two-photon luminescence imaging of cancer cells using molecularly targeted gold nanorods, Nano Lett, 2007; 7: 941–945.
- E.C. Dreaden, L.A. Austin, M.A. Mackey, M.A. El- Sayed, Size matters: gold nanoparticles in targeted cancer drug delivery, Therapeutic delivery, 2012;3: 457-478.
- El-Sayed, I. H., Huang, X., El-Sayed, M. A., Surface plasmon resonance scattering and absorption of anti- EGFR antibody conjugated gold nanoparticles in cancer diagnostics: Applications in oral cancer, Nano letters, 2005;5: 829-834.
- Elsayed, K. A., Imam, H., Ahmed, M., Ramadan, R., Effect of focusing conditions and laser parameters on the fabrication of gold nanoparticles via laser ablation in liquid, Optics & Laser Technology, 2013, 45, 495-502.
- Eustis, S., and El-Sayed, A., Why Gold Nanoparticles are more precious than pretty gold: Noble metal SPR and its enhancement of the radiative and nonradiative properties of nanocrystals of different shapes. Chem. Soc. Rev., (2006), 35, 209-217.
- Fernandes, A.R., Jesus, J., Martins, P., Figueiredo, S., Rosa, D., Martins, L.M.R.D.R.S., Corvo, M.L., Carvalheiro, M.C., Costa, P.M., Baptista, P. V., 2017. Multifunctional gold-nanoparticles: A nanovectorization tool for the

targeted delivery of novel chemotherapeutic agents. J. Control. Release 245, 52–61. doi:10.1016/j.jconrel.2016.11.021

- Foye, W. O., Principles of Medicinal Chemistry, Varghese publishing housing, 1989, 3, 757-784.
- Frens, G., 1973. Controlled Nucleation for the Regulation of the Particle Size in Monodisperse Gold Suspensions. Nat. Phys. Sci. 241, 20–22. doi:10.1038/physci241020a0
- Frens, G., Controlled nucleation for the regulation of the particle size in monodisperse gold suspensions, nature physical science, (1973), 241, 20-22
- G. Frens: Controlled nucleation for the regulation of particle size in monodisperse gold suspensions. Nature: Phys. Sci., (1973), 241, 20-22.
- Galbiati, E., Gambini, L., Civitarese, V., Bellini, M., Ambrosini, D., Allevi, R., Avvakumova, S., Romeo, S., Prosperi, D., 2016. ???Blind??? targeting in action: From phage display to breast cancer cell targeting with peptide-gold nanoconjugates. Pharmacol. Res. 111, 155–162. doi:10.1016/j.phrs.2016.06.007
- Galper, M. W., Saung, M. T., Fuster, V., et al., Effect of computed tomography scanning parameters on gold nanoparticle and iodine contrast, Invest Radiol 2012; 47: 475–481.
- Gangwar, R. K., Dhumale, V. A., Kumari, D., Nakate, U. T., Gosavi, S. W., Sharma, R. B., Kale, S. N., Datar, S., Conjugation of curcumin with PVP capped gold nanoparticles for improving bioavailability, Materials Science and Engineering: C, 2012;32: 2659-2663.
- Garg NK, Singh B, Kushwah V, Sharma R, Tyagi RK, Jain S, Katare OP. The ligand (s) anchored lipobrid nanoconstruct mediated delivery of methotrexate: an effective approach in breast cancer therapeutics. Nanomedicine: Nanotechnology, Biology, and Medicine 2016; 12: 2043–2060.
- Ghosh, P.,Han, G., De, M., Kim, C. K., Rotello, V. M., Gold nanoparticles in delivery applications, Advanced drug delivery reviews, 2008;60: 1307-1315.
- Gibson, J. D., Khanal, B. P., Zubarev, E. R., Paclitaxel-functionalized gold nanoparticles, J Am Chem Soc, 2007; 129: 11653–11661.
- GILJOHANN, D. A., SEFEROS, D. S., DANIEL, W. L., MASSICH, M. D., PATEL, P. C. & MIRKIN, C. A., Gold nanoparticles for biology and medicine. Angewandte Chemie International Edition, 2010, 49, 3280-3294.

- Giri, S., Trewyn, B. G, Stellmaker, M.P., et al., Stimuli-responsive controlledrelease delivery system based on mesoporous silica nanorods capped with magnetic nanoparticles, Angewandte Chemie, 2005; 117: 5166– 5172.
- Gole, A., Murphy, C. J., Seed mediated synthesis of gold nanorods: Role of the size and nature of seed. Chem, Mater., 2004, 16(19), 3633-3640.
- Goodman and Gilman's The Pharmacological Basis of Therapeutics, 11th Edition, McGraw-Hill Health Professional Div., New York, 2006.
- Guo, J., O'Driscoll, C.M., Holmes, J.D., Rahme, K., 2016. Bioconjugated gold nanoparticles enhance cellular uptake: A proof of concept study for siRNA delivery in prostate cancer cells. Int. J. Pharm. 509, 16–27. doi:10.1016/j.ijpharm.2016.05.027
- Hainfeld, J. F., O'Connor, M. J., Dilmanian, F. A., et al., Micro-CT enables microlocalisation and quantification of Her2-targeted gold nanoparticles within tumour regions, Br J Radiol, 2011; 84: 526–533.
- Harrison, E., Nicol, J.R., Macias-Montero, M., Burke, G.A., Coulter, J.A., Meenan, B.J., Dixon, D., 2016. A comparison of gold nanoparticle surface co-functionalization approaches using Polyethylene Glycol (PEG) and the effect on stability, non-specific protein adsorption and internalization. Mater. Sci. Eng. C 62, 710–718. doi:10.1016/j.msec.2016.02.003
- He, H., Xie, C., Ren, J., Nonbleaching fluorescence of gold nanoparticles and its applications in cancer cell imaging, Anal Chem, 2008; 80: 5951–5957.
- Hill, H. D., Vega, R. A., Mirkin, C. A., Nonenzymatic detection of bacterial genomic DNA using the bio bar code assay, Analytical chemistry, 2007; 79: 9218–9223.
- http://www.cytodiagnostics.com/store/pc/Introduction-to-Gold-Nanoparticle Characterization-d3.htm, accessed May 15, 2017.
- Huang, X., El-Sayed, M. A., Gold nanoparticles: Optical properties and implementations in cancer diagnosis and photothermal therapy, Journal of Advanced Research, 2010;1:13-28.
- Huo, Q., Colonm, J., Corderom, A., A facile nanoparticle immunoassay for cancer biomarker discovery. J Nanobiotechnology 2011; 9: 20.

- Hwu, J. R., Lin, Y. S., Josephrajan, T., et al., Targeted Paclitaxel by conjugation to iron oxide and gold nanoparticles, J Am Chem Soc, 2009; 131: 66–68.
- Imam, H., Elsayed, K., Ahmed, M. A., Ramdan, R., Effect of experimental parameters on the fabrication of gold nanoparticles via laser ablation, (2012).
- Iodice, C., Cervadoro, A., Palange, A., Key, J., Aryal, S., Ramirez, M.R., Mattu, C., Ciardelli, G., O'Neill, B.E., Decuzzi, P., 2016. Enhancing photothermal cancer therapy by clustering gold nanoparticles into spherical polymeric nanoconstructs. Opt. Lasers Eng. 76, 74–81. doi:10.1016/j.optlaseng.2015.04.017
- Jain, P. K., Lee, K. S., El-Sayed, I. H., El-Sayed, M. A., Calculated Absorption and Scattering Properties of Gold Nanoparticles of Different Size, Shape, and Composition: Applications in Biological Imaging and Biomedicine, The journal of physical chemistry B, American chemical society, 2006, 110(14), 7238-7248.
- Jain, P. K., Lee, K. S., El-Sayed, I. H., et al., Calculated absorption and scattering properties of gold nanoparticles of different size, shape, and composition: applications in biological imaging and biomedicine, J Phys Chem B, 2006; 110: 7238–7248.
- Jazayeri, M.H., Amani, H., Pourfatollah, A.A., Pazoki-Toroudi, H., Sedighimoghaddam, B., 2016. Various methods of gold nanoparticles (GNPs) conjugation to antibodies. Sens. Bio-Sensing Res. 9, 17–22. doi:10.1016/j.sbsr.2016.04.002
- Ji, X., Song, X., Li, J., Bai, Y., Yang, W., Peng, X., 2007. Size control of gold nanocrystals in citrate reduction: The third role of citrate. J. Am. Chem. Soc. 129, 13939–13948. doi:10.1021/ja074447k
- John, H., Fluorescence properties of gold nanorods and their applicationfor DNA biosensing, Chemical Communications, 2005; 3924– 3926.
- Jones, D. P, Carlson, J. L., Mody, V. C., et al., Redox state of glutathione in human plasma, Free Radic Biol Med, 2000; 28: 625–635.
- JunáZhen, S., YunáLi, J., FangáLi, Y. et al., Controllable preparation of metal nanoparticle/carbon nanotube hybrids as efficient dark field light scattering agents for cell imaging, Chemical Communications, 2010; 46: 4303–4305.

- Kah, J.C.Y., Wong, K.Y., Neoh, K.G., Song, J.H., Fu, J.W.P., Mhaisalkar, S., Olivo, M., Sheppard, C.J.R., 2009. Critical parameters in the pegylation of gold nanoshells for biomedical applications: an in vitro macrophage study. J. Drug Target. 17, 181–193. doi:10.1080/10611860802582442
- Khullar, P., Singh, V., Mahal, A., Dave, P. N., Thakur, S., Kaur, G., Singh, J., Singh Kamboj, S., Singh Bakshi, M., Bovine Serum Albumin Bioconjugated Gold Nanoparticles: Synthesis, Hemolysis, and Cytotoxicity toward Cancer Cell Lines, The Journal of Physical Chemistry C, 2012;116: 8834-8843.
- Kim, C. K., Ghosh, P., Pagliuca, C., et al., Entrapment of hydrophobic drugs in nanoparticle monolayers with efficient release into cancer cells, J Am Chem Soc, 2009; 131: 1360–1361.
- Kim, C. K., Ghosh, P., Pagliucha, C., Zhu, Z. J., Menichetti, S., Rotello, V. M., Entrapment of Hydrophobic Drugs in Nanoparticle Monolayers with Efficient Release into Cancer Cells, Journal of the American chemical society, ACS publication, 2009, 131(4), 1360-1361.
- Kim, K., Oh, K.S., Park, D.Y., Lee, J.Y., Lee, B.S., Kim, I.S., Kim, K., Kwon, I.C., Sang, Y.K., Yuk, S.H., 2016. Doxorubicin/gold-loaded core/shell nanoparticles for combination therapy to treat cancer through the enhanced tumor targeting. J. Control. Release 228, 141–149. doi:10.1016/j.jconrel.2016.03.009
- Kimling, J., Maier, M., Okenve, B., Kotaidis, V., Ballot, H., Plech, A., 2006. Turkevich Method for Gold Nanoparticle Synthesis Revisited.pdf. J. Phys. Chem. B 110, 15700–15707. doi:10.1021/jp061667w
- Kumar, S., Gandhi, K. S., Kumar, R., Modeling of formation of gold nanoparticles by citrate method. Ind. Eng. Chem. Res., (2007), 46, 3128-3136.
- Kumawat, M.K., Thakur, M., Lakkakula, J.R., Divakaran, D., Srivastava, R., 2017. Evolution of thiol-capped gold nanoclusters into larger gold nanoparticles under electron beam irradiation. Micron 95, 1–6. doi:10.1016/j.micron.2017.01.002
- Li, M., Liang, Z., Sun, X., Gong, T., Zhang, Z., 2014. A Polymeric Prodrug of 5-Fluorouracil-1-Acetic Acid Using a Multi-Hydroxyl Polyethylene Glycol Derivative as the Drug Carrier. PLoS One 9, e112888. doi:10.1371/journal.pone.0112888

- Li, M., Liang, Z., Sun, X., Gong, T., Zhang, Z., A Polymeric Prodrug of 5-Fluorouracil-1-Acetic Acid Using a Multi-Hydroxyl Polyethylene Glycol Derivative as the Drug Carrier, PLos ONE, 2014, 9(11), https://doi.org/10.1371/journal.pone.0112888
- Liao, H., Hafner, J., Synthesis and applications of gold nanorod bioconjugates, in abstracts of papers of the american chemical society; 2005: U1099.
- LIM, Z.Z. J., LI, J.E. J., NG, C.T., YUNG, L.Y. L. & BAY, B.H., Gold nanoparticles in cancer therapy. Acta Pharmacologica Sinica, 2011, 32, 983-990.
- Lin, G., Mi, P., Chu, C., Zhang, J., Liu. G., Inorganic Nanocarriers Overcoming Multidrug Resistance for Cancer Theranostics. Adv. Sci. doi: 10.1002/advs.201600134.
- Lin, Z., Monteiro-Riviere, N. A., Riviere, J. E., Pharmacokinetics of metallic nanoparticles, Wiley Interdisciplinary Reviews, Nanomedicine and Nanobiotechnology, 2015, 7, 189-217.
- Liu, G., Mao, X., Phillips, J. A., et al., Aptamer-nanoparticle strip biosensor for sensitive detection of cancer cells, Anal Chem ,2009; 81: 10013– 10018.
- Liu, Y., Shipton, M.K., Ryan, J., Kaufman, E.D., Franzen, S., Feldheim, D.L., 2007. Synthesis , Stability , and Cellular Internalization of Gold Nanoparticles Containing Mixed Peptide – Poly (ethylene glycol) Monolayers Synthesis , Stability , and Cellular Internalization of Gold Nanoparticles Containing Mixed Peptide-Poly (ethylene g. Anal. Chem. 79, 2221–2229. doi:10.1021/ac061578f
- Louis, C., Pluchery, O.,Gold Nanoparticles For Physics, Chemistry And Biology, Imperial College Press, 2012, 108-109.
- Manivasagan, P., Bharathiraja, S., Bui, N.Q., Lim, I.G., Oh, J., 2016. Paclitaxel-loaded chitosan oligosaccharide-stabilized gold nanoparticles as novel agents for drug delivery and photoacoustic imaging of cancer cells. Int. J. Pharm. 511, 367–379. doi:10.1016/j.ijpharm.2016.07.025
- Manson, J., Kumar, D., Meenan, B.J., Dixon, D., 2011. Polyethylene glycol functionalized gold nanoparticles: The influence of capping density on stability in various media. Gold Bull. 44, 99–105. doi:10.1007/s13404-011-0015-8

- Marcelo, G., Kaplan, E., Tarazona, M. P., Mendicuti, F., Interaction of gold nanoparticles with Doxorubicin mediated by supramolecular chemistry, Colloids and surfaces. B, Biointerfaces, 2015.
- Medley, C. D., Smith, J. E., Tang, Z., et al. Gold nanoparticle-based colorimetric assay for the direct detection of cancerous cells, Anal Chem, 2008; 80: 1067–1072.
- Miranda, O. R., Chen, H. T., You, C. C., et al., Enzyme-amplified array sensing of proteins in solution and in biofluids, J Am Chem Soc, 2010; 132: 5285–5289.
- Miranda, O. R., Creran, B., Rotello, V.M., Array-based sensing with nanoparticles: 'chemical noses' for sensing biomolecules and cell surfaces, Curr Opin Chem Biol, 2010; 14: 728–736.
- Mirza, A. Z., Shamshad, H., Preparation and characterization of doxorubicin functionalized gold nanoparticles, European journal of medicinal chemistry, 2011;46:1857-1860.
- Morgan, M. T., Nakanishi, Y., Kroll, D. J., et al., Dendrimer-encapsulated camptothecins: increased solubility, cellular uptake, and cellular retention affords enhanced anticancer activity in vitro, Cancer Res, 2006; 66: 11913–11921.
- Nag, M., Gajbhiye, V., Kesharwani, P., Jain, N.K., 2016. Transferrin functionalized chitosan-PEG nanoparticles for targeted delivery of paclitaxel to cancer cells. Colloids Surfaces B Biointerfaces 148, 363–370. doi:10.1016/j.colsurfb.2016.08.059
- Nakanishi, J., Nakayama, H., Shimizu, T., et al., Light-regulated activation of cellular signaling by gold nanoparticles that capture and release amines, J Am Chem Soc, 2009; 131: 3822–3823.
- Niidome, Y., Nishioka, K., Kawasaki, H., Yamada, S., Rapid synthesis of gold nanorods by the combination of chemical reduction and photoradiation processes; morphological changes depending on the growing processes. Chem. Commun., (2003), 2376-2377.
- Nirmala, J.G., Akila, S., Narendhirakannan, R.T., Chatterjee, S., 2017. Vitis vinifera peel polyphenols stabilized gold nanoparticles induce cytotoxicity and

apoptotic cell death in A431 skin cancer cell lines. Adv. Powder Technol. doi:10.1016/j.apt.2017.02.003

- Novotny, L., Bian, R. X., Xie, X. S., Phys. Rev. Lett.,1997, 79, 645.
- Panahi, Y., Mohammadhosseini, M., Abadi, A. J. N., Moafi, H. F., Akbarzadeh, A., Res, D., & Cell, S. (2016). Preparation, Surface Properties, and Therapeutic Applications of Gold Nanoparticles in Biomedicine. https://doi.org/10.1055/s-0042-115171.
- Patel, F., Shelke, M., Suryawanshi, S., AUV-spectrophotometric determination of methotrexate in tablet dosage form, international jounal of research in pharmacy and chemistry, 2015, 5(4), 641-644.
- Patra, C. R., Bhattacharya, R., Mukhopadhyay, D., Mukherjee, P., Fabrication of gold nanoparticles for targeted therapy in pancreatic cancer, Advanced Drug Delivery Reviews, 2010, 62,(3),346-361.
- Pedziwiatr-Werbicka E, Fuentes E, Dzmitrukd V, Sanchez-Nieves J, Sudas M, Drozde E, et al. Novel 'Si-C' carbosilane dendrimers as carriers for anti-HIV nucleic acids: Studies on complexation and interaction with blood cells. Colloids Surf B: Biointerfaces 2013;109:183-9.
- Perez AP, Romero EL, Morilla MJ. Ethylendiamine core PAMAM dendrimers/siRNA complexes as in vitro silencing agents. Int J Pharm 2009;380:189-200.
- Pérez-Herrero, E., Fernández-Medarde. A., Advanced targeted therapies in cancer: drug nanocarriers, the future of chemotherapy. Eur. J. Pharm. Biopharm. 93 (2015) 52-79.
- Perrault, S.D., Chan, W.C.W., 2010. Synthesis and Surface Modification of Highly Monodispersed, Spherical Gold Nanoparticles of 50-200 (vol 131, pg 17042, 2009). J. Am. Chem. Soc. 132, 11824. doi:10.1021/ja907069u
- Perrault, S.D., Walkey, C., Jennings, T., Fischer, H.C., Chan, W. C. W., Mediating tumor targeting efficiency of nanoparticles through design. Nano lett., (2009), 9(5), 1909-1915.
- Porcaro, F., Battocchio, C., Antoccia, A., Fratoddi, I., Venditti, I., Fracassi, A., Luisetto, I., Russo, M. V., Polzonetti, G., 2016. Synthesis of functionalized gold nanoparticles capped with 3-mercapto-1-propansulfonate and 1-thioglucose

mixed thiols and "in vitro" bioresponse. Colloids Surfaces B Biointerfaces 142, 408–416. doi:10.1016/j.colsurfb.2016.03.016

- Qian, W., Murakami, M., Ichikawa, Y., Che, Y., 2011. Highly efficient and controllable PEGylation of gold nanoparticles prepared by femtosecond laser ablation in water. J. Phys. Chem. C 115, 23293–23298. doi:10.1021/jp2079567
- Rafique, M., Rafique, M.S., Butt, S.H., Kalsoom, U., Afzal, A., Anjum, S., Usman, A., 2017. Dependence of the structural optical and thermo-physical properties of gold nano-particles synthesized by laser ablation method on the nature of laser. Opt. - Int. J. Light Electron Opt. 134, 140–148. doi:10.1016/j.ijleo.2017.01.015
- Saber, M.M., Bahrainian, S., Dinarvand, R., Atyabi, F., 2017. Targeted drug delivery of Sunitinib Malate to tumor blood vessels by cRGD-chiotosan-gold nanoparticles. Int. J. Pharm. 517, 269–278. doi:10.1016/j.ijpharm.2016.12.016
- Safwat, M.A., Soliman, G.M., Sayed, D., Attia, M.A., 2016. Gold nanoparticles enhance 5-fluorouracil anticancer efficacy against colorectal cancer cells. Int. J. Pharm. 513, 648–658. doi:10.1016/j.ijpharm.2016.09.076
- Sau, T. K., Murphy, C. J., Room temperature, High yield synthesis of multiple shapes of gold nanoparticles in aqueous solution. J. Am. Chem. Soc., 2004, 126, 8648-8649.
- Scaramuzza, S., Zerbetto, M., Amendola, V., Synthesis of Gold Nanoparticles in Liquid Environment by Laser Ablation with Geometrically Confined Configurations: Insights To Improve Size Control and Productivity, The Journal of Physical Chemistry C, 2016, 120, 9453-9463.
- Schaal, P. A.,Besmehn, A., Maynicke, E., Noyong, M., Beschoten, B., Simon, U., Electrically conducting nanopatterns formed by chemical e-Beam lithography via gold nanoparticle seeds. Langmuir, (2012), 28, 2448-2454.
- Semmler-Behnke, M., Kreyling, W. G., Lipka, J., Fertsch, S., Wenk, A., Takenaka, S., Schmid, G., Brandau, W., Biodistribution of 1.4- and 18-nm gold particles in rats, Small (Weinheim an der Bergstrasse, Germany), 2008, 4, 2108-2111.
- Senoudi, A. R., Chabane Sari, S. M., Hakem, I. F., Analysis of the Evolution of Tannic Acid Stabilized Gold Nanoparticles Using Mie Theory, International Journal of Analytical Chemistry, 2014:832657.

- Shaat, H., Mostafa, A., Moustafa, M., Gamal-Eldeen, A., Emam, A., El-Hussieny, E., Elhefnawi, M., 2016. Modified gold nanoparticles for intracellular delivery of anti-liver cancer siRNA. Int. J. Pharm. 504, 125–133. doi:10.1016/j.ijpharm.2016.03.051
- Shah, M., Badwaik, V., Kherde, Y., Waghwani, H. K., Modi, T., Aguilar, Z. P., Dakshinamurthy, R., Gold nanoparticles: various methods of synthesis and antibacterial applications. Front Biosci (Landmark Ed), (2014), 19; 2016:1320-1344.
- Sharma, N., Bhatt, G., & Kothiyal, P., Gold Nanoparticles synthesis, properties, and forthcoming applications, 2015, 3(2), 13–27.
- Shi, L., Buhler, E., Boué, F., Carn, F., 2016. How does the Size of Gold Nanoparticles Depend on Citrate to Gold Ratio in Turkevich Synthesis? Final Answer to a Debated Question. J. Colloid Interface Sci. doi:10.1016/j.jcis.2016.10.065
- Sivaraman, S. K., Kumar, S., Santhanam, V., Monodisperse sub-10 nm gold nanoparticles by reversing the order of addition in turkevich method- The role of chloroauric acid. J. Colloid Interface Sci., (2011), 361(2), 543-547.
- Skrabalak, S. E., Chen, J., Sun, Y., Lu, X., Au, L., Cobley, C. M., Xia, Y., Gold nanocages: synthesis properties and applications. Acc. Chem. Res., 2008, 41(12), 1587-1595.
- Suganya, K.S.U., Govindaraju, K., Kumar, V.G., Karthick, V., Parthasarathy, K., 2016. Pectin mediated gold nanoparticles induces apoptosis in mammary adenocarcinoma cell lines. Int. J. Biol. Macromol. 93, 1030–1040. doi:10.1016/j.ijbiomac.2016.08.086
- Suganya, U.S.U., Govindaraju, K., Kumar, G.G., Prabhu, D., Arulvasu, C., Dhas, S.S., Karthick, V., Changmai, N., 2016. Anti-proliferative effect of biogenic gold nanoparticles against breast cancer cell lines (MDA-MB-231 & MCF-7). Appl. Surf. Sci. 371, 415–424. doi:10.1016/j.apsusc.2016.03.004
- Sun, S., Mendes, P., Critchley, K., Diegoli, S., Hanwell, M., Evans, S. D., Leggett, G. J., Preece, J. A., Richardson, T. H., Fabrication of gold micro and nanostructures by photolithography exposure of thiol stabilized gold nanoparticles. Nano Lett., (2006), 6, 345-350.

- Taghdisi, S.M., Danesh, N.M., Lavaee, P., Emrani, A.S., Hassanabad, K.Y., Ramezani, M., Abnous, K., 2016. Double targeting, controlled release and reversible delivery of daunorubicin to cancer cells by polyvalent aptamers-modified gold nanoparticles. Mater. Sci. Eng. C 61, 753–761. doi:10.1016/j.msec.2016.01.009
- Tang, C., Sosa, C.L., Pagels, R.F., Priestley, R.D., Prud'homme, R.K., 2016. Efficient preparation of size tunable PEGylated gold nanoparticles. J. Mater. Chem. B 4, 4813–4817. doi:10.1039/C6TB00886K
- Tassa, C., Duffner, J. L., Lewis, T. A., Weissleder, R., Schreiber, S. L., Koehler, A. N., Shaw, S. Y., Binding Affinity and Kinetic Analysis of Targeted Small Molecule-Modified Nanoparticles, Bioconjugate Chem., 2010, 21 (1), 14–19
- Thaxton, C. S., Elghanian, R., Thomas, A. D., Nanoparticle-based biobarcode assay redefines "undetectable" PSA and biochemical recurrence after radical prostatectomy, Proc Natl Acad Sci USA, 2009; 106: 18437–18442.
- Tokonami, S., Yamamoto, Y., Shiigi, H., Nagaoka, T., Synthesis and bioanalytical applications of specificshaped metallic nanostructures: A review, Analytica Chimica Acta, 2012;716:76-91.
- Torchilin, V. P., Rammohan, R., Weissig, V., Levchenko, T. S., TAT peptide on the surface of liposomes affords their efficient intracellular delivery even at low temperature and in the presence of metabolic inhibitors. Proc. Natl. Acad. Sci. USA. 98 (2001) 8786-91.
- Torchilin, V., Tumor delivery of macromolecular drugs based on the EPR effect, Adv Drug Deliv Rev, 2011; 63: 131–135.
- Tripathi, K.D., Essentials of Medical Pharmacology, 5th edition, Jaypee Brothers Medical Publishers, New Delhi, 2003,769-775.
- Turkevich, J., Stevenson P. C., Hillier J., A study of the nucleation and growth process in the synthesis of colloidal gold. Discuss. Faraday Soc., (1951), 11, 55-75
- Turkevich, J., Stevenson, P. C., Hillier, J., A study of the nucleation and growth process in the synthesis of colloidal gold, Disc. Farad. Soc.,(1951), 11, 55-75.

- Turkevich, John; Cooper, P.H.J., 1951. A study of the nucleation and growth process in the synthesis of colloidal gold. Discuss. Faraday Soc. 55, 55–75. doi:10.1039/df9511100055
- van Schooneveld, M. M., Cormode, D. P., Koole, R., et al., A fluorescent, paramagnetic and PEGylated gold/silica nanoparticle for MRI, CT and fluorescence imaging, Contrast Media Mol Imaging, 2010; 5: 231–236.
- Vigderman, L., Manna, P., Zubarev, E. R., Quantitative replacement of cetyl trimethylammonium bromide by cationic thiol ligands on the surface of gold nanorods and their extremely large uptake by cancer cells, Angewandte Chemie, 2012; 124: 660–665.
- Wang, W., Wei, Q.Q., Wang, J., Wang, B.C., Zhang, S. hui, Yuan, Z., 2013. Role of thiol-containing polyethylene glycol (thiol-PEG) in the modification process of gold nanoparticles (AuNPs): Stabilizer or coagulant? J. Colloid Interface Sci. 404, 223–229. doi:10.1016/j.jcis.2013.04.020.
- Waters, C. A., Mills, A. J., Johnson, K. A., Schriffin, D. J., Purification of dodecanethiol derivatized gold nanoparticles. Chem. Commun., (2003), 540-541.
- Xia, H., Bai, S., Hartmann, J., Wang, D., Synthesis of monodisperse quasi-spherical gold nanoparticles in water via silver(I)-assisted citrate reduction. Langmuir, (2010), 26(5), 3585–3589.
- Yang, W. H., Schatz, G. C., Van Duyne, R. P., J. Chem. Phys., (1995), 103, 869.
- Yoo, J. W., Doshi, N., Mitragotri, S., Adaptive micro and nanoparticles: temporal control over carrier properties to facilitate drug delivery, Advanced drug delivery reviews, 2011; 63: 1247–1256.
- Yousefi, G., Foroutan, S. M., Zarghi, A., Shafaati, A., Synthesis and Characterization of Methotrexate Polyethylene Glycol Esters as a Drug Delivery System, Pharmaceutical society of japan, (2010), 58(2) 147—153.
- Zhang, J., Wang, L., Zhang, H., et al. Aptamer-based multicolor fluorescent gold nanoprobes for multiplex detection in homogeneous solution, Small, 2010; 6: 201–204.
- Zhang, Y., Yu, J., Birch, D. J., et al., Gold nanorods for fluorescence lifetime imaging in biology, J Biomed Opt, 2010; 15: 020504.

- Zheng, J., Petty, J. T., Dickson, R. M., High quantum yield blue emission from water-soluble Au8 nanodots, J Am Chem Soc, 2003; 125: 7780–7781.
- Zheng, J., Zhou, C., Yu, M., et al., Different sized luminescent gold nanoparticles, Nanoscale 2012; 4: 4073–4083.
- Zhi-Chuan, X., Cheng-Min, S., Cong-Wen, X., TianZhong, Y., Huai-Ruo, Z., Jian-Qi, L., Hong-Jun, G., Wet chemical synthesis of gold nanoparticles using silver seeds: a shape control from nanorods to hollow spherical nanoparticles. Nanotechnol., 2007, 18, 115608.
- Zhong, Y., Wang, C., Cheng, R., Cheng, L., Meng, F., Liu, Z. & Zhong, Z., cRGD-directed, NIR responsive and robust AuNR/PEG–PCL hybrid nanoparticles for targeted chemotherapy of glioblastoma in vivo. Journal of Controlled Release, 2014, 195, 63-71.